UNIVERSITY OF SOUTHAMPTON

Nonlinearity Mitigation by Optical Phase Conjugation

by

Yujia Sun

Thesis for the degree of Doctor of Philosophy

in the

Faculty of Physical Science and Engineering

Optoelectronics Research Centre

March 2019

UNIVERSITY OF SOUTHAMPTON

ABSTRACT

FACULTY OF PHYSICAL SCIENCE AND ENGINEERING
OPTOELECTRONICS RESEARCH CENTRE

Doctor of Philosophy

by Yujia Sun

As the demand for high data rates in optical fibre communication systems grows at an unprecedented speed, nonlinearity compensation of wavelength-division multiplexing (WDM) signals with advanced modulation formats is a key challenge for optical transmission. Nonlinearity compensation by optical means such as mid-link optical-phase conjugation (OPC) offers bit rate and modulation format transparency, and more importantly the capability of handling wideband WDM signals or densely packed super-channels simultaneously. In this project, a bandwidth-efficient polarisation-insensitive fibre optical parametric amplifier (FOPA) -based OPC scheme has been proposed and implemented, and its performance as a nonlinearity compensation (NLC) device has been tested experimentally using a variety of modulation formats and number of channels.

Mid-link OPC ideally requires link symmetry about the OPC module in order to provide optimal NLC efficiency. Mostly based on lumped amplification and single-mode fibres, practical link conditions lack symmetry. Investigations on the potential of applying mid-link OPC to these practical links are of great interest. In the experiments presented in the thesis, the implemented OPC module was placed in a field-installed transmission system with varied link conditions using several types of transmitted signals. For dispersion-managed and dispersion uncompensated links (having total lengths between 400 km and 800 km), Q factor improvements ranging between 3.0 dB and 0.5 dB, respectively, are reported. The experimental results have shown the great potential of OPC for NLC in real-world transmission systems.

Contents

List of Figures

List of Tables

UNIVERSITY OF Southampton

Research Thesis: Declaration of Authorship

Print name:	Yujia Sun

Title of thesis:	Nonlinearity Mitigation by Optical Phase Conjugation

I declare that this thesis and the work presented in it is my own and has been generated by me as the result of my own original research.

I confirm that:

1. This work was done wholly or mainly while in candidature for a research degree at this University;
2. Where any part of this thesis has previously been submitted for a degree or any other qualification at this University or any other institution, this has been clearly stated;
3. Where I have consulted the published work of others, this is always clearly attributed;
4. Where I have quoted from the work of others, the source is always given. With the exception of such quotations, this thesis is entirely my own work;
5. I have acknowledged all main sources of help;
6. Where the thesis is based on work done by myself jointly with others, I have made clear exactly what was done by others and what I have contributed myself;
7. Parts of this work have been published as listed in the List of Publications in the Appendix:

Signature:		Date:	

Acknowledgements

First of all, I would like to express my sincere gratitude to my supervisors Prof. Periklis Petropoulos and Dr. Francesca Parmigiani for their constant support and great patience. Their guidance has been the most valuable gift during my time at ORC. I would like to thank Prof. David J. Richardson for his encouragement and support all these years.

Many thanks are given to Dr. Kyle R. H. Bottrill who has offered generous help both in discussions and in the lab.

I would also like to thank Abel Lorences-Riesgo, Gabriel Saavedra Mondaca, Dr. Zhixin Liu, and especially Dr. Satoshi Yoshima, for their collaborations that helped form vital parts of this work.

Thanks to Dr. Shaif-ul Alam and Prof. Michael Zervas. Their comments and suggestions on my work have been extremely helpful.

More thanks go to Dr. Graham D. Hesketh, for sharing his insight into link optimisation, and to Dr. Cosimo Lacava, Dr. Mohamed Ettabib, Iosif Demirtzioglou, and all members of our group, for making our lab a wonderful place.

Finally, special thanks to my family, especially my parents and grandparents, for their support is indispensable. Last but not least, I would like to thank my wife for her company. This work, though trivial, is not possible without her.

Nomenclature

ASE	amplified spontaneous emission
BER	bit-error ratio
BW	bandwidth
CD	chromatic dispersion
CE	conversion efficiency
$CO-OFDM$	coherent orthogonal frequency division multiplexing
CP	circularly polarised
CW	continuous wave
DBP	digital back propagation
DCF	dispersion-compensating fibre
DCM	dispersion-compensating module
DM	dispersion-managed
DP	dual-polarisation
$DPSK$	differential phase shift keying
DRA	distributed Raman amplification
DSF	dispersion-shifted fibre
DUC	dispersion-uncompensated
EDC	electronic dispersion compensation
$EDFA$	Erbium-doped fibre amplifier
$ENOB$	effective number of bits
EVM	error vector magnitude
FOD	fourth-order dispersion
FWM	four-wave mixing
GVD	group velocity dispersion
$HNLF$	highly nonlinear fibre
IDF	inverse dispersion fibre
IQ	in-phase and quadrature-phase
LO	local oscillator
$MSSI$	mid-span spectral inversion
NF	noise figure
NLC	nonlinearity compensation
$NLPN$	nonlinear phase noise

$NLSE$	nonlinear Schrödinger equation
NLT	nonlinear threshold
$NWDM$	Nyquist wavelength-division multiplexing
NZ	non-zero
$OBPF$	optical bandpass filter
$OFDM$	orthogonal frequency division multiplexing
OMA	optical modulation analyser
OOK	on-off keying
OPC	optical phase conjugation
$OSNR$	optical signal-to-noise ratio
PD	photon detector
PM	phase modulation
PMD	polarisation mode dispersion
$PolMux$	polarisation multiplexing
PP	pump-pump
$PRBS$	pseudo-random bit sequence
PS	pump-signal
PSA	phase-sensitive amplifier
PSI	pump-signal-idler
QAM	quadrature amplitude modulation
$QPSK$	quadrature phase shift keying
RX	receiver
SBS	stimulated Brillouin scattering
SMF	single-mode fibre
SNR	signal-to-noise ratio
SOP	state of polarisation
SP	single-polarisation
SPM	self-phase modulation
SRS	stimulated Raman scattering
$SSFM$	split-step Fourier method
STS	scaled translational symmetry
TOD	third order dispersion
TX	transmitter
WDM	wavelength-division multiplexing
WSS	wavelength selective switch
XPM	cross-phase modulation
ZDW	zero-dispersion wavelength

Chapter 1

Introduction

In early years of fibre-optic communications, steady development of fibre technologies supported tremendous growth of data rate, which outgrew data demand. The advent of technologies such as the Erbium-doped fibre amplifier (EDFA) [Mears et al. (1987)], wavelength-division multiplexing (WDM) and dispersion-compensating fibres (DCF) ushered in a new era of fibre-optic communications. The electronic subsystems developed as rapidly as their optical counterparts. Digital coherent receivers have also revolutionised the field during the last decade, unlocking the advancement of higher modulation formats such as quadrature amplitude modulation (QAM) and more complex digital signal processing (DSP) technologies.

An important difference between fibre-optic communications and wireless communications is the presence of Kerr nonlinearity, or third-order nonlinearity in general. The well-known Shannon capacity limit assumes additive white Gaussian noise (AWGN) being the sole type of transmission impairments, establishing a relation between the signal-noise ratios (SNR) and the maximum achievable spectral efficiency. Kerr nonlinearity further reduces the maximum achievable spectral efficiency, causing a reduction of spectral efficiency with increasing SNR beyond an optimal SNR value.

This capacity limit as a function of SNR is called nonlinear Shannon limit. As more advanced modulation formats and the ever increasing symbol rates driven by the exponentially increasing data demand are becoming commonplace, the need for higher optical signal-to-noise ratio (OSNR) pushes transmission power higher than ever before. The nonlinear Shannon limit becomes the fundamental performance barrier for fibre-optic communications [Mitra and Stark (2001)].

Many technologies have been devised to compensate for Kerr nonlinear effects including digital back propagation (DBP), coherent superposition, and optical phase conjugation (OPC). Digital coherent receivers retrieve the amplitude, phase, and state of polarisation (SOP) of the received signals, allowing the use of DBP and digital versions of coherent

superposition. As DSP technologies, they are mostly limited by the computational complexity and limited receiver bandwidth (BW). On the other hand, all-optical signal processing solutions, such as OPC and optical versions of coherent superposition, provide a versatile yet flexible alternative to their digital counterparts, automatically exhibiting bitrate and modulation format transparency as well as a potentially wider operating bandwidth (BW).

The idea of mid-link OPC can be traced back to several decades. Transmission impairment compensation using inline OPC started from dispersion compensation. In 1970s, A. Yariv et al. demonstrated that by placing OPC at the mid-point of a transmission link, dispersion can be effectively compensated for [Yariv et al. (1979)]. The basic idea was that the accumulated chirp due to group-velocity dispersion (GVD) in the first half of the fibre transmission link is reversed by the second half after OPC. Phase conjugation was implemented by a four-wave mixing (FWM) -based FOPA. In subsequent years well into 1990s, OPC compensation of dispersion had been demonstrated for high speed fibre transmission systems [Watanabe et al. (1993), Jopson et al. (1993)].

Not only can dispersion be compensated for via OPC in the middle of a span of fibre, but it also applies to Kerr nonlinearity compensation. Pepper and Yariv discovered [Pepper and Yariv (1980)], shortly after Yariv's first paper on dispersion compensation by OPC, that distortion by the aberrating media due to Kerr nonlinearity is reversible by mid-span spectral inversion (MSSI), the other name of mid-link OPC.

Later on, this concept was extended by Fisher et al [Fisher et al. (1983)], attributing to OPC the compensation capability of the interplay between self-phase modulation (SPM) and GVD. This was shown by numerically simulating backward propagation of phase conjugated wave through the same aberrating media as for the forward direction. This was also experimentally confirmed in the following years as in [Pieper et al. (1994)] and [Watanabe et al. (1993)].

OPC became an intensive research topic again in 2010s, since the use of DSP for Kerr nonlinearity compensation in optical fibre communication systems with an increasingly large number of WDM channels has been deemed insufficient in many cases. The advent of digital coherent receivers unlocked the potential of advanced modulation formats, high baud rate, and the use of polarisation-division multiplexing. It needed to be shown experimentally that the use of OPC is compatible with these features of the transmitted signals.

Setting aside the advanced features of transmitted signals enabled by digital coherent receivers, the conditions of the link are critical to the performance gain provided by OPC. In particular, link symmetry is required for efficient nonlinearity compensation (NLC). Ideal link conditions are not realistic for real-world applications. Questions are then raised on the impact of the degree of link asymmetry on the performance gain by OPC.

The question whether OPC has the potential to benefit the ubiquitous field-installed single-mode fibre (SMF)-based transmission systems attracted our attention.

Turning to the design perspective of the OPC module, conventional OPC designs at the time neglected the concerns over efficient use of available bandwidth (BW). The wavelength shift of individual channels in phase conjugation parametric processes is an unavoidable side effect. A proper solution to this issue is one of the first steps towards the practical implementation of this technology.

To summarise, the main motivations for undertaking this project are

1. construction of an OPC module design with efficient BW utilisation using a single nonlinear medium;

2. Experimental evaluation of the NLC efficiency by mid-link OPC in a field-installed SMF-based transmission system with lumped amplification by EDFAs, using modulation formats ranging from on-off keying (OOK) up to 256 QAM, with and without polarisation multiplexing and inline optical dispersion compensation, etc.

Outline

The thesis is organised as follows.

Chapter 2 to Chapter 4 introduce the theoretical background for fibre-optic communication systems that use mid-link OPC to combat nonlinear impairments.

Chapter 2 starts from the fundamental impairments in fibre transmission, both linear and nonlinear. Their physical origins, mechanism, and interaction with each other are discussed, showing the capacity limitation they imposed and their compensation technologies.

Chapter 3 continues by examining the physics of a special type of fibres, highly nonlinear fibres (HNLFs), that allow intense FWM processes to take place, which in turn can be used to counter nonlinear impairments in transmission. HNLFs used in FOPA applications need to exhibit certain properties in order to provide desired performance. Balancing these properties and optimising the design of the FOPA as a subsystem are serious challenges for the implementation of a high-performance FOPA-based OPC module.

Chapter 4 then moves on to the background introduction of common NLC approches, namely DBP, coherent superposition (phase-conjugated twin waves), and mid-link OPC.

The pros and cons of each approach are discussed, especially in the context of their effects on the major nonlinear and stochastic impairments that signals in fibre transmission encounter. These impairments are broadly categorised in the text. Their characteristics are essential to the understanding of their remedy. Improved resilience to stochastic effects is also one of the key advantages of mid-link OPC compared to its counterparts. This chapter then turns its focus to mid-link OPC alone, with an emphasis on the approaches to achieving optimal link performance by optimising the transmission system as a whole when OPC is in place.

Chapter 5 to Chapter 7 present the major experimental works conducted during this project. The first two chapters recorded and discussed the characterisation of the transmitter, transmission links, and the OPC module that were used in the experimental demonstrations for the purpose of mitigating nonlinear impairments and led to the key findings of the thesis that are discussed in the following chapter.

Chapter 5 presents the various transmitters and transmission links. These experiments feature a network of field-installed SMF transmission links with lumped amplification at geographical locations that are non-uniformly separated. A variety of transmission links are individually discussed, according to their key features such as the length, the presence of inline optical dispersion compensation, etc. For identical transmitted signals, their differences manifest themselves mostly in the varied peak performance and optimal launch powers, which are to be improved through the application of mid-link OPC.

Chapter 6 presents the design flow, the optimisation procedures, and the quantitative performance characterisation of the FOPA-based OPC module. The description and analysis regarding the choice of key components for the FOPA take a large part of this chapter. Since the theoretical background has been discussed in Chapter 3, experimental comparisons among potential candidates and the subsequent verification of the optimal choice are highlighted. The OPC module is tested in a back-to-back configuration without transmission. These results serve as the upper limit for the link performance with the OPC in place.

Chapter 7 presents the main experimental findings of the thesis. Mid-link OPC is shown to have effectively mitigated nonlinear impairments in field-installed conventional transmission systems for various total distances, for various advanced modulation formats up to 256 QAM, for both densely packed super-channels and conventional WDM, and for a variety of signal band BW, regardless of the use of inline optical dispersion compensation, the use of polarisation multiplexing, etc. The improvements are normally observed in the improved peak performance, the improved performance in nonlinear regime, or the increased optimal launch power. The chapter concludes with a summary of all works conducted.

Chapter 2

Background theory on fibre transmission impairments

Fibre-optic transmission systems started evolving from 1960s. At their early stages multi-mode fibres formed the backbone of deployed links, until modal dispersion began to limit the bitrate from increasing further beyond 100 Mbps. This limitation resulted in the adoption of single-mode fibres (SMF), which has continued to be the dominant optical fibre technology until today.

In this chapter, the background theory on major signal impairments during the transmission in SMF transmission systems is introduced. Starting from linear impairments, namely attenuation, chromatic dispersion (CD), and polarisation mode dispersion (PMD), to nonlinear distortions, including stimulated scattering phenomena and the three basic types of Kerr nonlinearity, this chapter provide essential information that will be helpful in understanding both the obstacles faced for SMF-based systems and the solution we proposed and investigated.

2.1 Attenuation and amplification

One major linear impairment is loss, i.e. wave power attenuation. The physical origins of the exponential attenuation of light power along the fibre include mainly the Rayleigh scattering and material absorption due to impurity, dopants, and sub-wavelength density fluctuations. Material absorption in silica SMFs is less than 0.03 dB in the wavelength window between 1300 nm to 1600 nm. Rayleigh scattering, on the other hand, scatters light due to sub-wavelength density fluctuations, scaling with λ^{-4}, therefore, is most severe at shorter wavelengths.

Light wave power attenuates inside the fibres exponentially. Defining the loss coefficient as a constant α, the wave power evolution is given by

$$P(z) = P(0)\exp(-\alpha z). \tag{2.1}$$

The loss expressed in decibel terms per unit distance is then

$$\alpha_{\mathrm{dB}} = 4.342\alpha. \tag{2.2}$$

The wavelength-dependent nature of the loss coefficient is the fundamental reason of the use of the wavelength regime in 1550 nm in modern telecommunication applications. Power attenuation is the lowest in this wavelength regime in standard SMFs. A typical decibel loss coefficient α_{dB} in standard SMFs is 0.2 dB/km in the vicinity of 1550 nm. This value is sufficiently low to allow periodically placing optical amplifiers at an interval up to about 100 km.

Before the advent of EDFA technology, optical signals were demodulated at inline opto-electronic repeaters to recover the transmitted information and re-modulated to allow further transmission. Although this approach has the advantage of better cascadability, moving back-and-forth between optical and electronic domains complicates the inline repeater modules, and reconfigurations are required when changing transmitted signals.

EDFAs amplify the attenuated light power within the optical domain. They are bitrate and modulation format transparent, and compatible with WDM scenarios within their operating BW. However, they come at the cost of adding broadband amplified spontaneous emission (ASE) noise. ASE noise due to EDFAs can be modelled as an AWGN source, which directly degrades the OSNR of the signals. The quantum limited fundamental noise figure (NF) of EDFAs as phase-insensitive amplifiers (PIAs) is 3 dB, and the actual NF of a typical EDFA is in the range between 4 dB to 8 dB.

EDFAs are grouped according to their use into 1) preamplifier EDFAs that amplify the received signals before detection, 2) booster EDFAs that launch the signals onto the link, and 3) inline EDFAs that compensate for the loss incurred in the previous fibre span.

The gain spectrum for a typical EDFA features a double peak, and a small frequency-dependent variation of gain exists across its operating BW. This is a particularly serious problem for transmission link with a chain of inline EDFAs. For example, the total gain variation of 20 dB can be reached in a link with 100 inline EDFAs with only 0.2 dB difference in gain between two channels for each EDFA. A common solution is to have frequency-dependent filters to flatten the gain [Inoue et al. (1991)].

Distributed amplification schemes such as distributed Raman amplification often provide a superior performance NF-wise, however, at the expense of larger pump powers and case-specific pumping designs [Perlin and Winful (2002)].

2.2 Propagation constant and dispersion

Single-mode fibres exhibit no modal dispersion since only a single mode is allowed to propagate inside the fibre. However, material dispersion can also cause wavelength-dependent propagation speed of signal pulses and constitutes a major type of linear impairments for waves propagating inside SMFs.

For SMFs, the spatial propagation of waves inside SMFs are a harmonic function of longitudinal distance. The spatial frequency of the harmonic function is the propagation constant or the wave vector, represented in most literature by $\beta(\omega)$. The electric field denoted by $E(x, y, z, t)$, as a solution of the wave propagation along the fibre can be decomposed into

$$E(x, y, z, t) = A(t)F(x, y)\exp(i(\beta z - \omega t)). \tag{2.3}$$

The assumptions made in deriving this equation include slow varying envelopes of rapidly varying waves and a longitudinally invariant transverse mode. The spatial and temporal dependence of the longitudinally propagating waves can therefore be factored out, leaving a complex amplitude $A(t)$ to describe the feature of wave propagation such as the modulated information. Since the propagation constant is a function of frequency, $\beta(\omega)$ can be expanded in Taylor series with respect to a reference angular frequency ω_0. The Taylor series is given by

$$\beta(\omega) = \beta_0 + \beta_1(\omega - \omega_0) + \frac{\beta_2}{2!}(\omega - \omega_0)^2 + \frac{\beta_3}{3!}(\omega - \omega_0)^3 + \frac{\beta_4}{4!}(\omega - \omega_0)^4 + \ldots. \tag{2.4}$$

The first order derivative physically represents the time it takes for a pulse to cover a unit length, which is also the inverse of group velocity, $1/\nu_g$. Using its physical interpretation, the walk-off in time t between two pulses at ω_1 and ω_2 after travelling over distance L is given by

$$t(L) = L(\beta_1(\omega_1) - \beta_1(\omega_2)). \tag{2.5}$$

The second order derivative of the propagation constant β_2 is the GVD. It governs the wavelength dependent pulse spreading of different spectral slices of the pulse. β_2 is a function of frequency, whereas dispersion parameter D is a function of wavelength. It is defined as $d\beta_1/d\lambda$. D is more commonly available in most fibre specifications than the GVD parameter. The two parameters are related as

$$D = -\frac{\omega}{\lambda}\beta_2. \tag{2.6}$$

For standard SMFs, in the spectral range where $D < 0$, the fibre exhibits normal dispersion, In the normal dispersion regime, longer spectral components travel faster than shorter ones. In the spectral range where $D > 0$, the fibre exhibits anomalous dispersion, and longer spectral components travel slower than shorter ones.

Third order dispersion (TOD) β_3 and dispersion slope S are the next order of derivatives of GVD and D, with respect to angular frequency and wavelength, respectively. TOD and S are related as

$$\beta_3 = (\frac{\lambda^2}{2\pi c})^2(S + \frac{2}{\lambda}) \tag{2.7}$$

and

$$S = \frac{\omega}{\lambda^2}(2\beta_2 + \omega\beta_3). \tag{2.8}$$

The fourth order dispersion (FOD) and its counterpart in wavelength terms are related via the equation as follows.

$$\beta_4 = -\frac{\lambda^4}{(2\pi c)^3}(6D + 6\lambda S + \lambda^2\frac{dS}{d\lambda}) \tag{2.9}$$

FOD is an important parameter of HNLFs when designing parametric amplifiers. Usually the fibre manufacturers do not provide FOD directly, and its estimation can be drawn based on the dispersion plotted against wavelength using the relations given above. For most SMF-based transmission links, dispersion up to the fourth order is sufficient to cover most features and impairments during signal propagation.

2.3 Birefringence and PMD in SMF transmission links

Last but not least, another linear impairment that is less significant yet not completely compensable due to its stochastic nature is polarisation-mode dispersion (PMD). PMD in standard SMFs relates to the random variation of fibre birefringence with both time and distance.

Ideal isotropic SMFs allow polarisation-independent wave propagation. The state of polarisation (SOP) of the input waves does not alter during propagation. Such is not the case in reality, where internal stress builds up during the fibre drawing process and external influence such as temperature variation, bending, and stress all play a role in deforming the otherwise perfectly circularly symmetric core/cladding geometry. These factors combine causing birefringence which manifests itself in the presence along the fibre of two orthogonal polarisation axes having different refractive indices. Linearly polarised waves along the two axes exhibit different propagation speeds therefore causing walk-off effects.

The orthogonal polarisation axes retain their orientation and the refractive index difference in polarisation maintaining fibres (PMF), which are intentionally fabricated to

keep the index difference sufficiently large, on the order of 10^{-4}, to avoid polarisation mode coupling. Because of the refractive index difference, an initially linearly polarised wave launched at a finite angle between the two polarisation axes must return to its original SOP after a certain length equivalent to a 2π phase shift. This length is called the beat length, and the SOP of such waves undergoes periodic changes for each interval separated by its beat length.

This is not the case for standard SMFs where the birefringence more closely resembles a concatenation of birefringent segments whose orientation and index difference varies both with time and on a segment-by-segment basis. However, there does exist a set of polarisation axes, along which the input wave is aligned that maintains its original SOP after traversing these random birefringent segments. This set of polarisation axes are called principal states of polarisation (PSPs).

The stochastic nature of fibre birefringence manifests itself as PMD. To be specific, a wave whose spectral components split between these two axes broadens due to the first order PMD. Similar to (chromatic) dispersion, PMD is also a frequency-dependent property of fibres. Second order PMD, i.e. the first order derivative of PMD with respect to frequency, is also not negligible when considering WDM signals in SMF transmission that spread across a large BW. In this case, second order PMD causes uncorrelated polarisation drifts for spectrally separated WDM channels.

In standard SMFs, the refractive index difference between the two polarisation axes is of the order of 10^{-6}, which corresponds to a beat length of the order of one metre. Any randomly birefringent fibres including standard SMFs and non-PM HNLFs that have a length much longer than its beat length rotate the SOP of the input waves randomly, except those waves launched along one of the fibre's PSPs. In this particular case, the RMS differential group delay (DGD) between the two waves, each launched at one of the PSPs, is proportional to the square-root of the fibre length. The sub-linear dependence of standard deviation of DGD, which is the first order PMD, on the fibre length is associated with a constant coefficient for a given fibre, as given by

$$\sigma = D_p\sqrt{L}, \tag{2.10}$$

in which σ is the RMS DGD, i.e. the standard deviation of DGD, and L is the fibre length. The coefficient D_p is the PMD parameter [Agrawal (2012)], and its value indicates the strength of PMD effects of the fibre. PMD increases with the fibre length, and its stochastic nature means that there is no means to compensate for PMD completely. Together with other non-deterministic impairments, it sets the fundamental capacity limit of a SMF-based transmission system.

2.4 Stimulated scattering

Waves propagating in SMFs experience electric field strength-dependent nonlinear impairments. Light waves, especially at high intensity, interact with the dielectric material of the fibre, giving rise to these various nonlinear processes.

Third order nonlinear impairments can be broadly divided into two categories, stimulated scattering processes and Kerr nonlinearity. The first category includes stimulated Raman scattering (SRS) and stimulated Brillouin scattering (SBS). In both of the two scattering processes, a photon is scattered and reduced to a lower frequency, at the same time releasing either an optical or an acoustic phonon to conserve energy. There exists a threshold power for both types of processes, beyond which the scattered light power increases in an exponential manner. This means signals launched at sufficiently high powers may experience severe scattering impairments. The strength of SRS and SBS processes and their corresponding threshold power in standard SMFs are key parameters to examine when considering their detrimental effects in typical fibre-optic transmission systems.

The Raman gain BW in standard SMFs extends across 10 THz, the maximum gain of $6x10^{-14}$ m/W occurs at Raman shift of 13 THz for input wave at 1550 nm. The continuous Raman gain spectrum is a result of the amorphous nature of silica fibres. For standard SMFs, the threshold power for SRS is close to 1 W at 1550 nm. At this threshold power, half of the wave input power is transferred onto the SRS frequency. For fibre-optic transmission applications, signal power per channel must be kept well below this threshold power to avoid the onset of SRS. However, as Raman gain coefficient is generally much smaller than (about one third of) well phase-matched parametric gain coefficient for Kerr nonlinearity, this SRS threshold power is usually not possible to be reached before other types of nonlinear impairments start to set in.

On the contrary, the Brillouin gain BW is much smaller as a result of the relatively long damping time of the acoustic phonon involved, limited to within 100 MHz at wavelength near 1550 nm. This value varies from fibre to fibre due to the variation of core diameter. Although having a much smaller BW, the Brillouin gain coefficient is over two orders of magnitude larger than that for SRS, reaching $5x10^{-11}$ m/W for standard SMFs. This corresponds to a SBS threshold power per channel of the order of several dBm. SBS is more likely to limit the signal launch power per channel in transmission than SRS. However, this threshold power is still higher than the typical signal launch power for a fibre-optic transmission system, hardly posing any problem in practice.

Nevertheless, with proper nonlinearity compensation (NLC), the transmission system may still operate at the nonlinear regime where the signal power may exceed several dBm, which is the SBS threshold power for monochromatic waves in standard SMFs. However, the peak Brillouin gain is reduced as the signal spectrum is broadened through

phase modulation (PM), as is often the case for modulated signals in transmission, which leads to increased SBS threshold power. As a result, SBS, similar to SRS, is less severe a type of nonlinear impairment in transmission, especially compared to Kerr nonlinearity, which will be discussed in the next section.

2.5 Kerr nonlinearity

Dielectric materials such as silica in standard SMFs react to applied electric field by creating electric dipole moment through oscillating electron displacement. The induced polarisation is related to the electric field through the power series of a susceptibility tensor χ, as given by

$$P = \epsilon_0(\chi^{(1)} \cdot \mathbf{E} + \chi^{(2)} : \mathbf{EE} + \chi^{(3)} \vdots \mathbf{EEE} + \cdots), \tag{2.11}$$

in which ϵ_0 denotes the vacuum permittivity, $\mathbf{E}$ represents the electric field vector applied to the dielectric medium, and χ is the susceptibility tensor expanded in its power series with a superscript indicating its order.

The first-order linear susceptibility $\chi^{(1)}$ is dominant in strength, and its effects are mainly included in the linear refractive index and the loss coefficient. Silica is a material exhibiting inversion symmetry at the molecular level, therefore the second-order nonlinear susceptibility $\chi^{(2)}$ is zero in silica SMFs. In materials that lack the inversion symmetry property such as Lithium Niobate, $\chi^{(2)}$ accounts for the nonlinear Pockels effect including second harmonic generation (SHG), difference frequency generation (DFG), etc. all of which are absent in silica SMFs.

In silica SMFs, the third-order susceptibility $\chi^{(3)}$ is the lowest order nonlinear susceptibility, responsible for Kerr nonlinear effects such as self-phase modulation (SPM), cross-phase modulation (XPM), and four-wave mixing (FWM). Other third order nonlinear effects namely third harmonic generation (THG) and sum frequency generation (SFG) are rarely phase-matched, hence not going to be discussed.

The real parts of the susceptibility tensors encompass the refractive index contributions to the induced polarisation. The third order nonlinearity manifests itself through a modification to the linear refractive index, as given by

$$n = n_0 + n_2|E|^2, \tag{2.12}$$

in which, n_0 is the linear part of the refractive index of silica, and n_2 is the nonlinear index coefficient stemming from the third order nonlinearity. Note the absence of linear dependence of the overall refractive index on the electric field, n_1, in silica SMFs.

The imaginary part of the susceptibility tensors gives rise to absorptive effects. The linear absorption has been mentioned in the section on attenuation, while the third order nonlinear absorption gives rise to phenomena such as two photon absorption (TPA), an effect whose strength is proportional to the square of the field intensity and much less significant than that for linear absorption for silica materials. TPA is often ignored when studying silica SMFs.

2.5.1 Self-phase modulation

Since the propagation constant is a function of the refractive index, the phase shift is not only a function of distance and time but becomes also power dependent due to the third order nonlinearity. This power induced phase shift of the wave itself is called self-phase modulation (SPM). The additional phase shift of the propagating wave itself is given by

$$\phi_{\mathrm{NL}} = \gamma P L_{\mathrm{eff}}. \tag{2.13}$$

The nonlinear phase shift due to SPM is proportional to the effective length of the fibre, $L_{\mathrm{eff}} = (1 - \exp(-\alpha L))/(1 - \alpha)$, the signal power, and the nonlinear coefficient which is normally represented by γ and defined as

$$\gamma = \frac{\omega n_2}{c A_{\mathrm{eff}}} \tag{2.14}$$

The effective mode area Aeff is πw^2 if the wave mode is Gaussian and w represents the mode radius. Unlike the nonlinear index coefficient n_2 that is the same for all silica materials, nonlinear coefficient accounts for the waveguide impact on nonlinear effects by including the effective mode area of the fibre into its expression. It can often be assumed that the nonlinear coefficient γ is frequency-independent if the waves involved are closely spaced in the spectrum.

Nonlinear effects are useful in some applications. According to Equation 2.13, increasing the strength of nonlinear effects requires a fibre having an increased nonlinear index coefficient and a reduced effective mode area. These two approaches are found in the designs of most highly nonlinear devices. Nonlinear materials, such as Chalcogenide, Tellurite, Bismuth oxide, etc., are developed aiming to increase n_2. Fibre structures such as small-core silica HNLFs and tapered fibres are developed to decrease A_{eff}. On the contrary, fibres used in transmission links need to have minimal nonlinear effects. Fibre designs aiming to reduce nonlinearity often choose to have an increased effective mode area [Zhou et al. (2009)].

2.5.2 Cross-phase modulation

Waves co-propagating with the reference wave can also induce nonlinear refractive index changes that give rise to a nonlinear phase shift of the reference wave. This effect is called cross-phase modulation (XPM). Its physical mechanism is similar to SPM but its magnitude is twice as large as that for SPM. The nonlinear phase shift of one wave $\phi_{1,\mathrm{NL}}$ due to both SPM and XPM when two waves co-propagate is given by

$$\phi_{1,\mathrm{NL}} = \gamma(P_1 + 2P_2)L_{\mathrm{eff}} \tag{2.15}$$

For the cases that have more than two waves,

$$\phi_{i,\mathrm{NL}} = \gamma(P_i + 2\sum_{j\neq i} P_j)L_{\mathrm{eff}} \tag{2.16}$$

Where i represents the ith wave, and L_{eff} is defined following Equation 2.13.

2.5.3 Four-wave mixing

The nonlinear polarisation P_{NL} induced by the presence of strong electric fields in silica fibres is a function of the cube of the applied electric fields as given by the third order susceptibility term $\chi^{(3)}$ in Equation 2.11. In the presence of N non-degenerate monochromatic waves, the total number of generated mixing terms are $4N^3$. New frequency components are generated in this process, although a large number of these terms coincide in their frequencies. As a nonlinear $\chi^{(3)}$ process having a maximum four interacting waves, these processes are therefore called four-wave mixing (FWM).

From a quantum mechanical point of view, FWM can be interpreted as a process in which one or two waves donate two photons that combine and split into two new photons. According to the energy conservation principle, as for example in a non-degenerate FWM configuration, which will be introduced in the next chapter, the frequencies of the four photons involved are related as

$$\omega_1 + \omega_2 = \omega_3 + \omega_4 \tag{2.17}$$

According to the momentum conservation principle, the propagation constants of the four waves are related as

$$\beta_1 + \beta_2 = \beta_3 + \beta_4 \tag{2.18}$$

The concept of phase matching thus stems from this propagation constant relations. A measure of the degree of phase-mismatch is given by

$$\Delta\beta = \beta_3 + \beta_4 - \beta_1 - \beta_2 \tag{2.19}$$

Minimising the phase mismatch offers optimal efficiency for FWM processes.

FWM effects are detrimental in WDM transmission applications. In most WDM applications, the channel spacing is uniform, which makes FWM between closely located (therefore, possibly well phase-matched) channels fall onto other nearby channels in the spectrum, contaminating their encoded information by reducing the OSNR. New spurious frequency waves can also stem from these FWM interactions, further reducing the signal quality. For overlapping pulses in the same channel, intra-channel FWM can take place among these overlapping pulses or among their modulation sidebands in transmission, thus creating ghost pulses in empty bit slots.

Typical measures to avoid excessive FWM impairments include maintaining finite local dispersion, using no inline dispersion-compensating fibres (DCFs), etc. A finite local dispersion discourages FWM interference by introducing phase mismatch, so FWM efficiency can be effectively reduced. Inline DCFs periodically compress the pulse width, which keeps a higher average pulse power along the link, thus resulting in more severe nonlinear impairments. Removing inline DCFs and using digital or optical pre- or post- dispersion compensation can reduce the average pulse power and help prevent the build-up of nonlinear impairments including that from FWM.

While in transmission FWM is seen as the a detrimental impairment that the link designers invest efforts to avoid and mitigate, FWM processes can also be used constructively in applications of optical signal processing, which in turn can be used to mitigate nonlinear impairments in the link. The positive use of this parametric process is discussed in the next Chapter 3.

2.6 Wave propagation models

The wave propagation equation [Agrawal (2012)] is derived from Maxwell's differential equations and given by

$$\nabla^2 E - \frac{1}{c^2}\frac{\partial^2 E}{t^2} = \mu_0 \frac{\partial^2 P_{\mathrm{L}}}{t^2} + \frac{\partial^2 P_{\mathrm{NL}}}{t^2}, \tag{2.20}$$

in which the polarisation terms have been given in Equation 2.11, c is the speed of light, and μ_0 is the vacuum permeability. In this wave propagation equation, the nonlinear polarisation is treated as a perturbation to the linear polarisation term, which remains valid as long as the nonlinear effects are comparatively small. For silica SMFs, the linear and nonlinear induced polarisation are related to the first and third susceptibility tensors, respectively. The solution of this equation has been given in Equation 2.3, with the assumption of a slowly varying envelope.

The well-known scalar nonlinear Schrödinger equation (NLSE) can be derived from the wave propagation equation assuming that 1) all waves are linearly polarised along the

same SOP and that 2) GVD and TOD are sufficient to describe the dispersion among all spectral components of the wave. The derivation can be found readily in literature [Agrawal (2012)] [Marhic (2007)]. The NSLE is normally given by

$$\frac{\partial A}{\partial z} = -\frac{\alpha}{2}A - \frac{i}{2}\beta_2\frac{\partial^2 A}{\partial T^2} + \frac{1}{6}\beta_3\frac{\partial^3 A}{\partial T^3} + i\gamma|A|^2 A. \tag{2.21}$$

A is the complex amplitude of the electric field, α is the loss coefficient, β_2 and β_3 are the GVD and TOD parameters, γ is the nonlinear coefficient, and T is the moving time frame at group velocity. The terms on the right hand side of the NLSE represent loss, GVD, TOD, and Kerr nonlinearity, respectively. The contribution of each term to the evolution of the waves is clearly separated in the equation. The physical meanings of all terms are intuitively understood.

The length scales of the link determines the choice of the wave propagation model. Maxwell's equations are valid from the order of the diameter of fibre cores and the light wavelength, hence applicable to the analysis of the more fundamental wave propagation dynamics in fibres. The more commonly used scalar NLSE applies to a fibre length scale shorter than that associated with PMD impairments and longer than that where the slowly varying envelope assumption holds true.

For a length scale much larger than the typical silica fibres' birefringence correlation length of the order of 100 m, the random varying birefringence is averaged out and the scalar Manakov-PMD equation is thus a more practical model to estimate the wave propagation in silica SMFs. The Manakov-PMD equation is given by [Reimer et al. (2012)]

$$\frac{\partial \mathbf{A}}{\partial z} = -\frac{\alpha}{2}\mathbf{A} - \frac{i}{2}\beta_2\frac{\partial^2 \mathbf{A}}{\partial T^2} + \frac{1}{6}\beta_3\frac{\partial^3 \mathbf{A}}{\partial T^3} - \frac{1}{2}(\mathbf{b}\cdot\boldsymbol{\sigma})\frac{\partial \mathbf{A}}{T} + i\gamma|\mathbf{A}|^2\mathbf{A}. \tag{2.22}$$

The symbols have the same meanings as for the NLSE in Equation 2.21. $\mathbf{A}$ is the Jones vector of the complex amplitude of the electric filed, $\boldsymbol{\sigma}$ is the Pauli spin matrices, $\mathbf{b}$ denotes random varying PMD, and defined as in $E(\mathbf{b}(z_1)\cdot\mathbf{b}(z_2)) = D_p^2\delta(z_2 - z_1)$. $E(\cdot)$ is the expectation operator, D_p is the PMD parameter, and $\delta(\cdot)$ is the Dirac delta function. In the equation, the terms on the right hand side represent the effects of loss, GVD, TOD, linear PMD, and the Kerr nonlinearity, respectively. The nonlinear coefficient γ is multiplied by an 8/9 factor in the Kerr nonlinearity term to take into account the averaging effect of randomly varying birefringence on the strength of nonlinearity. When the linear PMD can be neglected, a scalar version of the Manakov-PMD equation, i.e. Manakov equation, can be obtained by removing the linear PMD term and substituting A with its scalar counterpart.

Manakov-PMD equation can cope with any SOP of interacting waves by taking into account both polarisation components of the waves. It can be used to derive and analyse the pattern and outputs of wave propagation in SMFs using numerical simulation methods such as split-step Fourier method (SSFM) [Agrawal (2012)].

2.7 Summary

This chapter introduces the theoretical background on the major transmission impairments, both linear and nonlinear, for signal propagation in SMF links. The chapter begins with introducing linear impairments, which are loss, dispersion, and PMD. It then moves on to describe third order nonlinear effects, namely SRS, SBS, and Kerr nonlinearity. It concludes by presenting three models for wave propagation in fibres taking into account of all these types of impairments. They are NLSE, Manakov-PMD, and Manakov equation, each suiting a different scenario. Numerical simulation using these models can predict the effects of the impairments on signal propagation. This chapter identifies practical issues for SMF transmission systems, with an emphasis on Kerr nonlinear impairments. Their potential solutions, by, for instance, OPC, will be discussed in the following chapters.

Chapter 3

Background on fibre optical parametric amplifiers

Fibre optical parametric amplifiers (FOPAs) make use of ultra-fast parametric processes for amplification and wavelength conversion of the signals. This chapter discusses only the phase-insensitive FOPAs where no idler is present at the fibre input. Similar to other phase-insensitive optical amplifiers such as EDFAs, FOPAs exhibit a quantum limited noise figure (NF) of 3 dB [Marhic et al. (2014)]. However, compared to phase-sensitive amplifiers that require strict phase relations among all interacting waves, phase-insensitive FOPAs offer robust, flexible, BW efficient solutions when used as inline amplifiers or NLC devices. This chapter introduces essential theoretical background on the understanding, design, and implementation of FOPAs that will be used for NLC in fibre-optic transmission systems.

3.1 Four-wave mixing in fibre optical parametric amplifiers

FWM is a parametric process that can take place in $\chi^{(3)}$ materials such as silica-based fibres as has been introduced in Chapter 2. In fibre-optic transmission systems, since it may cause inter-channel crosstalk and parametrically amplified noise in transmission, it is treated as a detrimental effect that needs to be eliminated or mitigated. However, FWM used in fibre optical parametric amplifiers (FOPAs) can be exploited for purposes such as wavelength conversion, optical switching, optical phase conjugation (OPC), etc. In this chapter, the positive usage of FWM is discussed, in the form of FOPAs. Their properties and characteristics are introduced in the theoretical background, leading to their use in the applications of OPC, which is in turn used to counter Kerr nonlinearity itself that impairs the signal quality in the link. FOPAs are based on specific types of FWM processes that are categorised based on the frequency degeneracy of the interacting waves, as illustrated in Figure 3.1. The common features of these FWM processes are 1)

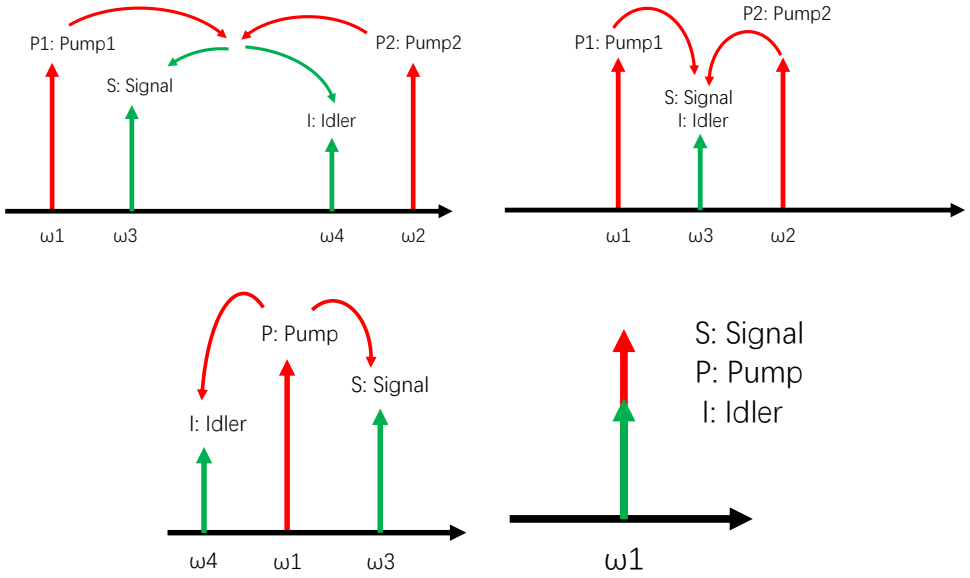

FIGURE 3.1: Schematics of different types of FWM processes; (top left) Non-degenerate FWM, (top right) signal-degenerate FWM, (bottom left) pump-degenerate FWM, (bottom right) fully degenerate FWM

the equally powered pumps that allow symmetric gain profiles and 2) a large pump-signal power ratio to avoid pump depletion and gain saturation.

1. If all four input waves are distinct in terms of their frequencies, the FWM process is non-degenerate.
2. If the signal and idler coincide in their frequencies, the FWM process is signal-degenerate.
3. If the two pumps coincide in their frequencies, the FWM process is pump-degenerate.
4. If the pumps and the signal share the same frequency, the FWM process is fully degenerate.

FOPA based on signal-degenerate and fully degenerate FWM processes usually require interferometric structures to extract the idler from its frequency-degenerate signal or/and pumps, and they are not used in this thesis. Only FOPAs that are based on the first two types of FWM processes are used, and they will be called hereafter dual-pump FOPA (2p-FOPA) and single-pump FOPA (1p-FOPA), respectively.

Since the maximum gain, gain bandwidth, gain profile, etc. are subtly different for these two types of FOPAs, an emphasis is made on 2p-FOPAs in the following discussions as they are the types of FOPAs that will be used in the experimental works.

In a 2p-FOPA configuration, there are three distinct types of first-order FWM processes taking place [Rancaño et al. (2013)]. They are denoted as phase conjugate (PC), Bragg

scattering (BS), and modulation instability (MI). The corresponding frequencies for these three processes are labelled in Figure 3.2. PC, as the phase conjugated copy of the signal, is the useful process for most 2p-FOPA applications, especially those for OPC. BS is a process in which the idler power is directly transferred from the signal rather than from the pumps, and no amplification is involved [Mechin et al. (2006)]. MI is a pump-degenerate FWM process. Similar to BS, MI does not involve phase conjugation. Therefore, BS and MI are treated as a possible cause for interference in 2p-FOPA configuration when it is used for OPC.

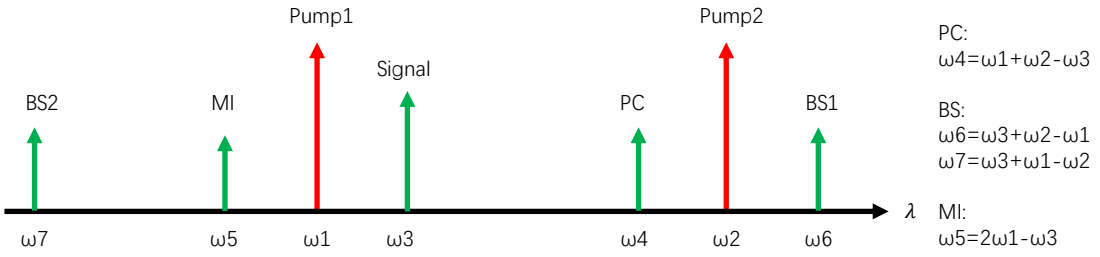

FIGURE 3.2: PC, BS, and MI terms for a 2p-FOPA

3.2 Phase-matching, conversion efficiency, and bandwidth

Derived from the wave equation in equation Equation 2.20, a set of coupled equations for 2p-FOPAs are given by [Agrawal (2012)]

$$A_1(z) = A_1(0)\exp(i\gamma(P_1+2P_2)z) \tag{3.1}$$

$$A_2(z) = A_2(0)\exp(i\gamma(P_2+2P_1)z) \tag{3.2}$$

$$\frac{dA_3(z)}{dz} = 2i\gamma((P_1+P_2)A_3 + A_1(0)A_2(0)\exp(-i\theta)A_4^*(z)) \tag{3.3}$$

$$\frac{dA_4^*(z)}{dz} = -2i\gamma((P_1+P_2)A_4^* + A_1^*(0)A_2^*(0)\exp(-i\theta)A_3(z)) \tag{3.4}$$

This set of equations are derived assuming 1) slowly varying envelopes, 2) a frequency-independent nonlinear coefficient γ, and 3) un-depleted pump power. A_i represents the ith normalised complex amplitude of the waves whose square directly equates to the wave's optical power P_i. The spatial mode distribution and time varying components of the complex amplitude $E(r,t)$ have been factored out of the expression, as $E(r,t) = A(t)F(x,y)\exp(i(\beta z - \omega t))$. The effects of integration of the spatial mode distribution $F(x,y)$ is included in the nonlinear coefficient γ. The terms on the right hand side of the last two equations in Equation 3.4 represent XPM-induced frequency shift of the signal and idler due to the two pumps and the FWM among the four waves. The SPM and XPM due to the signal and idler are neglected as a result of the assumption of the un-depleted pump power. If the effects of pump XPM are factored out of the complex amplitude expressions of the signal and idler, $B(z) = A(z)\exp(-2i\gamma(P_1+P_2)z)$. The

expressions for the evolution of the signal and idler then become

$$\frac{dB_3(z)}{dz} = 2i\gamma A_1(0)A_2(0)\exp(-i\kappa z)B_4^*(z) \tag{3.5}$$

$$\frac{dB_4^*(z)}{dz} = -2i\gamma A_1^*(0)A_2^*(0)\exp(i\kappa z)B_3(z) \tag{3.6}$$

The terms on the right hand side of the equations represent FWM processes among the four waves, in which the phase mismatch term is $\kappa = \Delta\beta + \Delta\beta_{\mathrm{NL}}$. $\Delta\beta$ and $\Delta\beta_{\mathrm{NL}}$ account for the linear and nonlinear phase mismatch terms, respectively, and are given by

$$\Delta\beta = \beta_3 + \beta_4 - \beta_1 - \beta_2 \tag{3.7}$$

$$\Delta\beta_{\mathrm{NL}} = \gamma(P_1 + P_2) \tag{3.8}$$

The conversion efficiency (CE) is defined in order to help evaluate the FOPA performance. CE is the ratio of idler output power to the signal input power, $P_4(L)/P_3(0)$. If the signal gain is unity or below, the signal input power can be approximated to the signal output power, hence the CE is directly measurable from the spectra as shown in Figure 3.3. For OPC applications, it is acceptable for the CE not to be larger than

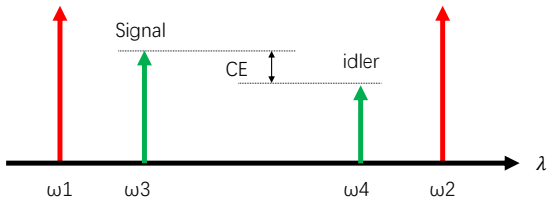

FIGURE 3.3: Definition of CE in a 2p-FOPA

0 dB. However, a lower or negative CE requires conventional amplification at the pre- or post-OPC stages and also reduces the idler OSNR, hence degrading the quality of the signal after OPC. This will be discussed in detail in the experimental chapters.

The approximate analytical expression for the idler CE is derived following Equation 3.6 [Marhic (2007)]. In 2p-FOPA configuration with an ideally lossless HNLF and sufficiently small signal powers, i.e. no pump depletion, the idler CE, G_4, can be expressed as follows

$$G_4(z) = P_4(z)/P_3(0) = |\frac{r}{g}\sinh(gz)|^2. \tag{3.9}$$

Note that the power gained by the signal and idler is identical so that

$$G_3(z) = P_3(z)/P_3(0) = G_4(z) + 1. \tag{3.10}$$

The signal gain and idler CE increase initially as z^2, and after a distance such that $gz \gg 1$, they increase exponentially. The parametric gain coefficient g is related to the

total mismatch and its maximum value as

$$g^2 = r^2 - (\kappa/2)^2 \tag{3.11}$$

$$r = g_{\max} = 2\gamma\sqrt{P_1 P_2} = \gamma P_0 \tag{3.12}$$

$$P_0 = P_1 + P_2 \tag{3.13}$$

κ is the total phase-mismatch as defined previously, and it reduces the parametric gain from its maximum possible value r.

Moreover, the linear contribution to the total phase mismatch in equation Equation 3.8 can be further expressed as

$$\Delta\beta = 2[\beta_{\text{even}}(\Delta\omega_s) - \beta_{\text{even}}(\Delta\omega_p)], \tag{3.14}$$

in which

$$\beta_{\text{even}}(\Delta\omega) = \sum_{m=0}^{\infty} \frac{\beta_{2m}}{2m!}(\Delta\omega)^{2m} \tag{3.15}$$

$$\omega_c = (\omega_1 + \omega_2)/2 \tag{3.16}$$

$$\Delta\omega_s = \omega_3 - \omega_c \tag{3.17}$$

$$\Delta\omega_p = \omega_2 - \omega_c = \omega_c - \omega_1 \tag{3.18}$$

$\Delta\omega_s$ and $\Delta\omega_p$ are the signal and pump detuning from the centre frequency, respectively. The subscript even indicates the remaining terms contain only even order dispersions, with the odd order dispersion terms cancelled in the subtraction in Equation 3.14. Note that the Taylor-expansion of the propagation constant, β is centred at the average frequency of the two pumps.

In most HNLFs and within typical operating BW of a FOPA, it is sufficient to take into account dispersion up to the fourth order. In this particular case, the linear phase mismatch is reduced to the following expression:

$$\Delta\beta = \beta_2(\Delta\omega_s^2 - \Delta\omega_p^2) + \frac{\beta_4}{12}(\Delta\omega_s^4 - \Delta\omega_p^4) \tag{3.19}$$

This expression can be used to design and achieve the phase-matching conditions. For example, if the pumps are placed symmetrically about the zero-dispersion wavelength (ZDW) of the HNLF, the GVD term vanishes. Hence, the linear phase mismatch is proportional to β_4. To achieve total phase-matching taking into account its nonlinear contribution , the terms containing β_4 need to be negative in order to balance the always positive nonlinear phase-mismatch contribution. Therefore, HNLFs with $\beta_4 > 0$ at ZDW is often the choice in 2p-FOPA designs to achieve a flat gain spectrum with a large gain BW that can reach the order of 100 nm [Radic et al. (2003)]. Combining theoretical

predictions with experimental adjustments, the pump placement for well-phase matched FWM processes can be determined.

In summary, designing and achieving a wide range of phase-matched FWM processes for signals across the range between the two pumps offers a FOPA relative flat signal gains and idler CE. Compared to 1p-FOPAs, pump detuning as the extra variable in the phase-matching expression provides an extra dimension to adjust the gain spectrum. The flatness of the gain and conversion spectrum is crucial to the uniformity of idler outputs for wideband WDM signals. This is precisely the reason why 2p-FOPAs are more favourable than 1p-FOPAs for OPC applications.

3.3 FOPA based on weakly birefringent fibres

Single-mode fibres can be classified according to their birefringent properties. They can be ideally isotropic, which only exists in theory. They can be highly birefringent, which is a feature of PM fibres that make use of an intentionally designed large DGD to avoid coherent mode coupling. The fibres can also be weakly birefringent exhibiting random signal SOP variations both in longitudinal distance and in time. This is a common feature of standard SMFs that are used in most deployed transmission links.

The randomness of birefringence of SMFs is related to both internal and external factors. In a real-world scenario, the imperfection on the cylindrical symmetry of the fibre core and the built-in asymmetric stress and strain on it prevent the fibre from being isotropic. External factors including lateral stress, bending, and twisting also add to a variation of the birefringence. As these external factors are influenced by environmental changes that vary with time, the time variation of fibre birefringence can therefore be attributed to them.

The time scale of birefringence variation ranges from the order of milliseconds due to acoustic vibration to over weeks due to seasonal temperature changes. It can be modelled by a concatenation of a random number of fibre segments, each having a random length and a random strength and direction of birefringence. Therefore, the overall DGD and PSP also vary with time. This randomisation of SOPs of the interacting waves induces PMD, which accounts for the dispersion due to random frequency-dependent polarisation drift with distance and time.

Provided that the fibre is much longer than the coherence length of the birefringence, which is defined as the length over which the SOPs of two frequency-separated waves remain correlated, its effects can be averaged out. The coherence length is usually of the order of ten metres for a typical D_p value of $0.1\,\mathrm{ps}/\sqrt{\mathrm{km}}$, so a typical 100 m Ge-doped silica HNLF is sufficiently long such that PMD can be considered to be averaged out

with a constant multiplicative modifier adjusting the nonlinear coefficient in the NLSE, thereby modifying the nonlinear interaction strength as a result of PMD.

The signal arrangement for a 2p-FOPA with linearly and orthogonally polarised pumps is illustrated in Figure 3.4. The figure shows a PC signal band having three channels between two orthogonally polarised pumps. The spectral inversion of the PC process is reflected by the reversal of the channel order indicated by their colour in the figure. The signals are decomposed into polarisation components along either of the pumps. The corresponding idlers are generated with their polarisation components orthogonal to those of the signals. Upon their recombination, the SOPs of the idlers are formed. Note that in this process, the change in signal SOPs only alters the power ratio between the two polarisation components of the idlers, without having an impact on the combined idler power. This makes 2p-FOPAs with orthogonally polarised pumps insensitive to the SOPs of the signals, however, at the expense of a reduced nonlinear interaction strength by a well-known 1/3 modifier on the nonlinear coefficient. [Marhic (2007)]. For the situation where the fibre is weakly birefringent with random variation in both

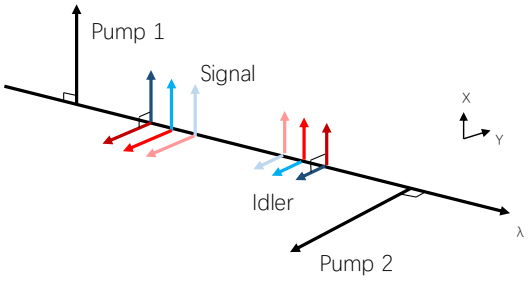

FIGURE 3.4: Orthogonally polarised 2p-FOPA

distance and time and the fibre length is much longer than the coherence length, the nonlinear coefficient for co-polarised pumps is modified by a factor of 8/9 to account for the averaged PMD effect, and a factor of 4/9 for orthogonally polarised pumps. Therefore, in weakly birefringent fibres the nonlinear interaction strength is actually increased by one third from 1/3 to 4/9 relative to the case of an isotropic fibre , which enhances the CE of orthogonally polarised 2p-FOPA and is beneficial for applications such as in a signal polarisation-insensitive OPC device.

The SOPs of the interacting waves in the 2p-FOPAs that have been considered so far have been linear. 2p-FOPAs that have circularly and orthogonally polarised pumps (right and left circularly polarised) provide an enhanced signal gain and idler CE, by an order of magnitude, as was shown in a theoretical estimation [Lin and Agrawal (2004b)] . It would be the most desirable to use circularly polarised (CP) pumps for 2p-FOPA applications. However, CP pumps can only maintain their SOPs over typical HNLF lengths in specialty fibres such as spun fibres, of which the PSPs are CP. Similar arguments apply to elliptically polarised pumps. For simplicity and practicality, only linear SOPs of interacting waves at the input of the HNLF are considered in this thesis.

3.4 Undesired effects

3.4.1 Noise

The idler quality, hence the performance degradation introduced by the FOPA, is greatly affected by the pump quality. The pump intensity noise and pump phase noise transfer to the idler causing idler intensity and phase noise. The phase noise, such as that due to finite linewidth and intentional PM of pump lasers, are transferred to the idler via FWM manifesting itself as phase noise, whereas the amplitude noise such as the ASE noise due to the pump EDFA and the RIN of the pump laser source are transferred to the idler phase via XPM.

To provide higher pump power that is crucial to the better performance of the FOPAs, each of the pump lasers is often followed by a high power EDFA. The ASE noise of pump EDFAs inevitably gives rise to additional pump intensity and phase fluctuations. To reduce the out-of-band ASE noise hence the performance degradation, an optical BPF is often installed after each of the EDFAs. The optical BPF has to be able to handle high powers and exhibit a BW as narrow as the pump wave linewidth allows.

3.4.2 Stimulated Brillouin scattering

SBS is an inelastic $\chi^{(3)}$ nonlinear process that backscatters incident light photons launched into the HNLF and at the same time generates acoustic phonons. The coupling of the electric field of the incident light wave and the acoustic wave is through the electrostriction processes. Since a second (acoustic) wave is generated through the process, the backscattered light wave has a reduced frequency to conserve the energy and momentum. The SBS BW and frequency shift at the vicinity of 1550nm are approximately 50 MHz and 10 GHz respectively in typical silica SMFs. The SBS threshold power can be defined as the input power beyond which the rate of change of back scattered light drastically increases in an exponential manner [Agrawal (2012)]. Other definitions also exist [Mermelstein (2009)]. It sets the power limit of the input light into the fibre. Therefore, the SBS needs to be suppressed by means that may include modifying either the FOPA setup or the HNLF design to allow a high pump power, which is crucial to the FOPA performance. It is worth noting that Brillouin gain is proportional to the effective length, $L_{\text{eff}} = [1 - \exp(-\alpha L)]/\alpha$, of the fibre, so reducing the effective length of the HNLF reduces the Brillouin gain, and therefore increases the SBS threshold power. Thus, a trade-off has to be made to balance the Kerr nonlinearity strength and the onset of SBS.

Phase modulation (PM) is a commonly used mechanism to suppress SBS, which effectively increases the SBS threshold power. The pump wave is phase modulated by a

single frequency (single-tone PM), or a set of sinusoids that are harmonics of a fundamental frequency (multi-tone PM), forming frequency side peaks or a pseudo-random bit sequence (PRBS) [Anderson et al. (2015)]. The single frequency or the fundamental frequency should be set to be higher than the Brillouin gain BW. The pump power seen by SBS is then reduced by the amount that has been transferred to the side peaks, thus increasing the SBS threshold power of the initial pump wave.

Counter-phase dithering techniques are vital to avoid the unintended idler linewidth broadening transferred from the PM of the pumps via FWM for 2p-FOPA [Ho et al. (2002)], and similar techniques can also be used for 1p-FOPA [Tan et al. (2014)] [Torii and Yamashita (2003)]. Attention should also be paid to avoid introducing pump IM that would transfer to the idler becoming the unwanted idler IM. These approaches are widely used in FOPA applications. Their choice is application-specific.

PM of the pump wave does not require to physically modify the HNLF, at the expense of the cost of additional devices and the extra noise introduced into the FOPA system by these devices. On the other hand, a variety of approaches to modify the HNLF design can be used to increase the SBS threshold. These approaches include the application of a linear strain gradient along the HNLF [Gruner-Nielsen et al. (2011)], which shifts the SBS gain peak and broadens the SBS gain BW, thereby increasing the SBS threshold power. Compared to PM techniques, straining the HNLF does not require additional components and operations. The drawbacks of this approach are the modified dispersion profile and the increased PMD of the HNLF, which may impact the FOPA's performance through modification of phase-matching conditions and the introduction of PMD-induced impairments. The increase of the SBS threshold through straining may reach and surpass 6dB [Gruner-Nielsen et al. (2011)]. Applying temperature gradient along the HNLF is also a feasible approach to suppress SBS, but it involves a more complex setup modification [Hansryd et al. (2001)].

3.4.3 FWM interference

The interfering FWM terms represent the unwanted FWM products generated among the original FOPA input waves and/or their FWM products. They are also called spurious FWM terms in some literature [Callegari et al. (2004)]. Depending on the waves involved in the FWM process, the FWM interference terms fall into two categories, namely signal-signal FWM interference terms and pump-signal interference terms.

The signal-signal FWM interference terms are also called signal-signal nonlinear crosstalk [Marhic et al. (2014)]. These FWM terms are either pump-degenerate or non-degenerate according to whether it is one or two signals of the FOPA that the FWM processes are based on. The number of the signal-signal FWM interference terms, M, is of the order

of N^3, where N is the number of interacting waves, and is specifically given by

$$M_{\text{non-degenerate}} = \frac{N^3}{2} - \frac{3N^2}{2} + N \tag{3.20}$$

for non-degenerate terms and

$$M_{\text{degenerate}} = N^2 - N \tag{3.21}$$

for pump-degenerate terms [Goebel and Hanik (2008)].

The distributions of the two types of FWM terms across the signal band and their relative ratios are shown in the top two plots in Figure 3.5, which illustrate the interference terms falling onto and close to the WDM signals when the channel count is three and four, respectively. As can be seen from the example for 4-channel signals, the middle channels of a signal band suffer more nonlinear impairments in FOPAs. As the number of signal channels increases, the dominance of the number of interference terms falling onto the middle channel becomes more visible [Goebel and Hanik (2008)]. The majority of these terms are non-degenerate. These statements hold both for SMF transmission links and FOPAs. Assuming that each FWM term counted above contributes equally to the total

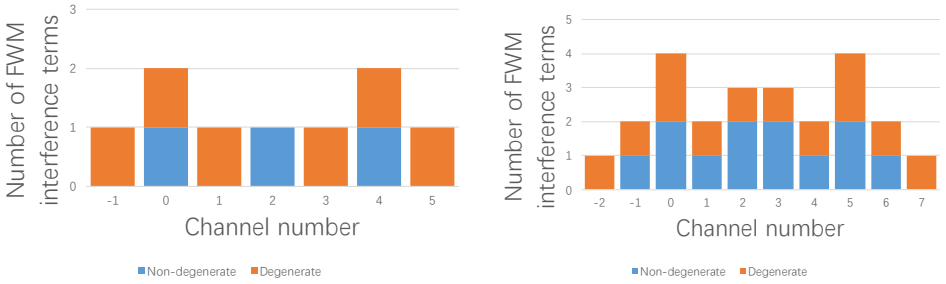

FIGURE 3.5: The numbers of signal-signal FWM interference terms for 3-channel (left) and 4-channel (right) signals

FWM interference power due to similar phase-matching conditions, the power of the signal-signal FWM interference for a single signal of interest in a 2p-FOPA is given by [Redyuk et al. (2015)].

$$P_{\text{signal-signal}}(L) = 4\gamma^2 \left(\int_0^L \sqrt{P^3_{\text{signal}}(z)} dz \right)^2 \tag{3.22}$$

In this equation, the growth rate of signal-signal interference power per channel Psignal-signal is proportional to the cube of the single signal power Psignal and the square of the HNLF length L. Therefore, given an identical CE, shortening the HNLF length and reducing the signal power reduces the absolute power of signal-signal nonlinear crosstalk.

Rather than speaking in terms of the absolute powers, the relative signal-signal crosstalk as compared to the signal power level is more relevant when considering its detrimental

impact on performance. This is given in [Marhic (2007)], assuming no loss and pump depletion for 2p-FOPAs, that

$$\frac{P_{\text{signal-signal}}}{P_{\text{signal output}}} = \frac{1}{4}\left(\frac{P_{\text{signal output}}}{P_{\text{pump input}}}\right)^2 \tag{3.23}$$

As can be seen, the relative signal-signal crosstalk is the square of the ratio of signal output power $P_{\text{signal output}}$ to pump input power $P_{\text{pump input}}$. Note that it does not depend on the signal gain, the signal input power, or the absolute pump and signal powers, of which the latter has been corroborated experimentally [Elschner et al. (2011)]. In the gain regime of a close-to-zero CE, increasing the pump-to-signal power ratio benefits the reduction of relative signal-signal FWM interference power.

The other major source of FWM interference is the pump-signal FWM interference terms. They are less detrimental to the FOPA performance provided that the signal bands are properly placed. The design of the signal band placement is discussed in the experimental chapters. However, since they involve the FOPA pump in the FWM processes, their power can be much larger than that of the signal-signal FWM interference terms assuming both are similarly phase-matched. Their relative power with respect to signal power is given by [Marhic (2007)]

$$\frac{P_{\text{pump-signal}}}{P_{\text{signal ouput}}} = \frac{4P_{\text{signal output}}}{P_{\text{pump input}}}, \tag{3.24}$$

in which the relative power of the pump-signal interference terms is seen to be proportional to the signal output power and inversely proportional to the pump input power $P_{\text{pump input}}$, regardless of the gain. Again, increasing the pump-signal power ratio reduces the impairments caused by the pump-signal FWM interference terms. A high pump power is therefore desirable to reduce pump-signal interference.

Higher order FWM interference terms and signal-noise interference have lower relative power compared the signal power level, hence being less significant. They can be ignored when considering their detrimental effects on the performance of FOPAs.

3.5 Summary

The chapter discusses the background theory, essential features, and general characteristics of FOPAs, especially the 2p-FOPAs that will be used in our experiments as the OPC device. It starts by categorising different types of FWM processes and the classification of FOPAs. It then moves on to the discussion of the key design parameters of 2p-FOPAs in order to achieve desired features and functions when used as a wideband polarisation-insensitive OPC device. The focus turns to the analysis of their major performance limiting issues, thereby providing an overview of the direction and challenges

towards the implementation of a high performance 2p-FOPA, which leads to the next chapter that discusses the use of a 2p-FOPA as the OPC device to combat nonlinear impairments in transmission systems.

Chapter 4

Background theory on mid-link OPC

In the previous chapter, the properties and functions of optical parametric amplifiers have been investigated for the specific purpose of constructing an OPC module. The primary function of an OPC module is to phase-conjugate input signals over a sufficiently large BW in an instantaneous fashion, such that the phase-conjugated BW is sufficiently large to accommodate WDM signals and the response speed of the phase conjugation is sufficiently fast to allow baud-rate transparency. Despite the fact that a noiseless OPC module only exists in theory, the optical properties of the transmission link are also a source of complicated linear and nonlinear impairments, both deterministic and stochastic in nature, which only result in their partial mitigation by mid-link OPC. The main sources of impairments that prevent ideally complete restoration of the transmitted signals are the stochastic ones, i.e. the signal-noise FWM interference and the PMD impairments [Ellis et al. (2016)].

The chapter begins with introducing various digital and optical techniques that are commonly used in research studies and commercial technologies. It then move on to identifying the origin and mechanism of these major types of nonlinear impairments. The advantages and disadvantages of various NLC techniques again these nonlinear impairments are discussed and compared. Literature survey emphasises the causes that prevent the ideally complete compensation by mid-link OPC.

After this, the ideal link conditions required by NLC by mid-link OPC are derived both intuitively and according to the NLSE. The requirement on these conditions have to be relaxed for practical links in lumped amplification SMF-based deployed transmission systems. Optimisation approaches targeting this practical scenario are also discussed.

At the end of this chapter, a general and brief review is given regarding the current research progress on mid-link OPC. The requirement for an investigation on NLC efficiency for practical employment leads to the following chapters of our experimental works.

4.1 Nonlinearity compensation techniques

4.1.1 Digital back-propagation

The propagation of waves in silica SMFs is often modelled by NLSE or its variant, the Manakov equation, which takes into account the averaging effects of random birefringence. SSFM that runs at the receiver side and back-propagates the received signals to the transmitter in a virtual link having the same parameters as the actual link can recover the transmitted signals by the effective compensation of the deterministic nonlinear impairments as well as dispersion. In principle, DBP can handle deterministic Kerr nonlinear impairments, i.e. the signal-signal inter- and intra-channel FWM interference, as long as they are within the NLC BW . The performance improvements brought about by DBP after the mitigation of signal-signal nonlinearity are ultimately limited by stochastic effects, namely signal-noise nonlinear interference [Rafique and Ellis (2011a)] and PMD impairments [Gao et al. (2012b)].

The complexity of DBP algorithms place high demand on the DSP electronics. It grows rapidly with increasing the processing BW or the number of WDM channels [Liga et al. (2014)]. Due to the complexity of commonly used DBP implementations and the processing speed associated with it, DBP application is still limited to a relatively narrow operating BW as of today, as compared to optical NLC techniques.

4.1.2 Digital and optical coherent superposition

It has been known for a long time that when a phase conjugated copy of a signal is transmitted along with it in a transmission medium, then the pair experiences correlated nonlinear impairments and, upon coherent superposition of the signal with its conjugate at the receiver, these nonlinear impairments can be undone [Liu et al. (2013)]. Additional SNR benefits as a result of the superposition operation may make coherent superposition schemes even more promising. The phase conjugated copy of the original signals can be multiplexed on an orthogonal polarisation [Olsson et al. (2015)], on alternating time slots [Eliasson et al. (2015)], or in subcarriers within the same super-channel [Yi et al. (2014)].

The inherent drawback of this simultaneous transmission of phase conjugated signals is the halving of the throughput. Unless the benefit of the improved spectral efficiency due

to the performance gain by these coherent superposition schemes outweighs the halving of throughput, coherent superposition schemes are not deemed beneficial. A balance can be struck between the performance improvement and the throughput by inserting one phase conjugated pilot for every few subcarriers [Le et al. (2015b)], making use of the fact that the nonlinear impairments of neighbouring subcarriers can be estimated by that experienced by the pilot subcarrier within certain correlation BW. The performance improvement has been shown to increase monotonically with the phase conjugated pilot overhead. Another way of utilising correlated nonlinear impairments among neighbouring subcarriers is to encode and process subcarriers simultaneously [Le et al. (2015a)], and its effectiveness has been demonstrated therein.

Phase conjugated signals can be generated in the digital domain at the transmitter side and superposed also in the digital domain at the receiver side. Similarly, they can also be generated by optical means such as parametric processes at the transmitter and superposed by a phase-sensitive amplifier (PSA) at the receiver [Olsson et al. (2012)].

An experimental attempt has been made to compare DSP-based and PSA-based coherent superposition schemes [Eliasson et al. (2014)]. In this particular experimental setting for the transmission of a single channel signal, the DSP-based solution requires higher received power for the same bit-error ratio (BER) by a margin, with no considerable difference in performance. The slight performance difference has been largely attributed to the difference in NF between EDFA that is used for DSP-based coherent superposition and PSA.

4.1.3 Mid-link OPC

Since coherent superposition schemes inevitably compromise the efficient use of the spectrum, phase conjugation performed within the link is the most attractive approach for NLC. In its simplest form, the idea of mid-link OPC is to reverse the nonlinear distortion imposed by the first half of the link so that similar nonlinear distortion experienced by the second half of the link recovers the transmitted signals. To this end, intuitively, the desirable link condition for mid-link OPC schemes is symmetry, such that the nonlinear distortion for both halves of the link is ideally the same. Mid-link OPC is therefore similar to DBP in the sense that the back-propagation is performed optically starting from the mid-link.

In generic terms, nonlinear distortion is proportional to the power involved, the link length, and the strength of nonlinear coefficient of the fibre itself, i.e. $\phi \propto \gamma L_{\text{eff}}$. In a link with fibres composed of the same material, the power and the nonlinear interaction length determine the strength of nonlinear distortion. Nonlinear FWM interference efficiency is affected by the degree of phase-mismatch, which in turn is determined by dispersion. Therefore, to achieve ideally identically distributed nonlinear distortion in

both halves of SMF-based links, the obvious approach is for the power and the accumulated dispersion to be symmetric about the OPC and the link length before and after the mid-link to be identical. These intuitive design requirements have been corroborated theoretically and experimentally [Watanabe and Shirasaki (1996)].

OPC compensation mechanism: mathematical representation and time reversal
The idea of NLC by OPC can also be interpreted based on an examination of the NLSE. Derived from Maxwell's equations by assuming a slowly varying envelope for the complex amplitude of signal waves and treating nonlinear effects as perturbations. NLSE describes the propagation of waves along fibres, covering a continuous spectrum. Its most common form is given in the following expression,

$$\frac{\partial A}{\partial z} = -\frac{\alpha}{2}A - \frac{i}{2}\beta_2\frac{\partial^2 A}{\partial T^2} + \frac{1}{6}\beta_3\frac{\partial^3 A}{\partial T^3} + i\gamma|A|^2A. \tag{4.1}$$

In which A represents the combined complex amplitude of all waves within the operating BW, and T represents the moving time frame at the group velocity of the field envelope ($T = t - \beta_1 z$). The terms on the right hand side of the NLSE relate to loss, GVD, TOD, and Kerr nonlinearity, respectively.

Taking the complex conjugate of the NLSE and after some manipulation with the signs, we get

$$\frac{\partial A^*}{\partial(-z)} = +\frac{\alpha}{2}A^* - \frac{i}{2}\beta_2\frac{\partial^2 A^*}{\partial T^2} - \frac{1}{6}\beta_3\frac{\partial^3 A^*}{\partial T^3} + i\gamma|A|^2A^*. \tag{4.2}$$

Equation 4.2 describes a backward propagating signal, which is the complex conjugate of the original one, in the same link but exhibiting a reversed power profile and a TOD that has an identical magnitude and a reversed sign. The physical interpretation of this modified NLSE then suggests that mid-link OPC is equivalent to optical back-propagation starting from the mid-point throughout the second half of the link, as opposed to the digital back-propagation technique which is performed at the receiver end tracing back the signal evolution over the entire link. Ideally, without the detrimental effects of stochastic impairments, upon arriving at the receiver, the signal's complex amplitude can be recovered in its phase-conjugated form.

According to the expression of the NLSE for OPC, the ideal link conditions can be summarised as follows.

1. a symmetric power profile about the OPC, i.e. $P(z) = P(-z)$
2. an identical even-order dispersion parameter after the OPC
3. a sign-reversed odd-order dispersion parameter after the OPC

OPC experiments in transmission systems designed based on these ideal conditions have been studied [Solis-Trapala et al. (2016), Solis-Trapala et al. (2014a)], and substantial

performance improvements have been observed. In a practical link with homogeneous constituent fibres, the third condition, requiring reversely signed odd-order disperison, is not satisfied, so it is impossible to compensate for odd-order dispersion terms by mid-link OPC. However, studies have shown that proper dispersion management can reduce the impact of TOD and higher order odd terms [Kaewplung et al. (2003)]. The comparison of the impact on NLC efficiency of mid-link OPC between transmission systems under ideal conditions and practical conditions is a recurring topic throughout the thesis. They are further discussed in respective theoretical and experimental sections.

4.1.4 Comparisons between DBP and OPC

DBP and OPC, as the representative NLC techniques for digital and optical solutions respectively, can both be interpreted as back-propagation-based techniques, whether performed digitally in a virtual transmission link or optically making use of the second half of the link to emulate the first. Under ideal conditions and neglecting stochastic impairments, both can restore dispersion- and Kerr nonlinearity-induced deterministic distortions inflicted on the signals. However, real-time processing BW for DBP is still limited by the state-of-art electronics [Galdino et al. (2017a)], such as the number of logic gates that can be crammed into a chip, the analogue-to-digital converter processing speed, and coherent receiver operating BW. Moreover, the algorithmic complexity for DBP and its variants scales superlinearly with channel count and BW [Ip (2010)], which makes full-field DBP that provides most performance improvements [Cartledge et al. (2017)] unrealistic in practice.

An advantage of DBP over OPC is that the latter makes stringent demands on the link conditions, namely the dispersion and power profile, for ideal compensation to take place, whereas DBP as a digital approach is not subject to physical constraints.

On the contrary, OPC benefits from the ultra-fast response time of parametric processes, which is on the femtosecond scale [Agrawal (2012)]. As an all-optical signal processing technique, OPC is inherently transparent to bitrate and modulation format, and compatible with WDM scenarios, which makes them increasingly beneficial for a larger number of channels compared to DBP variants. Although conflicting views exist regarding whether DBP [Rafique and Ellis (2011b)] or OPC [Ellis et al. (2015)] excels performance-wise for wideband transmission scenarios, which may depend on the case-specific conditions, the adaptability of OPC to include extra WDM channels to certain extent without additional cost and complexity is evident.

In the limit that deterministic nonlinear distortions are mostly recovered, the stochastic impairments come into play. Theoretical studies, often backed with numerical verifications, argue that OPC is advantagous as compared to DBP in its resilience to signal-noise nonlinear interference [Rafique and Ellis (2011a)], PMD impairments [Gao et al.

(2012a), McCarthy et al. (2016), Ellis et al. (2015)], and even the nonlinear evolution of transceiver noise [Galdino et al. (2017b)]. The mechanisms that result in all of these advantages relate to the halved back-propagation distance if OPC is considered as optical back-propagation from the mid-link rather than from the end of the link as for the case of DBP. Furthermore, with the use of multiple OPC schemes, these advantages are further enhanced due to the even shorter back-propagation intervals, making OPC an attractive solution both in principle and in practice to improve transmission system performance in nonlinear regime.

4.2 Nonlinear interference

Nonlinear interference in a transmission link is generally divided into three distinct categories. Signal-signal interference, signal-noise interference, noise-noise interference. Signal-signal interference stems from the SPM, XPM, and FWM among channels. Signal-noise interference involves the nonlinear interaction between channels and co-propagating ASE noise. Noise-noise interference results from the nonlinear interaction among spectral components of the ASE noise [Rafique and Ellis (2011a)]. However, in most systems the power level of noise alone is not sufficient to induce significant nonlinear interaction, so noise-noise interference is mostly neglected.

For deployed transmission systems, the OSNR requirement demands that the signal power should be significantly higher than the noise power. Therefore, signal-signal interference dominates all other types of nonlinear interference. As long as the signal-signal interference is not substantially mitigated, signal-noise interference together with noise-noise interference can be neglected.

4.2.1 Signal-signal interference

In the presence of NLC techniques, the finite NLC BW separates the nature of the signal-signal interference to within and outside this BW. In particular, if the interference originates completely outside the NLC BW, the nonlinear interference manifests itself as nonlinear interference noise (NLIN). The noise characteristics increasingly resemble that of AWGN for transmission links with lumped amplification that have a longer length and noisier link conditions [Poggiolini (2012)], so it can be treated similarly as ASE noise in most practical scenarios. For signal-signal interference that originates from within the NLC BW, it can potentially be completely compensated for by ideal NLC techniques.

The analytical expression for the relative power of the signal-signal FWM interference terms as compared to the ASE noise power and signal power for without and with mid-link OPC in a SMF-based EDFA-amplified transmission link is given in the SNR

expression as follows [Al-Khateeb et al. (2017b)].

$$\mathrm{SNR} = \frac{I_s}{NI_N + \eta\frac{3}{8}\frac{\gamma^2}{\pi\alpha|\beta_2|}I_s^3 N\alpha \sinh\left(\frac{\pi^2|\beta_2|B_w^2}{\alpha}\right)} \tag{4.3}$$

All symbols have their typical meanings as in other parts of the thesis. The residual nonlinearity $\eta = 1$ for without OPC and $\eta = 0$ for ideal NLC. The actual residual signal-signal nonlinearity for incomplete NLC by OPC is given as follows.

$$\eta = 1 - \frac{2\alpha}{\pi^2|\beta_2|B_w^2}\alpha \sinh\left(\frac{\pi^2|\beta_2|B_w^2}{\alpha}\right) \tag{4.4}$$

I_s, N, and I_N are the signal power spectral density, the number of spans, and the ASE noise power spectral density per EDFA, respectively. γ, α, and β_2 are the nonlinear coefficient, the loss coefficient, and the GVD parameter of the transmission fibre, respectively. Bw is the total BW of the signal band.

The accuracy of the analytical closed form expression is numerically and experimentally verified in studies as in [Al-Khateeb et al. (2017a)]. The expression can be used to estimate the signal-signal FWM interference power, either that falling onto existing channels or that stands alone as spurious terms. FWM interference in both of these two cases contribute to the overall performance degradation.

Since it is deterministic, neglecting the deleterious stochastic effects mainly of signal-noise interference and PMD that undermine NLC efficiency, signal-signal interference can be fully compensated for by ideal NLC schemes .

4.2.2 Signal-noise interference

Since the signal-signal interference are deterministic and at least partially compensated for by NLC techniques, the stochastic signal-noise interference then becomes one of the major limiting factors for the performance improvement by NLC. It is the result of the FWM interaction between signals and ASE noise along the link and presents a challenge for the efficiency of NLC.

Maintaining a high local dispersion is a common solution for reducing all types of FWM interference (including signal-noise interference) that require the phase-matching conditions to be satisfied [Agrawal (2012)].

For a large signal launch power, it is sometimes not sufficient to consider only the first-order signal-noise interference, but also the second-order signal-noise interference that is the FWM along the link between the signal and the first-order terms. In systems operating at the nonlinear regime, the optimal launch power is increased as a result of the mitigation of deterministic nonlinear impairments. In this case, neglecting the impact

of second or even higher order signal-noise interference may lead to overestimation of the performance as signal launch power is high [Ellis et al. (2017)].

As compared to DBP, an important benefit of mid-link OPC schemes is the interruption of the accumulation of signal-noise FWM interference. The accumulation of signal-noise interference is reversed at the mid-link where OPC is inserted. Thus, the effective length of the accumulation of signal-noise interference is halved for mid-link OPC schemes as compared to DBP.

The signal-noise interference generated by noise stemming from the transmitter can be fully compensated for by ideal mid-link OPC schemes. The signal-noise interference terms generated by the ASE noise stemming from the subsequent EDFAs in the first half of the link are, however, subject to over-compensation at the receiver , since the path lengths they take are not symmetric before and after the mid-link OPC. For this reason, DBP can be combined with mid-link OPC to improve the NLC performance. The inevitable presence of residual signal-noise interference makes mid-link OPC more beneficial in terms of NLC efficiency, as in-line NLC can effectively interrupt and reverse the accumulated signal-noise interference (and similarly the same applies to PMD). The NLC efficiency increases with the number of inline OPC modules in general, as the reversal of accumulated signal-noise interference becomes increasingly frequent. The compensation of second order signal-noise interference follows the same pattern.

The extra benefit of the dispersion compensation capability of mid-link OPC can also help reduce the power consumption for the receiver DSP by a large fraction for the current generation of DSP technology [Ellis et al. (2017)].

4.2.3 PMD impairments

PMD is another stochastic impairment in SMF transmission that contributes to the ultimate performance improvement limitation of NLC. The benefit that mid-link OPC offers as compared to DBP is better tolerance to PMD impairments in transmission. PMD randomly rotates the SOPs of signals with a frequency dependent magnitude. It is similar in its stochastic nature to signal-noise interference. However, it has been shown that PMD degrades the performance improvements offered by NLC to a larger extent than signal-noise interference [Gao et al. (2012b)]. Similarly to the interruption of the accumulation of signal-noise FWM interference, the frequency dependence of PMD-induced polarisation drift along the link becomes significant over link lengths longer than polarisation correlation length. It grows in a sub-linear fashion with the fibre length. Therefore, the PMD accumulated for the same total length is interrupted by the mid-link OPC module [McCarthy et al. (2016)], effectively increasing the PMD tolerance as compared to DBP.

4.3 OPC implementation and link conditions

4.3.1 OPC implementation

OPC in most literature is generated by parametric processes in highly nonlinear media. Parametric processes in both $\chi^{(2)}$ and $\chi^{(3)}$ materials can satisfy this purpose. The most typical $\chi^{(2)}$ nonlinear medium used for OPC experiments is PPLN [Hu et al. (2010)] [Umeki et al. (2016)]. In these experiments, phase conjugation is achieved by a cascade of SHG and DFG. The frequency difference between the signal and the second harmonic of the pump gives rise to the idler. The process is qualitatively equivalent to a third-order degenerate FWM process. PPLN-based OPC benefits from the significantly reduced signal-signal FWM interference due to their finite phase-matching BW. Third-order nonlinear effects namely SPM, XPM, and SBS are also absent from PPLN-based OPC devices [Morshed et al. (2013c)], which constitutes a significant advantage.

Common $\chi^{(3)}$ materials for OPC applications include SOAs [Anchal et al. (2016), Matsuura and Kishi (2013)], silicon waveguides [Gajda et al. (2018)] [Rong et al. (2008)], HNLFs. In an exemplary non-degenerate FWM process, the idler phase is given by

$$\phi_4 = \phi_1 + \phi_2 - \phi_3, \tag{4.5}$$

in which the ϕ_i, $i = 1, 2, 3, 4$ represent the phase of the two pumps, the signal, and the idler, respectively. The equation clearly shows the phase conjugation property of the idler. Novel waveguides such as silicon nanowire have also attracted attention due to their benefits relating to the absence of SBS, widely tuneable dispersion engineering, etc. [Vukovic et al. (2015)]. However, due to the ease of integration and dispersion engineering, among all these options, HNLFs are the most commonly used nonlinear media for generating OPC using parametric processes, if SBS can be suppressed.

4.3.2 Signal polarisation insensitivity

Signals enter the mid-link OPC module with random SOPs after traversing SMF-based links that exhibit random birefringence. Therefore, the OPC module design needs to take this into account and achieve signal polarisation insensitivity. The two commonly used methods are polarisation diversity schemes [Stephens et al. (2014), Sackey et al. (2014), Solis-Trapala et al. (2016), Ros et al. (2014)] and orthogonally polarised dual-pump FOPA configurations [Hu et al. (2016)] [Hu et al. (2016)]. Polarisation diversity schemes work with both dual-pump and single-pump FOPA configurations. They usually involve a PBS to form a Sagnac loop-like structure by splitting the input signals into two orthogonal polarisation components. These components are phase conjugated separately before being recombined in the same PBS before exiting the loop. Pump power is equally split between these two paths. The HNLF in the loop is used bi-directionally,

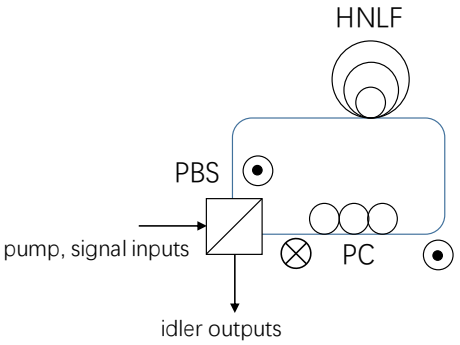

FIGURE 4.1: The polarisation diversity scheme

with two sets of FWM processes taking place inside the HNLF simultaneously from both directions. A polarisation controller is often used to adjust the SOPs of the two sets of waves such that they become orthogonally polarised until the PBS and can be combined as the output. The counter-propagation of two sets of parametric processes may degrade the idler quality due to additional nonlinear phase shift from counter-propagating pumps, Rayleigh scattering, etc. [Lei and Marhic (2014)]. To avoid the potential detrimental effects on performance, there are also works using a polarisation diversity scheme with two nonlinear media in the loop [Umeki et al. (2015)], however, at the expense of their possibly different optical properties.

Orthogonally polarised 2p-FOPAs also achieve signal polarisation insensitivity. The nonlinear interaction strength for FWM with orthogonally polarised two pumps is modified by a factor of 1/3 [Marhic (2007)], which causes reduced signal gain and idler CE . However, due to its simple form and reduced nonlinear interference power, this configuration is an attractive solution and is used in the experimental chapters of the thesis. It is discussed further as in Chapter 6.

4.3.3 Raman-assisted OPC

HNLF-based optical parametric amplifier with backward or bidirectional Raman pumping can be used to reduce the signal input power for the same idler output power [Huang et al. (2015a)], because of the distributed amplification by Raman pumping. Keeping signal input power low, relative to the pump input power, is crucial to reduce the pump-signal FWM interference power, because the pump to signal power ratio is roughly equal to the power ratio of the signal to pump-signal FWM interference. Furthermore, the signal-signal FWM interference and signal-noise FWM interference is also reduced, thus improving the idler output quality. If instead of reducing the signal input power, the benefit of increased CE can be exploited to increase the idler output power, thus achieving a higher OPC module output OSNR and improved OPC back-to-back performance [Huang et al. (2015b)]. The additional noise associated with the Raman-pumping may discourage its use.

4.3.4 Power symmetry and OPC offset

The power symmetry is critical for the performance improvement of a transmission link mid-link OPC [Rosa et al. (2015),Rosa et al. (2016)]. Minimising power asymmetry has been shown to lead to optimised performance improvements by OPC [Solis-Trapala et al. (2014b)]. Power symmetry is often implemented by distributed amplification schemes, generally based on Raman amplifiers [Solis-Trapala et al. (2016), Kaewplung and Kikuchi (2007), Rosa et al. (2015), Ellis et al. (2015)], which compensate for the link loss with improved OSNR, and also allow for tailored and optimised link power profile by tuning the Raman pump parameters.

Dispersion relates to phase-matching of the nonlinear FWM processes. The requirement by OPC on dispersion can be specified as an equal ratio of nonlinearity and dispersion at corresponding positions about the mid-link [Watanabe and Shirasaki (1996)]. TOD, and odd-order dispersion in general, is not able to be compensated for by mid-link OPC, so for ideally perfect compensation of all dispersion terms, the link fibre design may be modified to meet the requirement by inverting the sign of TOD for the second half of the link using specialty fibres [Solis-Trapala et al. (2014a)].

The place at which the OPC module is inserted into the link is also a factor that contributes to the effectiveness of dispersion and nonlinearity compensation. For single band signals, if the phase conjugated idler band is wavelength-shifted, the corresponding dispersion and phase-matching conditions also change accordingly, which makes OPC placed at a slightly offset distance about the mid-link the optimal configuration [Yu et al. (1995)]. With increased deviation of the OPC offset from the ideal position, the NLC efficiency decreases [Ros et al. (2018)].

4.3.5 Dispersion map design

For dispersion-managed (DM) links, the dispersion map design is crucial to the compensation efficiency of mid-link OPC [Wei and Plant (2004), Kaewplung et al. (2003)]. A dispersion map that is symmetric about the mid-link, i.e. the order of SMFs and DCFs are reversed after OPC, often offers better overall performance than that for keeping the same order of SMFs and DCFs [Wei and Plant (2004)]. This scaled translational symmetry (STS) dispersion map design benefits both FWM interference and XPM interference. The latter manifests itself mostly as nonlinear phase noise [Hesketh and Petropoulos (2016)].

The idea of STS is developed for both DM and DUC transmission systems in pseudo-linear regime, where the nonlinear effects can be considered as perturbations on top of the linear impairments. OPC in STS transmission systems can cancel the perturbative nonlinearity to the first order. Unlike the ideal link conditions where the power

profile is required to be mirror symmetrical about the mid-link OPC, the STS principle permits a translational symmetric power profile, naturally exhibited in EDFA-based lump-amplification schemes. The order of SMFs and DCMs that possess sign-reversed GVD parameters is desired, but not necessarily, to be mirror symmetrical about the mid-link OPC. The essence of STS is to ensure that the corresponding spans before and after phase conjugation generate nonlinearity at sign-reversed accumulated dispersion, so that the first-order nonlinear perturbation terms in corresponding fibre spans are equal in magnitude and reversed in sign. Due to their additive nature, they cancel each other, resulting in a zero net nonlinearity to the first order.

A proof-of-concept simple scenario of the application of dispersion map optimisation for practical links therefore considers simultaneously the accumulated dispersion and the corresponding power by adding pre-dispersion compensation, i.e. inserting certain lengths of DCFs before the OPC module and at the end of the link. In this way, fibre segments are arranged such that the nonlinear interaction strength matches the negatively signed accumulated dispersion at corresponding positions after OPC [Minzioni et al. (2006)]. The performance improvements by such arrangements have been verified in several other works numerically [Kumar and Liu (2007)] and experimentally [Kim et al. (2016)], in which the BER noise floor is reduced by three orders of magnitude for 13 dBm signal launch power per channel. A theoretical study has also been carried out [Ali et al. (2017)], providing the analytical expressions for signal-signal interference powers in links with both OPC and pre-dispersion compensation.

The mid-link OPC is desirable to be placed right at the middle of the link if the fibre parameters in both halves are identical. Slight offset must impact the overall performance negatively. A study in [Kim et al. (2014)] demonstrates the monotonic performance degradation with increasing offset from the mid-point. Some early work as in [McKinstrie et al. (2003)] showed numerically that the OPC should be placed at 2/3 position between the TX and RX so as to minimise nonlinear impairments, which was limited to nonlinear phase noise (NLPN) for purely phase modulated signals at the time. Though not factually invalid, the assertion concerns mainly with NLPN that is likely to be dominant in transmission links that extend over thousands of kilometres for a specific variety of signals [Minzioni (2009)]. It would shed further insight to investigate the effects of OPC positions in relation with NLC efficiency for various link conditions where different types of nonlinear effects dominate. However, as a rule of thumb, conforming either to STS principle or to ideal OPC link conditions, OPC is often expected to be placed right at the mid-point.

4.4 A summary and OPC survey

Mid-link OPC was originally proposed for the compensation of GVD alone [Yariv et al. (1979), Jopson et al. (1993)]. Its use was extended to nonlinearity compensation, SPM and SPM induced nonlinear phase noise in particular [Jansen et al. (2006)], in theoretical studies [Marhic et al. (1995)]. Experimental demonstrations [Watanabe et al. (1993)] showed the simultaneous compensation of nonlinearity and dispersion. Compensation of WDM signals was also proposed [Watanabe and Shirasaki (1996)].

As an all-optical signal processing technique based on parametric processes, OPC is independent of the modulation format of the signals. The experimental works relating to Kerr nonlinearity compensation were initially limited to unmodulated pulses [Royset et al. (1996)] and single-channel intensity modulated signals [Watanabe and Shirasaki (1996), Minzioni et al. (2006)]. Research interests soon turned to phase modulated signals and advanced modulation formats that employ both quadrature dimensions [Stephens et al. (2014), Tan et al. (2015)]. It is also applicable to systems with digital subcarrier multiplexed signals [Marti and Ramos (1997)] and spectrally efficient superchannels such as Nyquist-WDM [Schmidt-Langhorst et al. (2017)] and coherent optical-orthogonal frequency-division multiplexing (CO-OFDM) [Shoreh (2014)]. Demand of high spectral efficiency pushes the limit towards ever higher order of QAM signals, from the applications of OPC on 16 QAM signals [Morshed et al. (2013a)], a single-channel 64 QAM signal [Solis-Trapala et al. (2015)], and a single-channel 256 QAM signal [Ros et al. (2017)]. Our work pushed the boundary of ever higher order modulation formats in an OPC-assisted transmission system, demonstrating the first use at the time of 64 QAM WDM signals and 256 QAM Nyquist-WDM signals in OPC applications. A detailed discussion on these experimental work is given in Chapter 7.

OPC implemented by parametric processes can be viewed as two sides of the same effect, which are spectral inversion in the frequency domain and phase conjugation in both time and frequency domains.

$$A(t) \quad => \quad A^*(t) \tag{4.6}$$

$$\tilde{A}(\omega) \quad => \quad \tilde{A}^*(-\omega) \tag{4.7}$$

Phase conjugation is the property that one makes use of, whereas spectral inversion is the inevitable side effect. Ideally, wavelength shift-free operation on a channel basis is desirable. Some work uses signal-degenerate parametric process to generate OPC. Orthogonal SOPs are exploited to identify and seperate the signal and the idler [Schmidt-Langhorst et al. (2017)]. However, because of spectral inversion in the process of wavelength conversion by parametric processes, even with BW efficient OPC solutions to date [Sackey et al. (2018)], the wavelength of the channels within the signal band still needs to be

altered usually in a symmetric fashion. This inevitable side effect may become more undesirable in a flexible network environment, where special care needs to be taken to track the right channel of interest. Without careful design, the change of dispersion properties after the wavelength shift may also reduce NLC efficiency. One way to circumvent the issue is to carry out two wavelength-shift processes so that the signals return to their original spectrum. However, it may not be a favourable solution as the additional noise introduced by the extra OPC device reduces the signal quality, maximum number of cascadable OPC devices, achievable reach, etc.

OPC is a broad category as a means to compensate for nonlinearity inline in an all-optical manner, which does not limit its use in the mid-point of transmission links. The scaled link symmetry conditions, as has been discussed in the sections regarding dispersion map optimisation, can be exploited to offer all-optical nonlinearity precompensation solutions that involve OPC modules set up at the transmitter or the receiver, instead of being inserted inline. A theoretical fundation was built in [Watanabe and Shirasaki (1996)], and numerical simulations proved its feasibility therein. The scaling principle may be summarised as keeping identical accumulated even-order dispersion and identical nonlinearity interaction strength at any mirror-symmetric corresponding locations across the two sides of OPC. Increasing the magnitude of the even-order disperion terms and the strength of nonlinear interaction of the fibre segment before or after OPC is able to shorten this fibre segment, so that the shorter segment may be effectively modularised into a pre- or post-transmission nonlinearity compensating device. These two experimental demonstrations [Pelusi and Eggleton (2012), Pelusi (2013)] show performance gain across a large part of nonlinear transmission regime for OOK and DPSK WDM signals. This approach may be useful as long as the pre- or post-compensation modules provide an improved overall performance. In fact, the residual nonlinearity introduced by the pre- or post- compensation modules, especially that caused by the high launch power into the shortened fibre segment that usually have a small effective mode area, as compared to the case without NLC, may not overweigh the benefits it creates. Quantitatively speaking, the reach enhancement gained by the pre- or post-compensation module should be more than twice in order to justify its use. Once the issue with the extra and residual nonlinearity is overcome, it remains to be a feasible direction to go.

Under ideal conditions, mid-link OPC has been shown to improve the optimal launch power by 10 dB and the Q factor for peak performance by 5.3 dB for 4-channel 16 QAM signals in a 2000 km recirculating loop [Solis-Trapala et al. (2014a)]. The transmission fibres are tailor-made non-zero dispersion-shifted fibres (NZ-DSF) to provide oppositely signed TOD and identical GVD before and after wavelength conversion in the phase conjugation process. Loss is compensated for by distributed Raman amplification (DRA) in order to conform to the ideal symmetric power profile.

This set of experiments were supplemented [Solis-Trapala et al. (2016)] with the use of both mid-link and end-link OPC to retain the wavelength range of 4-channel signal

band within limit to emulate a 12-stage multiple OPC scheme using only two physical OPC modules. For a total transmission distance of 144 km, the 12-stage multiple OPC scheme increases the optimal launch power by 8 dB, and the peak performance in terms of Q factor is improved by 1 dB.

These two results set approximately the upper limit for the performance improvement permitted by inline OPC in a practical transmission system for similar types of transmitted signals (DP-QPSK). This has been shown to be the case in the following literature survey. Table 4.1 summarised recent works on OPC, with an emphasis on those under practical link conditions that are with EDFAs and SMFs.

Reference	Signals	Link Cdn	Distance	Q factor gain	NLT increase
Solis-Trapala et al. (2016)	DP 6x4xQPSK	DRA+NZ-DSF	144 km	1 dB	8 dB
Solis-Trapala et al. (2014a)	DP 4x16 QAM			5.3 dB	10 dB
Jansen et al. (2006)	1xDPSK	EDFA+SMF	800 km	0.9 dB	
	44xDQPSK	EDFA+SMF	10206 km	2 dB @ 7100 km	
Morshed et al. (2014)	DP 10comb x2chn x154sub x16 QAM OFDM	EDFA+SMF	800 km	0.2 dB	3 dB
Phillips et al. (2014)	DP 8xQPSK	DRA+SMF	10400 km	1 dB	4 dB
	DP 8xQPSK	EDFA+SMF	5200 km	0.4 dB	1 dB
Sackey et al. (2015)	DP 1x16QAM	EDFA+SMF(SLA)+IDF	480 km	1.8 dB	3 dB
			800 km	2.2 dB	3 dB
	DP 5x16QAM		480 km	0.7 dB	2 dB
			800 km	0.9 dB	2 dB
Vukovic et al. (2015)	3xQPSK	EDFA+SMF	800 km	0 dB	>3 dB
Umeki et al. (2016)	DP 92x16QAM NWDM	DRA+SMF	5120 km	0.4 dB	4 dB
Sackey et al. (2018)	DP 8x16QAM	EDFA+SMF	800 km	0.7 dB	1 dB
Al-Khateeb et al. (2018)	DP 8xQPSK	EDFA+SMF	3000 km	0.7 dB	2 dB
	DP 4xQPSK		3000 km	1 dB	2 dB
	DP 2xQPSK		3000 km	1.8 dB	3.5 dB

TABLE 4.1: Summary of recent OPC works for practical links in literature; NLT: nonlinear threshold, i.e. optimal launch power; IDF: inverse dispersion fibre; NZ-DSF: non-zero dispersion-shifted fibre

The majority of the works with EDFAs and SMFs have a throughput in the range between 0.1 to 1 Tbps. The Q factor improvements are mostly below 1 dB, which translate to marginal reach and spectral efficiency enhancements. A noticeable exception is the Q factor improvements of 1.8 and 2.2 dB for single-channel transmission in [Sackey et al. (2015)], in which the link is DM using inline inverse dispersion fibres (IDFs) to compensate for dispersion optically. The significantly higher performance gain by OPC may be attributed to the use of IDFs, similar to DCFs, which usually possesses a higher nonlinear coefficient than SMFs. DM links also exhibit a higher average local dispersion due to the periodic pulse compression, enhancing the detrimental nonlinear interaction efficiency. The increasingly nonlinearly impaired signals in DM links provide mid-link OPC higher potential for improving performance gain. The difference in NLC efficiency between DM and DUC links will be experimentally investigated in the thesis. The conclusions drawn from my work are mostly in agreement with the discovery from this survey.

It is also evident from this set of measurements that OPC benefits links with longer transmission distance for the same type of transmitted signals, for the power of nonlinear impairments is roughly a quadratic function of effective transmission distance [Agrawal (2012)]. The increasingly nonlinearity-inflicted signals may allow larger performance gain by OPC. The experimental chapters will discuss this issue.

Another noticeable work by [Al-Khateeb et al. (2018)] contains three sets of measurements for signal bands with three different BW. A pattern has been concluded and generalised in the paper as that increasing the BW leads to the reduction of both the performance gain and the improvement of optimal launch power by OPC. This series of works paralleled with ours. The experimental investigation of this pattern will be discussed in the following chapters of the thesis.

Direct comparisons across different works are impractical and complicated, because each work utilises distinctly different types of signals and link conditions that are generated with a variety of optoelectronic devices. However, the performance gain obtained was similar across these works. They demonstrated the potential, though relatively moderate, performance improvement by using mid-link OPC in lump-amplified SMF-based practical links. The experimental chapters of the thesis will focus on similar issues, shedding our own insight into the performance limiting factors and the characteristics of OPC-assisted transmission systems.

4.5 Conclusions

This chapter introduces the nonlinearity compensation techniques with a strong emphasis on mid-link OPC. A comparison between representative digital nonlinearity compensation techniques and OPC is given. The advantages of using OPC as an ultra-fast optical signal processing technique make it attractive especially for wideband and heterogeneous transmission scenarios where digital means find their limits. Besides deterministic nonlinear effects that can ideally be compensated by OPC and various other means, stochastic effects, be it linear or nonlinear, set the ultimate limit for nonlinearity compensation. OPC excels in this regard. The chapter continues with the implementation of OPC devices and the link conditions required to release its full potential. Fibre-based phase conjugation is the choice for the rest the thesis. The link symmetry required by OPC includes both of its power and dispersion profile. Practical link conditions compromise OPC performance gain, but scaled translational symmetry principles still offer nonlinearity compensation to the first order. This chapter ends with a general literature survey of relevant peer works that preceded and paralleled this thesis. This in turns leads to justification of the scope of the work, which is the design and investigation of real-world mid-link OPC systems.

Chapter 5

Characterisation of the transmission link

5.1 Introduction

Transmitter and link characterisation is performed in this chapter. The aim is to provide a performance framework based on which nonlinearity compensation (NLC) efficiency of mid-OPC can be compared. The various transmitters and links will be used in Chapter 7 for the OPC experiments. A few issues encountered when setting up and optimising these links are also discussed.

The chapter starts by introducing the transmitter setup for various modulation formats, including binary modulation formats and M-ary quadrature amplitude modulation (QAM) signals.

A way to generate an electro-optic-based frequency comb is introduced as a technique to emulate an array of laser sources for WDM transmission. The effect of adopting the optical comb for the generation of multiple carriers to be used in the transmitter for WDM transmission is also characterised.

Furthermore, a polarisation multiplexing (PolMux) scheme we developed to emulate dual-polarisation (DP) signal is introduced and its impact on the performance is measured.

Upon the completion of the transmitter characterisation, the subsequent link performance characterisation and optimisation is carried out in the following sections, mainly focusing on the EDFA power settings and the dispersion-compensating module (DCM) allocations.

As dispersion compensation can be moved from the optical to the digital domain after coherent detection, a performance comparison is carried out between the DM links and

dispersion-uncompensated (DUC) links, both based on the same field-installed transmission system.

Lastly, because of the gain tilt of inline EDFAs, channel power equalisation is also experimentally investigated and optimised for both DM and DUC links.

5.2 Transmitter characterisation

The performance evaluation of the signal quality at the output of the transmitter is the first crucial step of any link characterisation. Depending on the modulation format that the transmitter uses, performance metrics such as Q factors, error vector magnitude (EVM), and BER are measured.

Signals in a fibre-optic transmission link can make use of the four degrees of freedom to enlarge its information carriage. These four degrees of freedom are quadrature (in-phase and quadrature-phase), wavelength (frequency), polarisation, and time. All of these four dimensions are used in these experiments and their specific implementation is discussed in this section.

5.2.1 Generation of advanced modulation formats

The first set of experiments works with transmitters using intensity modulators and binary modulation formats. A single continuous wave (CW) laser source is modulated with an intensity modulator to generate binary signals such as on-off keying (OOK) and differential phase shift keying (DPSK) as in Figure 5.1(a). The direct detection (DD) receiver in the figure is for demodulating OOK and DPSK signals. After adding ASE noise source into this setup, BER measurements in Figure 5.2 show an OSNR of 25 dB is required to achieve a BER of 1×10^{-12}. The single CW source can also be modulated with an IQ (in-phase and quadrature-phase) modulator to generate quadrature phase shift keying (QPSK), 16 QAM, 32 QAM and 64 QAM signals as in Figure 5.1(b). In this case an arbitrary waveform generator (AWG) is used to drive the IQ modulator. A commercial optical modulation analyser (OMA) is used as the optical coherent receiver that is equipped with built-in real-time DSP algorithms. The OMA can also be used to capture signal waveforms for offline processing. The purpose of the B2B characterisation is to estimate whether the quality of signal of the transmitter is good to be sent over the proposed transmission link.

For binary modulation formats, namely on-off keying (OOK) and differential phase shift keying (DPSK), error free operation (BER $< 1 \times 10^{-13}$) is readily achieved for the B2B configuration as in Figure 5.1(a) at baud rates up to 40 GBd. For more advanced modulation formats i.e. M-ary QAM, three different baud rates are tested, namely 2.5 GBd,

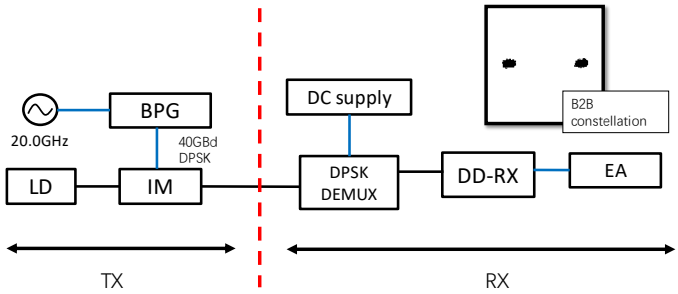

(a) Experimental setup for DPSK transmitter and receiver; inset: the constellation for a B2B DPSK signal at 40 GBd; TX and RX: transmitter and receiver; BPG: bit pattern generator; IM: intensity modulator; DD-RX direct detection receiver; EA: error analyser

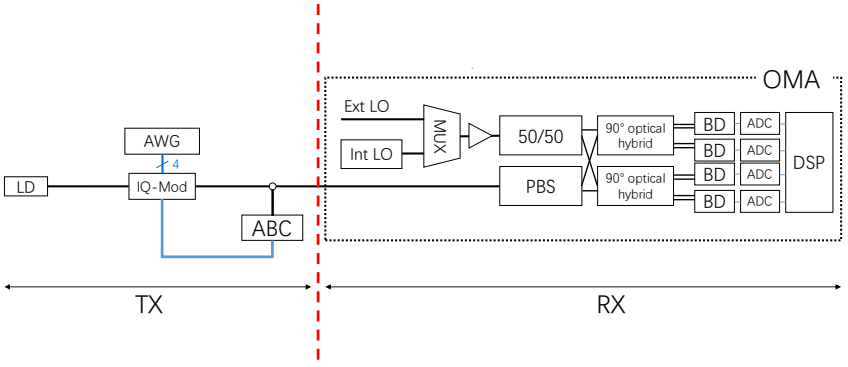

(b) Experimental setup for M-ary QAM transmitter and receiver; TX and RX: transmitter and receiver; ABC: automatic bias control; BD: balanced detector; ADC: analogue-to-digital converter

FIGURE 5.1: Basic transmitter and receiver setup

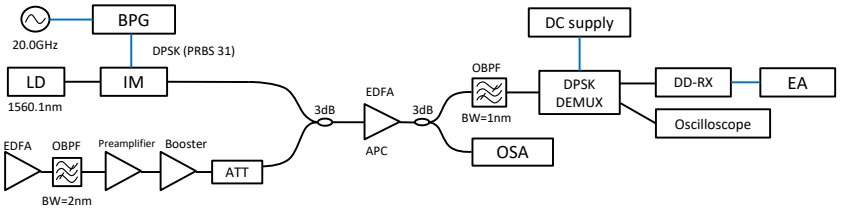

(a) The setup

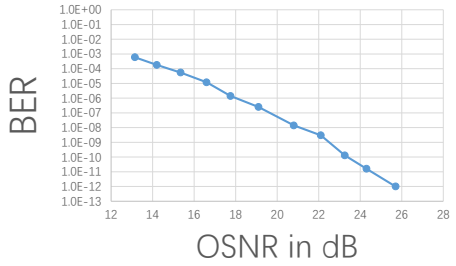

(b) BER plotted as a function of OSNR

FIGURE 5.2: BER as a function of OSNR for the B2B configuration of the DPSK transmitter in (a)

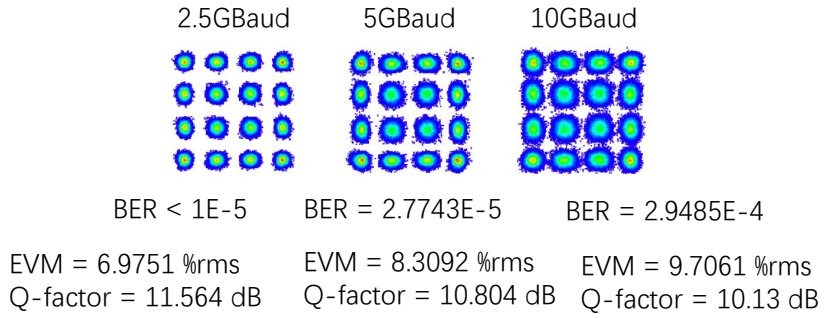

(a) 16 QAM

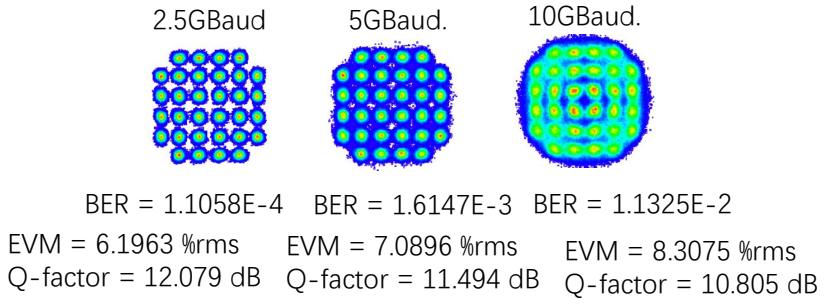

(b) 32 QAM

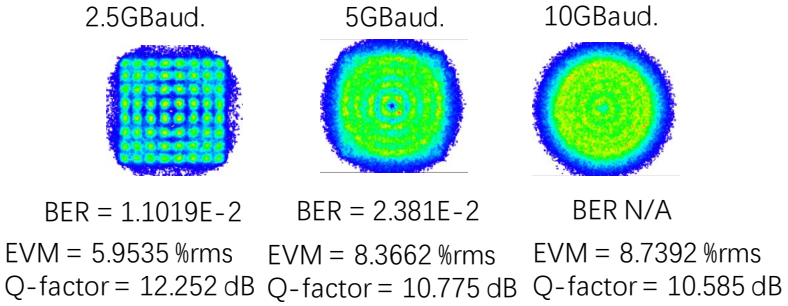

(c) 64 QAM

FIGURE 5.3: The constellations and experimental results for the B2B performance of the transmitter setup in Figure 5.1(b) for three QAM formats at three baud rates

5 GBd, and 10 GBd for the same received power of 5 dBm. As a point of reference, the BER of 1.4×10^{-4} is defined as the HD-FEC limit for hard-decision RS(255,239) FEC code for a post-FEC BER of 1×10^{-13}. As shown in Figure 5.3, not all cases for the three modulation formats surpass the HD-FEC threshold. The limitation of the signal quality of the transmitter is mainly due to the bandwidth (9.6 GHz), maximum sampling rate (24 GSa/s) and the vertical resolution of the AWG (8 bits). Typically, in our work we are interested in a comparative characterisation of different link configurations rather than the absolute received performance, and the above limitation has not been a problem for my experiments. However, it is worth noting that the performance of the transmitters used in our experiments may change the effectiveness of the technique that we proposed

in our work to mitigate the nonlinearity. In Chapter 7, this is also discussed further as part of the future work.

To overcome the limitation of the signal quality of the 16 QAM generated by the AWG, I investigated another approach to generate them. Better B2B performance is ensured starting from a QPSK signal and emulating a 16 QAM constellation by using a delay line interferometer (DLI). The corresponding operating principle is shown in Figure 5.4. A QPSK signal is split into the two arms of the DLI, the signal in one arm being delayed to decorrelate with the other and attenuated by 6 dB in power. Upon recombination, a 16 QAM signal with a equidistant constellation is generated. Clearly, this technique can only emulate rather than generate 16 QAM due to the fact that half of the information is duplicated.

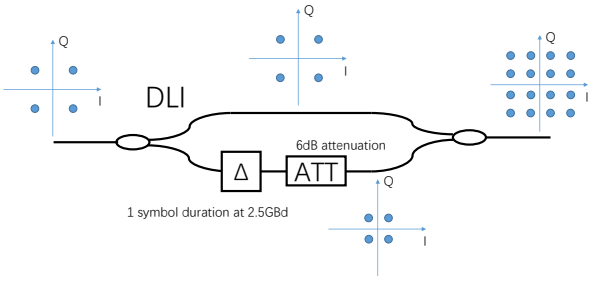

FIGURE 5.4: The principle of emulating a 16 QAM signal starting from the generation of a QPSK signal followed by a DLI; Δ is equivalent to one symbol duration at 2.5 GBd; the attenuation is 6 dB in power for emulating a 16 QAM signal with an equidistant constellation

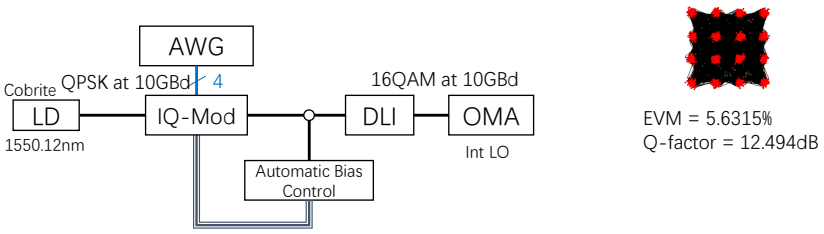

FIGURE 5.5: Performance characterisation of the emulated 16 QAM signal generated using a QPSK signal followed by a DLI

A proof-of-concept experiment is set up to verify the feasibility of the emulation of the 16 QAM signal at 10 GBd. The Q factor at the output of the transmitter is 12.5 dB (as in Figure 5.2.1), 2 dB higher than that obtained with the direct generation of the 16 QAM signal at 10 GBd. The experimental setup and the constellation is shown in Figure 5.5.

A conclusion can be drawn that the generation of 16 QAM from QPSK using the DLI method indeed improves the back-to-back performance with a maximum Q factor margin close to 2 dB, however, at the expense of data correlation to some extent. The choice between the DLI method and the direct generation method then depends on specific applications.

5.2.2 Frequency comb generation

WDM is a common multiplexing technique that utilises the wavelength dimension to increase the transmission capacity. In a WDM optical transmission system, individual CW signals that are separated in wavelength are modulated with independent information content such that the spectrum utilisation efficiency is greatly enhanced compared to a single-channel transmission. These multiple CW signals can be achieved by either an array of individual laser sources or an optical frequency comb based on a single CW source. Such a frequency comb can be generated in a number of different ways, for example by exploiting parametric processes or by using an electro-optic modulator [Torres-Company and Weiner (2013)]. Due to its simplicity, in the following experiments, the electro-optic-based approach is adopted to generate the optical comb.

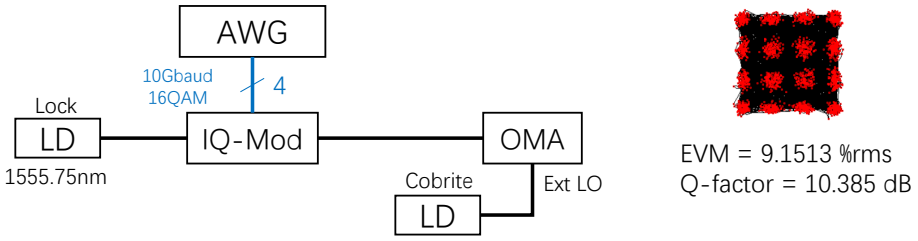

(a) Experimental setup and results for the B2B performance of a single-channel signal

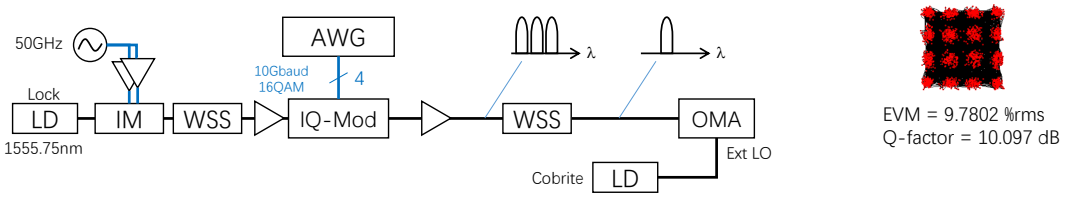

(b) Experimental setup and results for the B2B performance of 3-channel WDM signals generated using the frequency comb

FIGURE 5.6: The effect of the addition of the frequency comb module to generate WDM signals

The use of an optical comb to generate multiple carriers may have the advantage of cost reduction (only one CW source is needed instead of multiple ones) and of phase coherence among all comb lines. An example of the latter can be found in [Lundberg et al. (2017)], where the complexity of a joint carrier recovery DSP algorithm is reduced.

The linewidths of the generated new comb lines replicate that of the input master signal. Additional signal quality impairments such as the RF noise are from the synthesiser and the RF amplifiers.

In the following experiment I report a comparison of the performance of the signal before and after adding the comb to quantify the degradation. Note that after the comb generator, an EDFA is used to compensate for the attenuation.

The setup of the frequency comb generation module can be found in Figure 5.6(b), which is built based on the original setup as in Figure 5.6(a), and consists of an intensity modulator, two RF electrical power amplifiers for push-pull operation, a 50 GHz signal generator, and a wavelength selective switch (WSS) for comb line equalisation. As previously discussed, an EDFA is followed to compensate for the overall loss in the comb. Figure 5.7 shows typical spectra of the transmitter before and after the WSS where three comb lines spaced by 50 GHz are generated, with a measured OSNR of around 40 dB for each comb line.

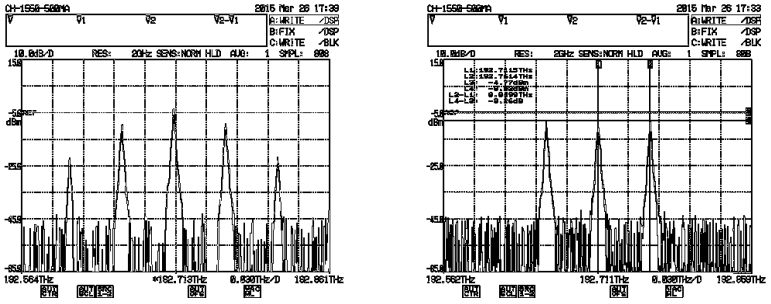

(a) The spectrum before the WSS in the frequency comb setup

(b) The spectrum after the WSS in the frequency comb setup

FIGURE 5.7: The spectra within the frequency comb setup

Initially, a back-to-back performance for a single-channel signal is measured as a reference to which the effect of adding a comb is compared, as shown in Figure 5.6(a). The local oscillator (LO) is separated from the signal laser source, having a similar linewidth of 100 kHz. The performance is slightly better than in Figure 5.3(a), reaching a Q factor of 10.4 dB. Then, the comb is inserted. The performance in terms of Q factor is now 10.1 dB, with a moderate degradation of 0.3 dB as compared to the case for a single-channel signal. The comb can thus be integrated as part of this transmitter to generate WDM signals.

5.2.3 Polarisation multiplexing

As previously discussed, polarisation is an extra degree of freedom that can be utilised to double the information capacity. The most common way to make use of this extra dimension is to use DP modulators. In lab settings, a PolMux emulator is often used to emulate a DP signal originating from a single-polarisation (SP) one, at the expense of duplicated information. The correlation of the two copies of bit sequence makes the experimental results deviate further from those obtained in actual transmission, thus necessitating a decorrelation scheme. Since the SP signal bit sequence is often a PRBS, decorrelation can be readily realised by time delaying one signal copy relative to the other on the two polarisation components by a finite number of bit slots.

The setup of the PolMux emulator can be found in Figure 5.8(a). The incoming signal is split into two copies, one of them being time delayed via the use of a 2m long PM SMF which is equivalent to about 100 symbols for signals at 10 GBd, before being combined in a PM PBC to form a PolMux signal.

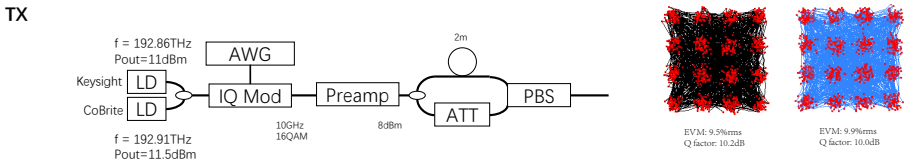

(a) PolMux transmitter setup

(b) Back-to-back performance for DP-16 QAM

FIGURE 5.8: Back-to-back setup and performance for DP-16 QAM signals

The B2B performance when a PolMux emulator is added into the transmitter to generate a 16 QAM signal is measured. The performance in terms of Q factor for the two polarisation components are 10.0 dB and 10.2 dB respectively, with an average of 10.1 dB, which is only marginally lower than that of a SP-16 QAM signal (no more than 10.5 dB). Therefore, it can be concluded that the PolMux emulator can effectively emulate DP-16 QAM signals with balanced performance between the two polarisation components with negligible penalty.

5.3 Characterisation of the link to Reading

FIGURE 5.9: A map of the NDFIS network; courtesy of Zhen Yang from UCL, London

Many of the transmission experiments presented in this thesis have been carried out on a two-pair link to Reading, which is part of the NDFIS (national dark fibre infrastructure service) network or Aurora2 network. Its map is shown in Figure 5.9 and consists of two round trips with a total of four spans of SMFs with identical length. This configuration allows the transmitter, the mid-link, and the receiver to be placed at one

place at Southampton. In the majority of the characterisation experiments , the link is DM with periodic DCMs installed along the link. In order to implement a completely compensated link, the addition of some legnths of extra SMFs was required. These lengths were decided based on calculations and residual CD measurements.

Then, the first half of the completely compensated link is characterised and compared for different modulation formats (DPSK and QPSK signals) and channel counts (single- versus three WDM signals). The characterisation of the second half and the two-pair link is also performed using a single-channel DPSK signal and a a single-channel QPSK signal. Subsequently, the EDFA output powers and the dispersion map are adjusted to optimise the performance. The same optimisation procedure was also applied when the link was extended to Telehouse, London.

Finally the link is also characterised without DCMs. Compared to a DM link, a DUC link may be more favourable as a result of its reduction in nonlinearity impairments. The performance between them is compared and the pros and cons of a DUC link are discussed.

5.3.1 Residual CD measurements

The transmission link in this experiment is based on standard SMFs, amplified by EDFAs, and dispersion-managed using discrete DCMs. The available DCMs fully compensate for the second and third order dispersion that is accumulated in the SMFs. The EDFAs compensate for the transmission loss. Due to the limited availability of DCMs in our lab and the requirement of complete optical compensation of CD in each round trip, the exact values of the residual CD need to be known in order to decide whether extra lengths of SMF are required. The CD compensation calculations of the link suggest the use of two extra spools of SMFs of 9.2km and 19.2km. The locations of the two spools of SMFs are shown in Figure 5.10(a). Furthermore, for a better performance of the mid-link OPC module, which will be introduced later, the net GVD should ideally also be zero at both the mid-link and the end of the link. The extra SMFs required may be different than the calculated length. An actual measurement of the residual CD by the OMA is therefore carried out to determine the exact length.

The transmission setup is shown in Figure 5.10. The transmitter side includes a single DPSK signal at 1550nm, operating at a baud rate up to 40 GBd. This setup also includes two optical bandpass filters (OBPFs) at both the mid-link and the receiver to suppress the out-of-band noise due to the EDFAs along the link, and to improve the overall performance. The purpose of the first experimental link characterisation is to decide the lengths of extra SMFs required for both paths to be fully compensated.

Three baud rates are tested, namely 10 GBd, 16 GBd, and 22 GBd, in order to reduce the possible dependence of calculated residual CD on baud rates. Figure 5.10(b)

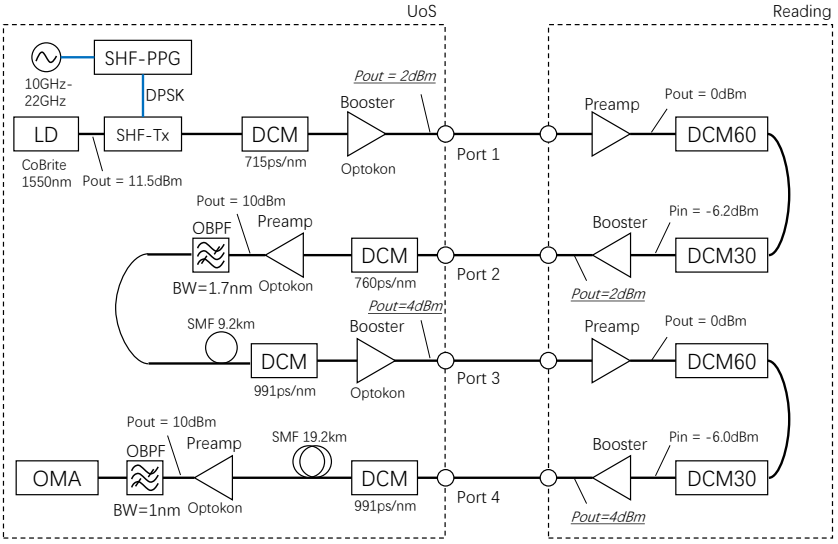

(a) Experimental setup of the link to Reading

(b) Results of the transmission of a single-channel DPSK signal

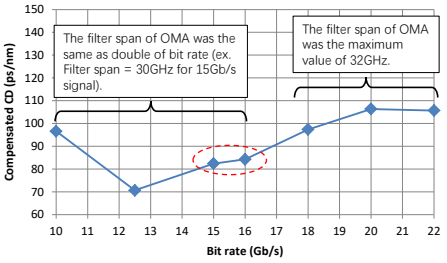

(c) Residual CD calculated from the sweeping for optimal value of CD by a CD compensation algorithm

FIGURE 5.10: Characterisation of the transmitter with DLI to emulate 16 QAM with QPSK

shows the constellation and the residual CD, as calculated by the OMA, which ranges from 84 ps/nm at 16 GBd to 106 ps/nm at 22 GBd. The discrepancy is approximately 22 ps/nm, i.e. 25% of the residual CD at 16 GBd. Figure 5.10(c) shows the detailed plot sweeping the residual CD values for baud rates between 10Gbd to 22 GBd. The average residual CD is about 85 ps/nm at the baud rate of 16 GBd, equivalent to about 5 km SMF, which is then added to the setup via the 1.5 km, 2 km, and 0,8 km SMFs as shown in Figure 5.11.

5.3.2 Link performance

After adding the extra SMFs required to fully compensate each round trip in terms of CD, a set of characterisation experiments are carried out on the link using the same single-channel DPSK signal generated with the transmitter as in Figure 5.1(a) over the first pair link Figure 5.12(a). The plot of the EVM performance as a function of launch power shows the optimal launch power is 0 dBm per channel at Point B in Figure 5.12(b).

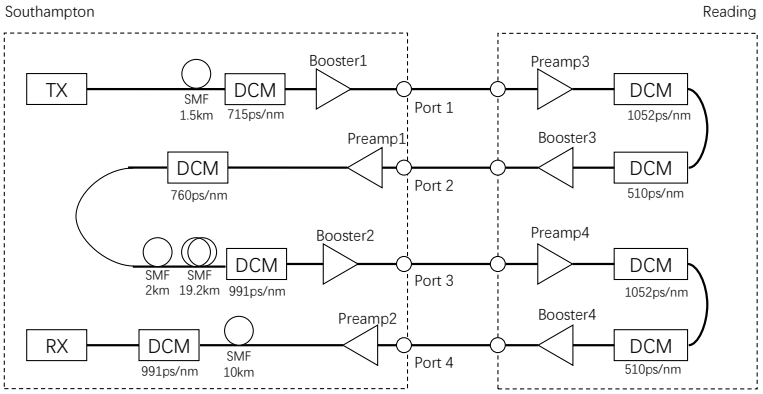

FIGURE 5.11: The link to Reading with complete CD compensation

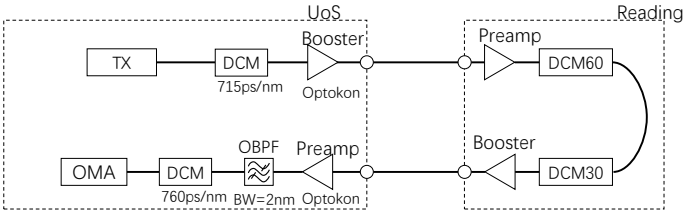

(a) Transmission link setup, the first pair link

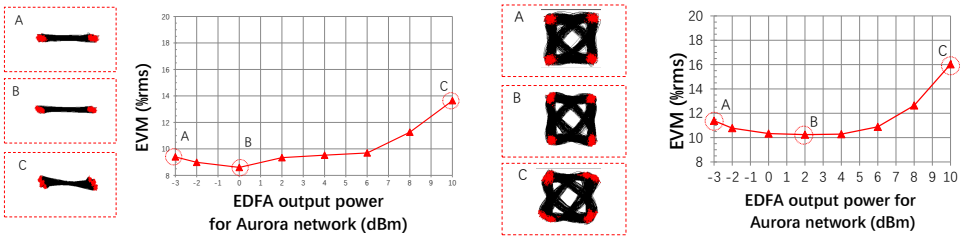

(b) Performance for the DPSK signal and constellations at key powers

(c) Performance for the QPSK signal and constellations at key powers

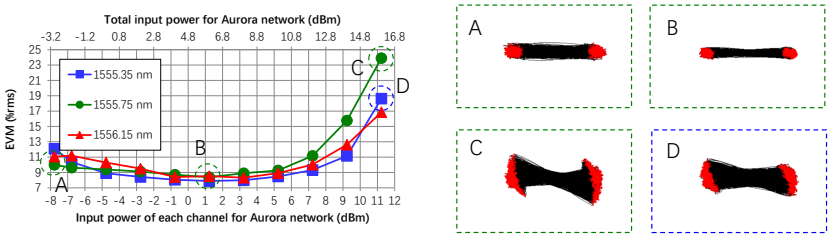

(d) The plots for performance vs. launch powers and constellations for at various points

FIGURE 5.12: Transmission link performance characterisations

In order to get a more thorough characterisation of the link, the transmitter is swapped to allow experimenting on different types of signals to be sent over the same first pair link. These different types of signals include 1) a single-channel QPSK signal as in Figure 5.1(b) and 2) 3-channel WDM signals in Figure 5.6(b), which correspond to the cases of different modulation formats and WDM scenarios, respectively.

The performance for a single-channel QPSK signal also peaks between 0 dBm to 4 dBm (close to Point B in Figure 5.12(c)). Then for the WDM DPSK transmitter, the transmission performance peaks at 1 dBm per channel with a similar EVM value of around 8%rms as for the single-channel case. The plots for all three channels are shown in Figure 5.12(d). Although these findings are not comprehensive, they still show a fairly consistent performance of the link (optimal launch power per channel at about 0 dBm and 1 dBm) regardless of the modulation formats and the number of channel counts.

The second pair link (Figure 5.13(a)) and the two-pair link (Figure 5.13(b)) to Reading have also been characterised using a single-channel DPSK and a QPSK signal. The optimal launch powers are both at -2 dBm and 0 dBm, respectively, similar yet slightly lower figures to the first. It suggests an early onset of significant nonlinear impairments, which can be attributed to the additional spools of SMFs in the second pair of fibres adding an extra length of 30 km. This optimal values are labelled as B in the plots Figure 5.13(c), Figure 5.13(d), Figure 5.13(e), and Figure 5.13(f). Their constellations show cleaner signals than point A where the amplified spontaneous emission (ASE) noise dominates, and point C where the phase noise dominates. The performance as functions of total launch power is also plotted in Figure 5.13.

5.3.3 Link amplifier output power optimisation

The purpose of this set of experiments is to characterise the performance of the link to Reading (the two round trips combined) by optimising the output powers of all EDFAs along the link, so that the optimal power settings can be found.

Two signals separated by 80 GHz are modulated with PRBS31 DPSK at 40 GBd. The received signals are demodulated to measure BER. The experimental setup is shown in Figure 5.14.

All EDFAs in the link are set to constant power mode. To test the impact of repeater power settings on the performance, the optimisation method used is as follows. At first, every EDFA is set to a power that is sufficient for supporting the transmission of the signal from start to finish. Then, a launch power sweep is carried out to locate the optimal launch power. Note that the EDFAs that launch signals into the transmission link are set to the same output power at any given time during measurements for all experiments. Following that, after the launch power being fixed at the optimal value, a power sweep for the rest of the EDFAs is conducted to locate the optimal operating powers. Since the link is symmetric about the mid-point, this amplifier power sweep can be done in pairs where mirror symmetrical amplifiers with respect to the mid-link vary their output powers simultaneously. The other approach that is used later for the extended link to Telehouse in London is on a sequential basis where each EDFA output

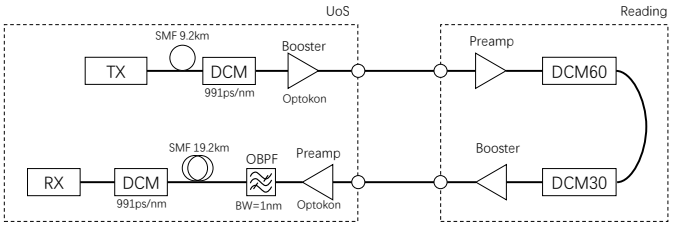

(a) Experimental setup for the second pair link to Reading

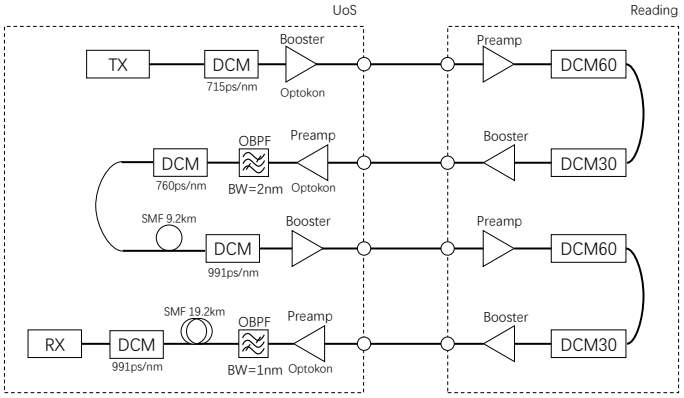

(b) Experimental setup for the two-pair link to Reading

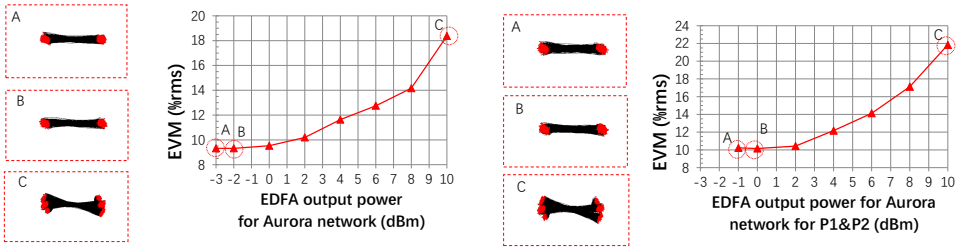

(c) Constellation and plots for the transmission experiment of single-channel DPSK signals for the second pair link to Reading

(d) Constellation and plots for the transmission experiment of single-channel DPSK signals for the two-pair link to Reading

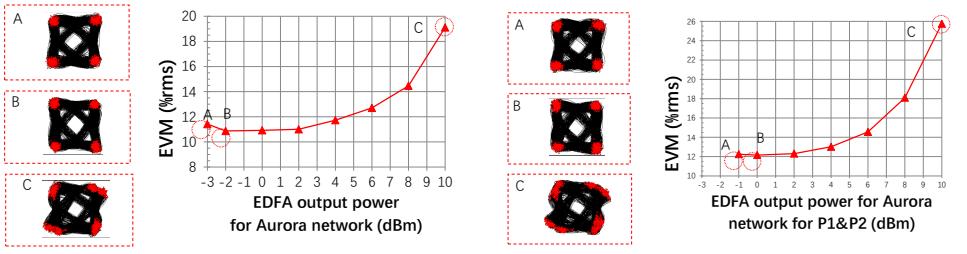

(e) Constellation and plots for the transmission experiment of single-channel QPSK signals for the second pair link to Reading

(f) Constellation and plots for the transmission experiments of single-channel QPSK signals for the two-pair link to Reading

FIGURE 5.13: Transmission experiments for a single-channel DPSK or QPSK signal over the second pair link or the two-pair link to Reading

power is individually optimised, as the link in this case is less mirror-symmetric about the mid-link.

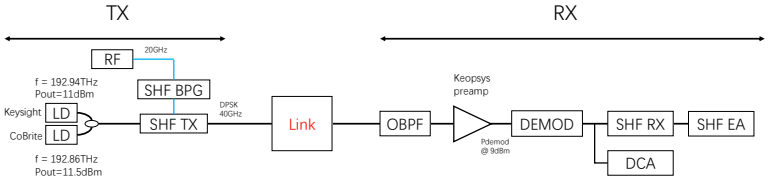

(a) Transmitter and receiver setup

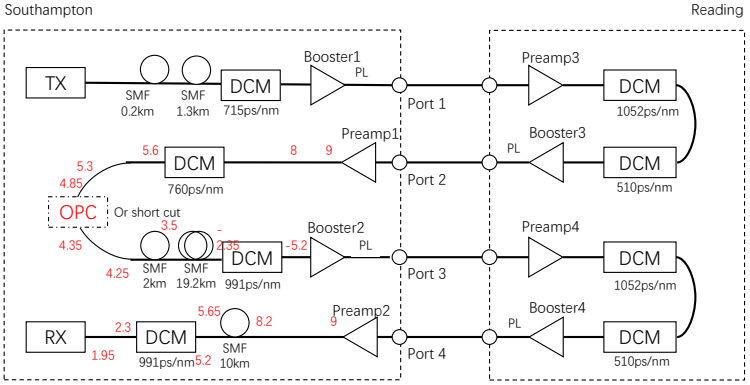

(b) Transmission link setup, red figures showing the power metre readings along the link, from which the loss in passive optical components can be calculated

FIGURE 5.14: The experimental setup before the EDFA output power settings optimisation

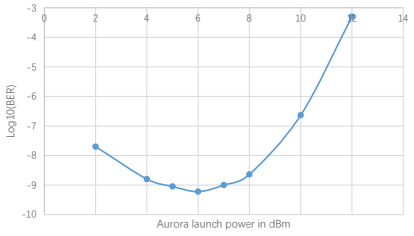

(a) BER as a function of launch power

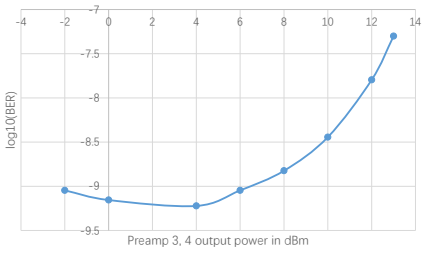

(b) BER as a function of remote preamplifier output power

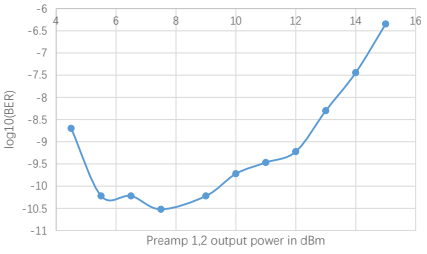

(c) BER as a function of local preamplifier output power

FIGURE 5.15: The experimental results of repeater optimisation

The results of the measurements are shown in Figure 5.15, the optimal total launch power for two 40 GBd DPSK signals is 6 dBm. The subsequent amplifier power sweep is based on fixing the launch power to this value and done in pairs. The optimal remote preamplifier output power is found to be 4 dBm in total as in Figure 5.15(b), while

that of the local preamplifiers is around 8 dBm in total as in Figure 5.15(c). Fixed on these optimal power settings, the launch power sweep is done another time to verify or re-adjust the optimal launch power. The 6 dBm total launch power is confirmed to be the optimal. The final link performance characteristics are shown in Figure 5.15(a). Subsequent link performance measurements in the following chapters make use of these findings.

Although this approach might not be able to locate the very best operating point, this procedure in practice ensures the discovery of the narrow range in which this best operating point can be found.

5.3.4 Dispersion map optimisation

The interaction among the three types of optical elements, namely the SMFs, the EDFAs, and the DCMs, determines the overall performance and the attainable capacity of the system [Agrawal (2012)].

The DCFs used in the DCMs throughout our transmission systems are HFDK [Gruner-Nielsen et al. (2005)], a product from OFS, with a dispersion of -250 ps/nm·km and dispersion slope of -0.9 ps/nm^2·km at 1550 nm, equivalent to 15 times as those of SMFs. Hence these DCMs compensate simultaneously for both dispersion and dispersion slope of the SMFs in the link.

Transmission links that are set up according to scaled translational symmetry (STS) principles [Wei and Plant (2004)] provide enhanced resilience to nonlinear impairments through the compensation of nonlinearity on a perturbative basis up to the first order, hence improving link performance without conforming to the ideal power symmetry and dispersion profile. Transmission systems with OPC operating in nonlinear regime also benefit from STS [Hesketh and Petropoulos (2016)]. The STS principle permits natural power profiles in a lump-amplified transmission system. Sign-reversed even order dispersion terms and identical odd order dispersion terms in the second half of the link after OPC are desirable, as opposed to the ideal dispersion profiles required by perfect NLC by OPC, where the requirements on dispersion are exactly the opposite.

For the particular cases of the two-pair link to Reading and the two-pair link to Telehouse, London, the power profile naturally follows STS principle. The arrangement of SMFs and DCMs before and after OPC is reversed in order. The corresponding accumulated dispersion profile, however, becomes highly asymmetrical as in Figure 5.17(b), especially for the longer link, which will be discussed in Chapter 5.4, deviating considerably from that dictated by STS. This deviation will certainly compromise the performance gain on top of other aspects of link asymmetry, but certain improvement may still be present with the reversely ordered SMFs and DCMs after optimisation as arrow-indicated in the dispersion map. As shown in Figure 5.16, the DCMs right after the

OPC module are launched with high powers to correspond and form an anti-symmetric accumulated dispersion in the previous fibre span. The same principle is applied to the end of the link, although the impact may be negligible. This modification, perhaps trivial, conforms to the STS principle. Its impact will be verified experimentally.

The comparison between before and after dispersion map optimisation based on STS demands unnecessarily complicated mathematical integration over the asymmetric non-linear profile as has been theoretically demonstrated in [Hesketh and Petropoulos (2016)]. For practical applications where the ultimate purpose of dispersion map optimisation is not to study the impact of link asymmetry on the performance but to discover the link conditions that offer improved performance with OPC, performance comparison should be carried out experimentally to justify its use.

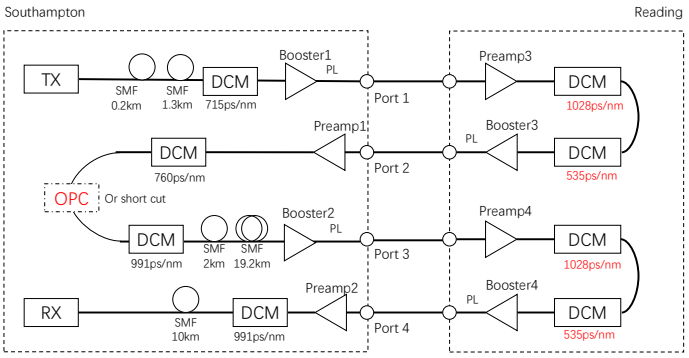

(a) The rearranged experimental setup after dispersion map optimisation

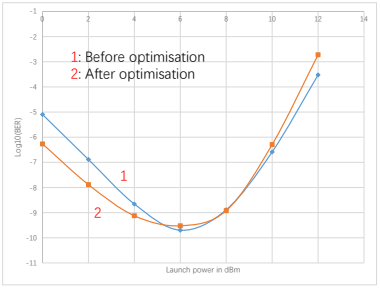

(b) Performance before and after the dispersion map optimisation as a function of launch power

FIGURE 5.16: The experiment on dispersion map optimisation

The modified setup that is optimised according to the STS principle in Figure 5.16(a) can be compared with the original setup as in Figure 5.14(b). The dispersion map for the two cases are given in Figure 5.17(a) and Figure 5.17(b). In this field-installed transmission link, the span lengths and the choice of the DCMs are limited. Therefore, the optimisation process can only approximate the ideal arrangement suggested by the theory. The overall improvement with the application of STS principles, therefore, may not be significant, but it is applied in all subsequent DM link setup in the hope that

it positively impacts the performance with OPC despite the considerably non-ideal link conditions.

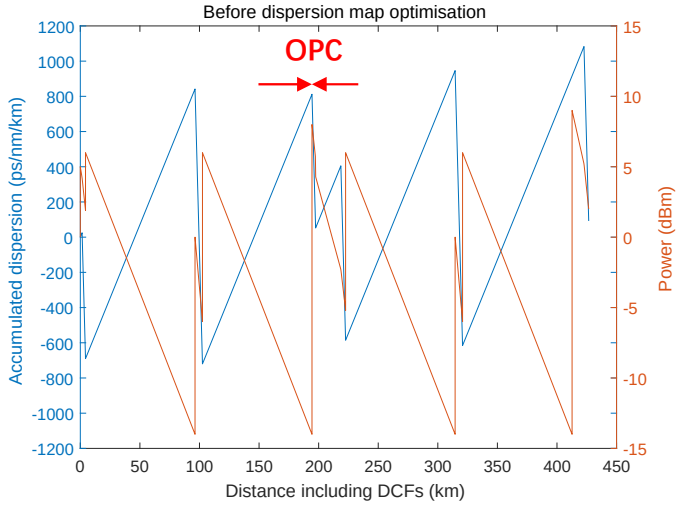

(a) The dispersion map and power profile before optimisation

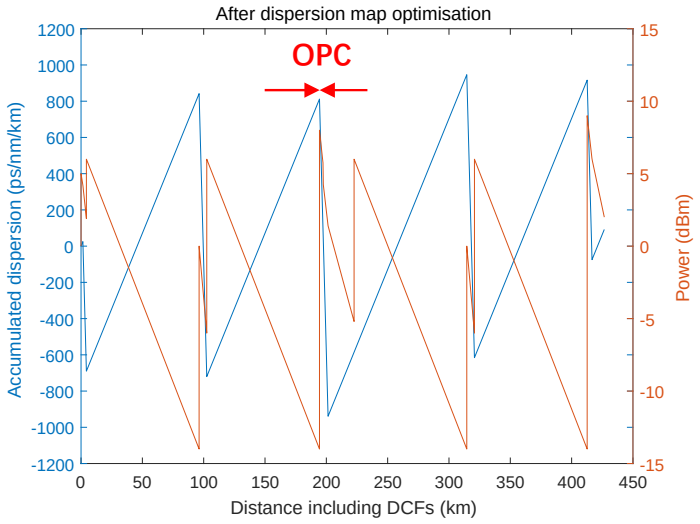

(b) The dispersion map and power profile after optimisation using the STS principles

FIGURE 5.17: Dispersion map optimisation for the DM link to Reading; the horizontal axes are distance in kilometres including the length of DCFs in DCMs.

In order to compare the link performance before and after dispersion map adjustments, the transmitter is set up to include two CW sources modulated with DPSK signals at 40 GBd, and the receiver monitors the eye diagram while error analysing to count the BER. A launch power sweep is carried out for the two cases before and after the optimisation.

Two curves are produced and plotted in the same figure in Figure 5.16(b). The optimised link generally shows a similar performance and the peak power is close to that of the

original setup. The slightly worse nonlinearity tolerance and slightly better performance in the low power regime are still within the range of experimental errors. The performance at the two peaks is almost identical without significant performance degradation or improvements.

The main conclusion from this is that the performance without OPC is not degraded with the use of the dispersion map optimisation, and its benefit is to be seen when mid-link OPC is in place, which is covered in Chapter 7.

5.3.5 Performance comparison between single- and dual-polarisation signals

The link is prepared for PolMux signal transmission. Transmitters that emulate and generate PolMux signals have been introduced in Section 5.2.3 and the transmitter setup that generates a DP two-channel 16 QAM signal at 10 GBd has been shown in Figure 5.8(a). A test is carried out in this section to characterise the two-pair link to Reading with this transmitter. It consists of two CW sources lasing at two wavelengths separated by 50 GHz, modulated with 16 QAM PRBS15 signals at 10 GBd. There is a choice whether to bypass or to launch the signal into the PolMux emulator. The receiver side is a pre-amplified optical modulation analyser (OMA).

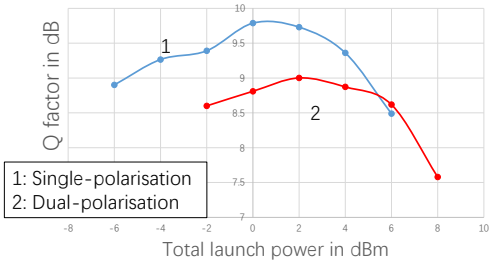

FIGURE 5.18: Performance as a function of launch power for SP and DP signals

One set of measurements compares link performance versus launch power for both the cases of SP and DP signals. Figure 5.18 shows the curves for these two cases. It should be noted that the launch power on the horizontal axis of the plot is the total launch power for two channels and two polarisation components combined, so for the case of DP the actual launch power per polarisation component is 3 dB lower than for the case of SP. Therefore, the optimal launch powers in the two cases are almost identical at around 0 dBm per polarisation for two channels combined. The absolute performance in terms of Q factors is separated by 0.6 dB, which may be seen as the performance penalty for having DP instead of SP.

The other set of measurements optimises EDFA power settings for PolMux signals. The results show that the peak performance occurs at preamplifier powers of 0 dBm at Reading and of 5 dBm at Southampton regardless of the use of the PolMux emulator.

These results verify the performance consistency when DP signals are used instead of SP ones.

5.4 Characterisation of the link to Telehouse in London

The link to Reading in previous sections is further extended to Telehouse London, via two other locations, Reading and Powergate, to increase the number of spans so that the total transmission distance amounts to 800 km. Longer transmission distance degrades the signal quality further mainly due to the ASE noise from the larger number of EDFAs in the link and the nonlinear impairments from all sources.

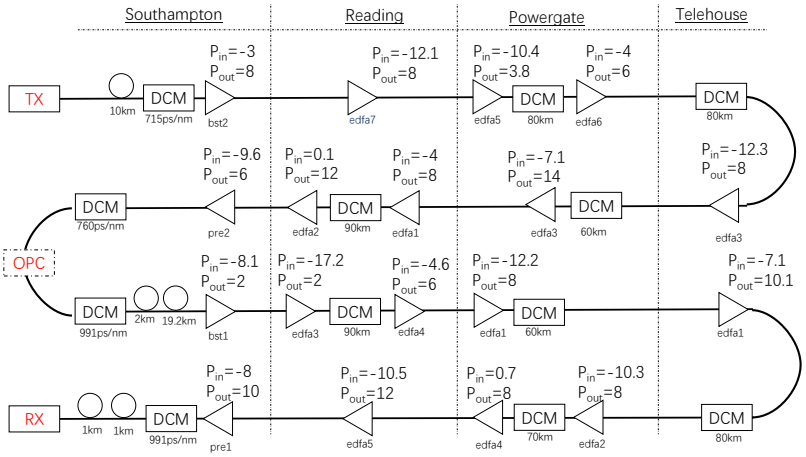

FIGURE 5.19: Power budget along the optimised link to Telehouse in London

The transmission setup has been arranged according to the STS principles and is shown in Figure 5.19. The dispersion map is given in Figure 5.20. The optimisation mainly involves the reversed ordering of the SMFs and DCMs after OPC. Other link symmetry conditions concerning dispersion in a field-installed SMF link can hardly be completely satisfied, as in the case to Reading.

A testing signal has been sent through the link to check the power losses at critical connecting points, confirming the uninterrupted transmission and the absence of excessive losses. The amplifier output power optimisation procedure is carried out based on the same method as for the link to Reading. This optimisation process is done on a sequential basis rather than done in pairs due to the lesser degree of symmetry of this link to London. The results of EDFA output power optimisation for the link to Telehouse are labelled in the link setup. These power settings permit the maximum allowable performance for this given setup, offline DSP algorithms, and this particular transmission link therefore are used as a reference for subsequent experiments. However, the link performance variation with the power settings is not substantial and the main performance limitations are on other factors such as the signal quality at the transmitter output, the nonlinear impairments along the link, etc.

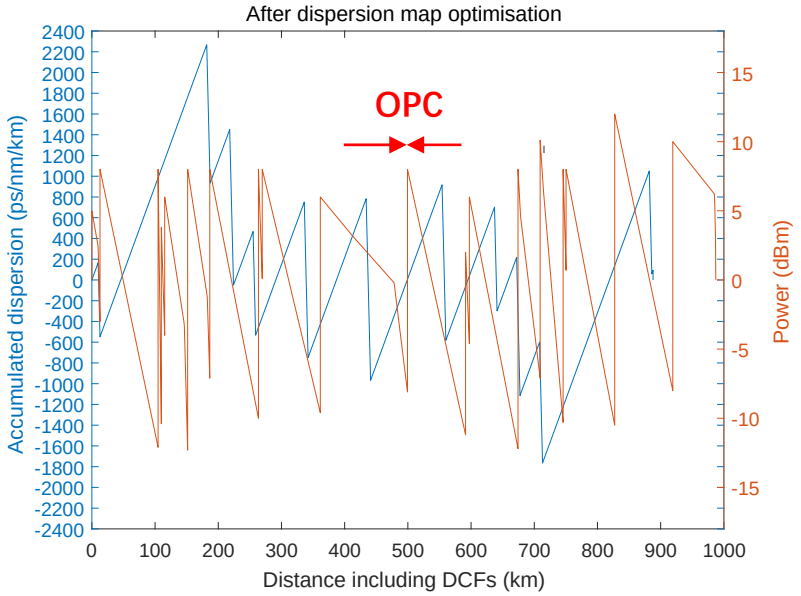

FIGURE 5.20: Dispersion map and power profile for the link to Telehouse, London; the horizontal axis is distance in kilometres including the length of DCFs in DCMs.

5.5 DM links and DUC links

Depending on the approach to dealing with dispersion, a transmission link can be categorised into two broad types, namely a DM link and a DUC link. In a DM link, dispersion is compensated optically usually by periodically-installed DCMs, whereas in a DUC link, the dispersion is either compensated at the transmitter by digital pre-compensation or left uncompensated until dealt with by receiver DSP. In Chapter 4, the difference between these two types of dispersion compensation strategies for a field-installed transmission link is discussed in more detail. In general, DUC links are more commonplace in today's optical transmission systems. The major driving force of the transformation to DUC links lies in the advancement of electronics, which enables the implementation of increasingly complex DSP algorithms, replacing the function of all the DCMs that contribute to the addition of noise and nonlinearity impairments [Xu et al. (2010)].

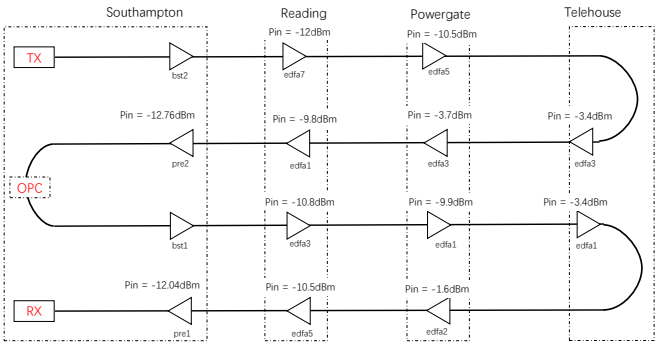

FIGURE 5.21: The experimental setup of the DUC link to Telehouse London

The link to Telehouse in the previous experiments in Section 5.4 is a typical example of a DM link. It is transformed into a DUC link by removing all DCMs and associated EDFAs, as shown in Figure 5.21. In order to measure the losses of all fibre spans as indirectly given in the figure by the input powers of the inline EDFAs, these amplifiers are set to constant output power mode at 8 dBm. No excessive losses are discovered along the link.

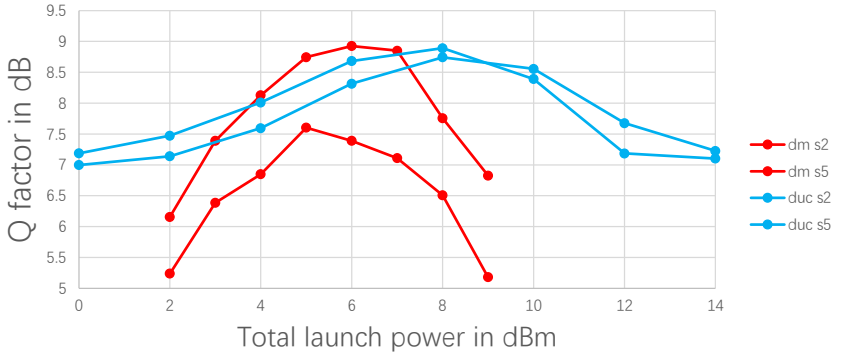

FIGURE 5.22: Performance comparison of the DM link and DUC link based on the same field-installed transmission system from Southampton to Telehouse in London

The performance comparison between this DUC link and its DM counterpart is also carried out using a 6-channel PolMux transmitter modulated with 16 QAM at 10 GBd, and the respective setups are shown in Figure 5.19 and Figure 5.21. The plots of Q factor as a function of total launch power for the two middle channels in both signal bands are shown in Figure 5.22. For the DM link, the optimal launch power is 2 dB lower than that for the case of the DUC, which is the result of a stronger presence of nonlinearity due to the use of the DCMs and the greater number of EDFAs. The absolute performance for the two links is similar, achieving a Q factor of around 9 dB, but the plots for the DM link show a larger vertical performance spread across the channels. Two reasons may be the causes of the observation: Firstly, the larger number of EDFAs introduces a larger tilt in the gain profile, increasing the OSNR imbalance across the transmitted channels. Secondly, the DCMs in the DM link are not able to compensate for higher order dispersions, hence further spreading the performance of spectrally separated channels. However, its effect may be minimal due to the limited frequency separation of a mere 500 GHz.

5.6 Channel power equalisation

The transmission link is amplified by EDFAs that do not have built-in filters or other mechanisms to equalise the gain tilt across their operating bandwidths. The cumulative gain imbalance can reach more than 7 dB for the two signal bands, which are separated by 500 GHz, over the 800 km link, so the location at which the power of all channels is

equalised has a crucial impact on the performance discrepancy between them. It also affects the optimal launch power of each signal band as well as its absolute performance.

Channel power equalisation is carried out in the experiments by varying the source laser output power, so that the channel powers can be made equal at the target location. Another possible approach to adjust the power of each signal band is to attenuate one of the signal bands at the transmitter WSS. Both approaches produce similar performance at the end of the link.

The channel power can be equalised at two obvious positions: 1) the output of the transmitter and 2) the mid-link. Equalisation at transmitter (or at the receiver) produces maximum possible channel power differences in average. Whether this approach necessarily leads to larger channel performance differences remains to be tested. In most of our experiments the equalisation is done at the mid-link so as to balance the uneven power growth of the two signal bands, by having the signal band that has a higher power in the first half of the link a lower power in the second half. More importantly it allows the channel powers to be equalised at the input to the mid-link OPC module, as shown in the spectrum in Figure 5.24(b). An experiment is set up to compare this commonly used approach with the first one.

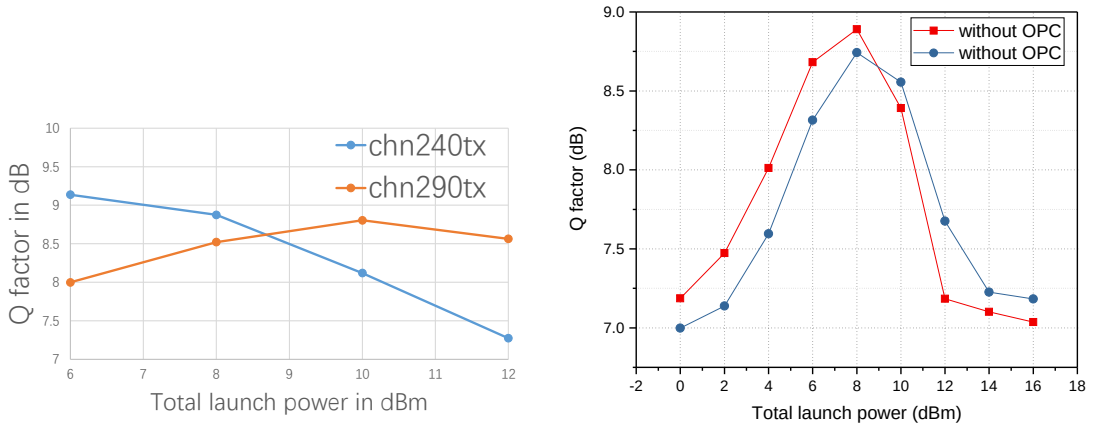

(a) Performance as a function of total launch power when the channel powers are equalised at the transmitter

(b) Performance as a function of total launch power when only one signal band is sent at the mid-link

FIGURE 5.23: Impact of the location of channel power equalisation

The transmitter is set up to generate six DP-16 QAM signals at 10 GBd, grouped into two signal bands. When the channel power is equalised at the output of the transmitter, Figure 5.23(a) shows the performance in terms of Q factor as a function of launch power for the two middle channels of the two signal bands, Chn240 at 192.4 THz and Chn290 at 192.9 THz. Chn240 has its optimal performance at a total launch power of 6 dBm, whereas this value is 10 dBm for Chn290. The earlier onset of nonlinearity for Chn240 is a manifestation of the higher band power of the longer-wavelength signal band of which Chn240 is in the middle.

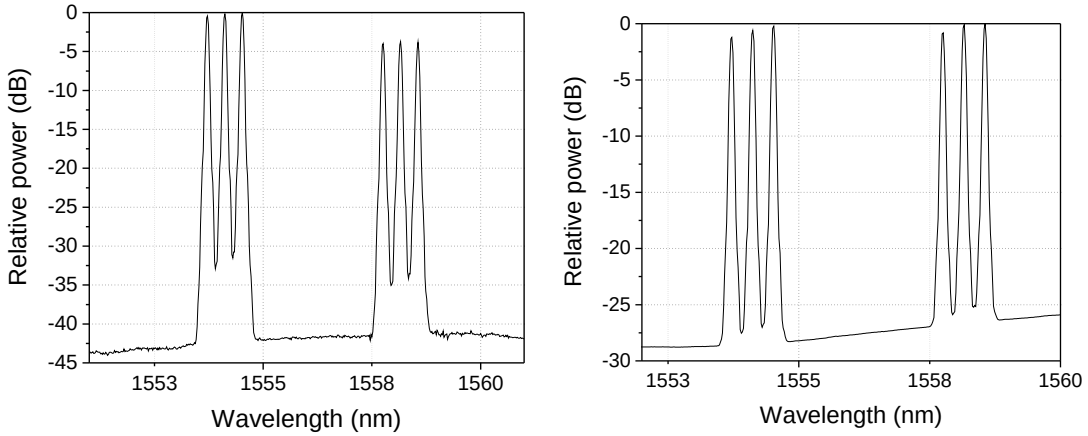

(a) The spectrum at the transmitter of the link to Telehouse when the channel powers are equalised at the mid-link; the maximum channel power difference is around 5 dB

(b) The spectrum at the mid-link when the channel powers are equalised at the mid-link

FIGURE 5.24: The spectra at the transmitter and the receiver when the channel powers are equalised at the mid-link

The other situation is where the powers of the two signal bands are equalised at the mid-link. Figure 5.24 shows the spectrum taken at the transmitter and the mid-link for all six channels. The tilt of channel peak power is visible and the difference amounts to 5 dB at the transmitter and is equalised at the mid-link. As shown in Figure 5.23(b), the optimal launch powers are the same, both at 8 dBm. The relatively balanced and comparable performance between the two middle channels confirms that the performance imbalance can be greatly reduced by proper equalisation of signal band powers. Therefore, mid-link equalisation is preferred in all subsequent experiments.

5.7 Conclusions

In this chapter, experimental studies for fibre-optic communication systems begins with setting up the transmitter. Like its wireless counterpart, fibre-optical transmitters pursuing full utilisation of available bandwidth exploit additional dimensions of the quadrature and the orthogonal polarisation. While links combat power loss by inline EDFAs, the approach coping with distortions caused by GVD, TOD, etc, divides the links into those that are dispersion managed with inline DCMs, and those that are dispersion uncompensated. The residual dispersion in the latter case is often dealt with by EDC or OPC. Other unavoidable issues, as a result of the gain spectral imbalance due to imperfection of inline EDFAs, are addressed by careful evaluation of possible positions where the gain equalisation should be performed. With links to Reading and London set up and made ready, the characterisation of the OPC module remains the last step towards a complete OPC-assisted transmission system.

Chapter 6

Characterisation of the OPC module

Applying OPC at the mid-link is an effective nonlinearity mitigation technique. The OPC operation can be implemented in a variety of approaches. Most common approaches make use of the phase conjugation property of parametric processes such as FWM in $\chi^{(3)}$ nonlinear materials including silica HNLFs. Conventional OPC schemes typically 'waste' at least half of the bandwidth that is available for the signal to be transmitted and require co-polarised signal input co-propagating with the pumps in the parametric process, thus requiring cumbersome polarisation diversity schemes to ensure the overall signal polarisation insensitivity. Therefore, the OPC design in this thesis aims to address these limitations by implementing the following three major features:

1. efficient bandwidth utilisation,

2. compactness and simplicity of the OPC module using a single nonlinear medium, and

3. signal polarisation insensitivity.

The chapter begins by discussing the approaches that allow these features to be implemented in the final OPC module design. It continues by discussing the choice of the nonlinear medium used for the OPC module that has been implemented. A variety of HNLFs that are available in the telecommunication laboratory have been compared in terms of SBS power threshold, their dispersion and nonlinear properties, which lead to different CEs and CE bandwidths of the generated phase-conjugated signals. Other parameters of the OPC module, such as the signal band placement, the signal power into

the HNLF, etc., all play important roles in the optimisation of the OPC performance. Some practical techniques including the control of the pump orthogonality are discussed, as they are critical to maintaining a stable and optimal operation of the OPC module, which is a crucial aspect of the OPC design as it allows the turn-key operation of the module. Finally, the complete implementation of the OPC module is characterised and discussed in terms of the signal OSNR degradation and the B2B performance for various types of signals that are used in transmission.

6.1 Design

6.1.1 OPC module design criteria

Since the OPC operation involves spectral inversion, i.e. wavelength conversion, typical mid-link OPC schemes often make use of at most half of the available bandwidth. In such systems, half of the bandwidth is reserved in the first half of the link for the wavelength converted idler band in the second half of the link, whereas the original bandwidth of the signal band is vacated and wasted after OPC, see the left schematic of Figure 6.1. As the spectral inversion with respect to the central frequency is an inevitable property of OPC operation implemented by parametric processes, a natural approach to recycle the bandwidth is to propagate two signal bands at the transmitter such that they swap their bandwidths after the mid-link OPC, continuing the transmission without reserving or wasting any bandwidth resources in the link. Clearly, it must be guaranteed that in the very same band, the signals should be filtered out at the end of the OPC module before the generated idlers can be transmitted. This scheme is demonstrated in Figure 6.1, where the left and right block diagrams depict the signal band arrangement in a typical OPC scheme and the OPC scheme proposed in this thesis, respectively, in terms of bandwidth utilization.

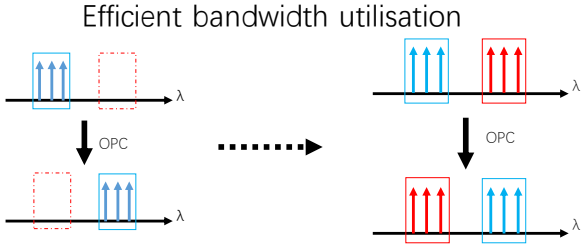

FIGURE 6.1: Schematic diagram of the typical (left) and the proposed (right) OPC schemes in terms of bandwidth utilisation

However, the feature of efficient bandwidth utilisation involves two separate OPC operations, one for each band, hence typically requiring two identical nonlinear media for the processing of the two signal bands, as illustrated in Figure 6.2(left). The second feature

of this OPC scheme is, thus, to use a single nonlinear medium and process simultaneously both bands in it. This is achieved by allowing the two signal bands to propagate through the nonlinear medium in opposite directions via the use of two circulators. This idea is illustrated in Figure 6.2(right). Making use of a single nonlinear medium not only has the advantage of having almost identical performance for the two signal bands (the fibre properties are the same in both cases), but also the cost of the extra HNLF can be saved, one of the most expensive components in the OPC module. If the two pumps are shared between the two FOPAs, the saving of an extra pair of narrow-linewidth high quality lasers is even more significant.

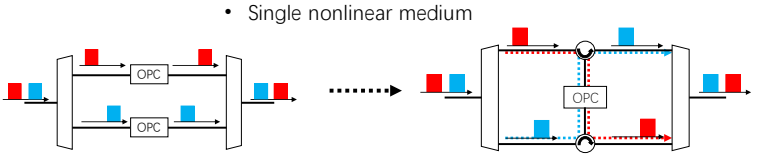

FIGURE 6.2: Schematic diagram of OPC schemes that use two (left) or one (right) nonlinear media

The third feature of this OPC scheme is signal polarisation insensitivity. Transmission systems based on SMFs do not maintain the SOP of the signals. When entering the mid-link OPC module, the signal is randomly polarised. The OPC module must be able to be agnostic to the signal polarisation, which means the CE and performance variation must be minimised with the signal polarisation. The signal polarisation insensitivity is also crucial for a PolMux system, since otherwise the signals on the two polarisation components will exhibit different performance when going through a system with polarisation-dependent operation. Typical approaches include orthogonally-polarised dual pump FWM configurations as in Figure 6.3 or the use of polarisation diversity schemes based on either single-pump FWM or dual-pump FWM configurations. The corresponding mechanism is introduced in Chapter 3. Polarisation diversity schemes achieve simultaneous OPC operations for each polarisation component, requiring either two extra nonlinear media, one for each polarisation component, or a counter-propagation scheme. As the counter-propagation configuration has already been used to address the second feature of this OPC scheme, the orthogonally-polarised dual-pump FWM configuration has been chosen to address the polarisation insensitivity feature in this design. This is due to its simplicity in control and tuning, but it comes at the cost of a lower CE for the same pump powers used.

6.1.2 Design versions

The three essential features or requirements on the OPC design described in the previous section are summarised as follows.

1. BW efficient OPC operation, which involves two FOPAs that separately phase-conjugate two individual signal bands

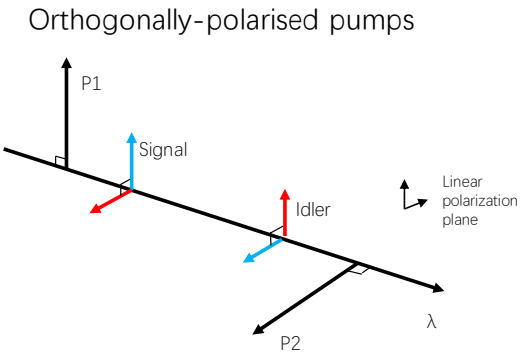

FIGURE 6.3: Schematic diagram of the OPC design realising the input signal polarisation insensitivity by orthogonally polarised dual-pump FOPA configuration

2. Two OPC operations taking place in one single nonlinear medium and making use of only one single pair of pump lasers

3. Signal polarisation insensitivity realised by orthogonally polarised 2p-FOPAs

Achievable pump powers are the most important design consideration. A large fraction of pump powers is inevitably lost during propagation through the module. The two counter-propagating FOPAs share one common pair of pumps, which involves at least 3 dB power reduction. As pumps need to be coupled with signals before the nonlinear medium, this causes another power reduction of 1 to 2 dB. The insertion losses after the pump sources and before the HNLF and the bending losses in polarisation controllers (PC) all amount to another few decibels' loss. At the HNLF input, for better noise performance and higher CE, higher pump powers are always desirable as long as significant SBS is not triggered. Therefore, the high-power EDFAs after the pump lasers are set to operate at their maximum of 37 dBm (5 W). The first two versions of OPC module design mainly differ by the remaining pump powers at the input of the HNLF.

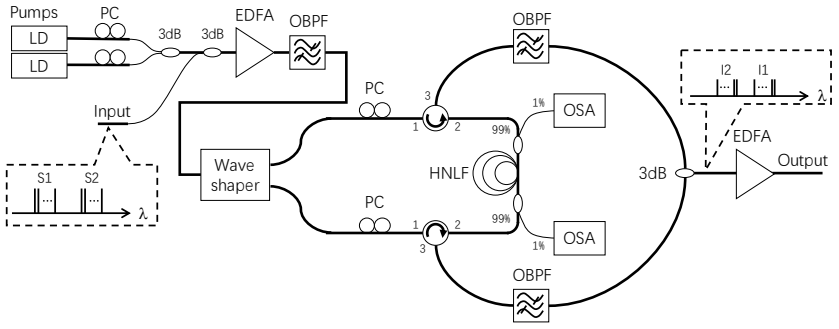

FIGURE 6.4: First version of the OPC module

The very first design of the OPC module that is used in this project is shown in Figure 6.4. The design was carried out mainly by Dr. Satoshi Yoshima. The subsequent modifications towards the second and third versions of the design were carried out jointly between the two of us, while I was mainly responsible for the system characterisation.

In this first design, the pumps are combined with signal bands before a high power EDFA. Each pump is degraded by more than 6 dB going through the PC and two couplers before being combined with the two signal bands. Together, they are amplified by a single booster EDFA that has a maximum allowable input power of 5 dBm, and a maximum joint output power of 37 dBm, which in turn greatly limits the maximum usable pump power. In this case, the pump powers reaching the HNLF is not more than 20 dBm, which does not provide the targeted CE hence sufficient output OSNR. Therefore, we decided that the design should be modified to amplify the pump and signal band separately.

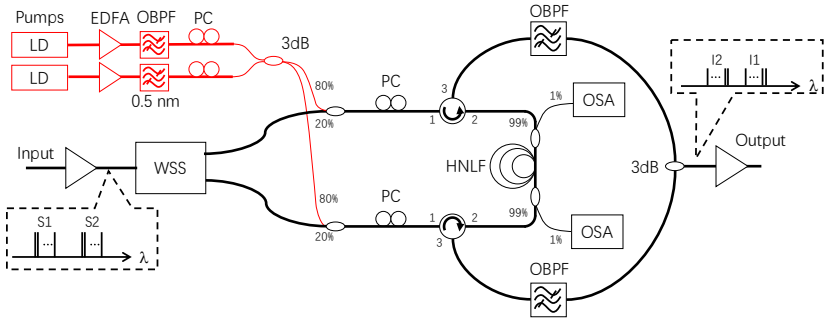

FIGURE 6.5: Second version of the OPC module

The second design shown in Figure 6.5 demonstrates this modification, where the pumps are separately amplified to 37 dBm before combining with the signal bands via a pair of couplers. The couplers should maximise the transmitted pump power while maintaining sufficient signal band power into the HNLF, so as to improve the pump-signal power ratio as well as allowing a sufficient signal OSNR. To this end, the splitting ratios of the couplers have been chosen experimentally among 70%-30%, 80%-20%, and 90%-10%, and through the 70%, 80%, and 90% ports, respectively, are the pumps transmitted. The 80%-20% coupler provides the best performance and is used in all subsequent experiments.

This second design was used in some early works, but there had been a potential problem with the signal power, which is also an important consideration for the proper function of the module. There exists an optimal signal band power into the HNLF that provides maximised back-to-back and overall OPC performance [Morshed et al. (2012)]. With an increased channel count or the use of PolMux, both of which reduces the power per channel per polarisation, the optimal signal power into the HNLF may fall out of the range allowed by the second design.

To be more specific, the signal bands share a common EDFA and its output power is limited by the succeeding WSS which permits only a power of 13 dBm per channel and a total of 20 dBm at its input. This problem has been addressed with another modification of the setup.

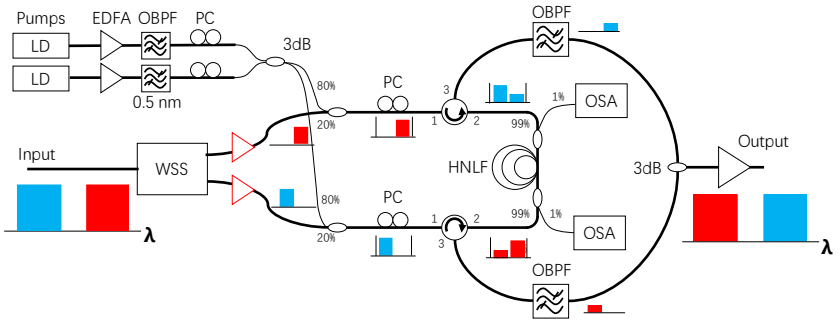

FIGURE 6.6: Third version of the OPC module

In the third design as in Figure 6.6, This signal power limitation is addressed by splitting the signal bands before they are amplified by separate EDFAs. This modification increases the maximum signal band power from around 12 dBm to beyond 20 dBm, which is determined solely by the signal band EDFAs' maximum power outputs. The range within which the optimal signal power into the HNLF can be located is largely increased. This flexibility, however, comes at the cost of not filtering each signal band after amplification using the WSS. This noise reduces the signal quality after OPC. The trade-off is made by comparing both the back-to-back and the overall transmission performance between the two designs, and the outcome of the comparison generally favours the third version of design. It has been used in all experiments with PolMux signals.

The final design is based on the conceptual schematics presented in Figure 6.1 to Figure 6.3 and evolves through the three versions of design. In Figure 6.6, the two pumps are amplified, filtered, combined, and split into two copies, each coupled with only one signal band (the other has been properly filtered out by the WSS) and launched into one of the two ends of the nonlinear medium, where the two FWM processes take place, performing the two OPC operations, which are effectively two FOPAs. Each generated idler band is then selected, filtered, and combined with the other at the output of the OPC module, before being amplified for their transmission in the second half of the link. As previously discussed, the two signal bands effectively swap spectral positions and no bandwidth is wasted in this process.

The manual adjustment for proper functioning of the OPC module mainly involves the tuning of PCs. They are worthy of some discussions. There are four PCs in the setup, one pair inserted in the optical paths with each permits the transmission of three input waves of one FOPA, the other pair inserted after the high-power EDFAs for the pumps. The aim of the four PCs is firstly to adjust and make the SOPs of the two pumps orthogonal with respect to each other, and secondly to align the SOPs of the two sets of input waves of the two FOPAs to those of the principle axes of the HNLF. The purpose of this practice is to achieve input signal polarisation insensitivity, while maintaining stable and efficient operation of the parametric processes.

There are a variety of other factors that influence the OPC performance. These factors include the selection of the HNLF, the power and wavelength allocations of the pump and the signal bands, etc. With the satisfaction of all these requirements, the OPC module design can be finalised. They will be discussed in subsequent sections.

6.1.3 HNLF choice

As discussed in Chapter 3, the OPC operations in this thesis are essentially FOPAs that are based on the parametric process taking place in a highly nonlinear medium. However, there are a variety of candidates of nonlinear media to choose from including both $\chi^{(2)}$ and $\chi^{(3)}$ materials, such as PPLN, Si-based nonlinear waveguides, silica HNLFs, and non-silica soft glass fibres. Since the transmission system is fibre-based, although HNLFs do not offer as compact integration solutions as some non-fibre-based nonlinear media, they have the primary merit of easier coupling with the rest of the fibre-based components. Future development of this scheme may find non-fibre-based solutions more attractive; however, this is not the main concern in this thesis.

The HNLF needs to satisfy a few requirements as follows.

1. Large γL_{eff} product (nonlinear coefficient times effective length) to support a high CE and OSNR
   (a) Large nonlinear coefficient
   (b) Long fibre length
   (c) Low fibre loss for large effective length
2. High SBS threshold power of the nonlinear medium to allow the use of high pump powers
3. Dispersion properties (engineered dispersion) to fulfil phase-matching;
   (a) ZDW close to the two pumps
   (b) Low dispersion and dispersion slope across the operating wavelengths of the FOPAs
   (c) Short fibre length to reduce the impact of longitudinal dispersion property variation
4. PMD to reduce the polarisation-dependent performance, especially if PolMux signals are used.
   (a) Small absolute PMD values
   (b) Short fibre lengths

The idler CE at the output of the HNLF is a pivotal parameter of the two FOPAs in the OPC module, as it relates to the OSNR, phase-matching, etc. In order to achieve a high idler OSNR, the CE needs to be as high as possible. Pump powers are directly related to the CE by the relation in Equation 3.9. However, they are limited by the SBS threshold power of the HNLF. Usually, to obtain the highest CE, the pump powers are set to values that are only slightly lower than the SBS threshold. The CE is also dependent on the fulfilment of the phase-matching condition, which is influenced by the dispersion properties of the HNLF. Phase-matching for the dual-pump FWM often requires the two pumps to be symmetric in wavelength about the ZDW of the HNLF. This means the ZDW needs to be approximately 1550 nm for the wavelengths that are typically used in this design. Unless the two pumps can be conveniently placed symmetric about the ZDW, a low dispersion and dispersion slope across the operating wavelengths of the FOPAs also facilitates the phase matching required by the parametric processes. PMD is another issue that reduces the efficiency of the parametric processes. For a PMD of the order of 0.1 $\mathrm{ps}/\sqrt{\mathrm{km}}$, the beat length is of the order of a few metres. Therefore, substantial SOP changes of all waves in the HNLF are expected, leading to the random variation of the effective principal SOP of the HNLF over time, hence the undesirable random variation of performance over time. This makes HNLFs with smaller PMDs more suitable choices. Given similar PMD values, shorter HNLFs are less affected by the detrimental effects caused by PMD.

Name	Length	ZDW	γ	D@1550 nm	S@1550 nm	SBS	α@1550 nm	A_{eff}	PMD
Unit	m	nm	/W/km	ps/(nm· km)	ps/(nm^2· km)	N/A	/km	μm^2	ps/$\sqrt{\mathrm{km}}$
Sumitomo 220 m	220	1550	N/A	0.01	0.03	nonstrained	0.53	10.3	0.02
Ge 100 m	101	1531	11.6	0.36	0.018	strained	0.79	11.5	0.31
Ge 160 m	163	1534	11.6	0.39	0.018	strained	0.79	11.5	0.33
Ge 300 m	302	1555	11.6	-0.08	0.018	strained	0.88	13.6	0.5
Al 100 m	103	1559	6.9	-0.022	0.025	strained	6.3	15.3	0.46

TABLE 6.1: The optical properties of the HNLFs available

The first set of characterisation measurements towards determining the optimal choice of the HNLF are the SBS threshold measurements, so that in subsequent experiments the pump power levels can be determined according to this threshold value. The corresponding CEs are then measured to determine the HNLF that has potentially the best performance. It is worth noting that due to the signal-signal FWM interference and ASE noise of the signal band EDFA (defined in the design section), higher idler power inside the HNLF may not always provide the better performance. Therefore, the B2B performance with OPC is measured to confirm the choice. The performance variation over time is finally measured in the PMD section. Table 6.1 reports the most important optical properties of the fibres that have been investigated. It might be worth noting that these are the characteristics provided by the fibre manufacturers, i.e. no specific information on the core profiles and diameters are available.

6.1.3.1 SBS threshold

Since the OSNR and CE of the idler bands increase with pump power, the pump power need to be as high as the components in the OPC module allow, until reaching the SBS threshold of the HNLF. Beyond the SBS threshold, the back scattered light power exceeds that which is transmitted forward, thereby forming an upper limit on the pump power. Chapter 3 describes two feasible approaches to increasing this threshold level: either the HNLF can be linearly strained, or the CW pumps can be frequency dithered.

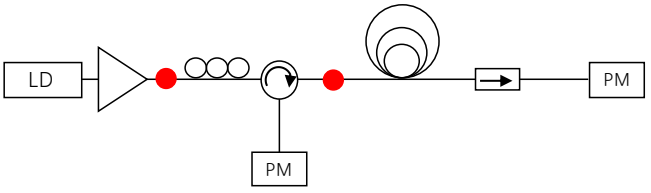

FIGURE 6.7: The experimental setup for SBS threshold measurements

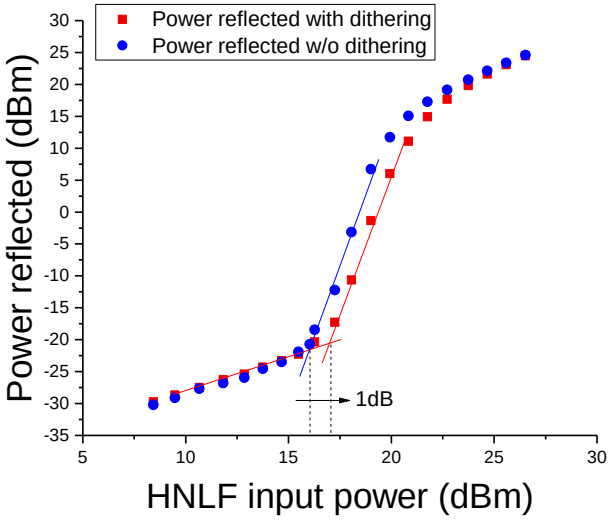

FIGURE 6.8: Plots for reflected power at a function of HNLF input power, before and after applying the single-tone dithering

A simple attempt is made on the frequency dithering technique by using the built-in dithering function of the pump laser source for the non-strained Sumitomo 220 m Ge-doped HNLF. Please refer to Table 6.1 for its optical properties. A single dithering tone is pre-set at the frequency of 1 GHz. The experimental setup for the SBS threshold characterisation is shown in Figure 6.7. The CW laser source is connected to a PC to align the CW wave polarisation with the principal axis of the HNLF via a circulator. Port 3 of the circulator is then connected to a power meter to monitor the back scattered light from the HNLF. The plot in Figure 6.8 is the reflected SBS power as a function of HNLF input power, and the SBS threshold powers before and after applying dithering are clearly shown. As can be seen, the SBS threshold is increased by 1 dB

from approximately 16 dBm to 17 dBm, which is not a substantial improvement for the specific application. It is worth mentioning that typically multi-tone dithering is able to achieve much higher SBS threshold [Torounidis et al. (2006)]. However, dithering of the pump broadens its bandwidth, and this phase modulation of the pump is transferred to the idler, thereby degrading the idler performance. In the non-degenerate FWM configuration, this is the result of the phase relationship:

$$\phi_4 = \phi_1 + \phi_2 - \phi_3, \tag{6.1}$$

in which ϕ_i, $i = 1, 2, 3, 4$ represent the phases of the pumps, the signal, and the idler, respectively. Counter-dithering the two pumps with out-of-phase RF waves that are phase-shifted by π can effectively cancel the phase modulation of the idler output and reduce the impact of the pump dithering on the idler performance [Ho et al. (2002)]. Even if the more effective multi-tone approach and counter-dithering technique are applied, the degradation of the idler performance by RF noise is still inevitable, which makes dithering techniques less attractive in increasing the SBS threshold.

A different way to increase the SBS threshold, at the cost of an increase in PMD and altered dispersion properties, is to apply a linear strain on the HNLFs [Gruner-Nielsen et al. (2011)].

I have considered four strained different HNLFs in my work. To measure their SBS threshold power, the same experimental setup as in Figure 6.7 is used. Figure 6.9 shows the corresponding curve for a Ge-doped 160 m linearly strained HNLF. The SBS threshold power is clearly shown to be about 24 dBm (as compared to 16 dBm for a 220 m of unstrained fibre with similar nonlinear properties). The SBS threshold powers for other linearly strained HNLFs including 100 m Ge-doped, 300 m Ge-doped, and the 100 m Al-doped are summarised in Table 6.2. Al-doped silica HNLFs have higher SBS tolerance at the expense of a reduced nonlinear coefficient relative to Ge-doped fibres [Mermelstein (2009)]. For the same chemical composition, the SBS threshold decreases with increasing length, as can be shown for the cases of Ge-doped HNLFs with the three different lengths.

HNLF	SBS threshold power in dBm
Ge-doped 100 m	26 dBm
Ge-doped 160 m	24 dBm
Ge-doped 300 m	23 dBm
Al-doped 100 m	28 dBm

TABLE 6.2: The SBS threshold power measurements for a selection of strained HNLFs

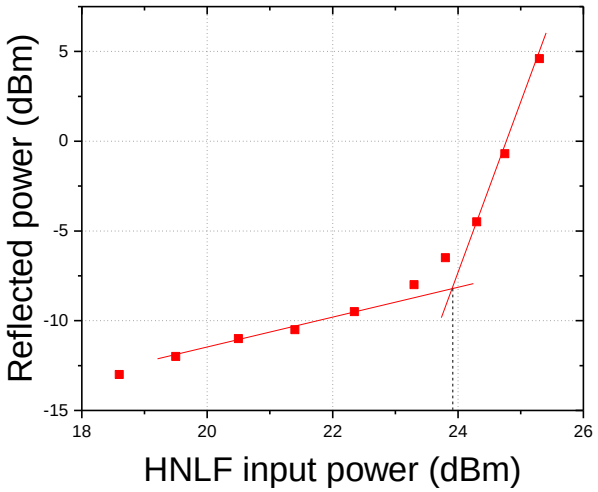

FIGURE 6.9: SBS reflection power as a function of fibre input power for the Ge-doped 160 m linearly strained HNLF

6.1.3.2 Conversion efficiency and B2B performance

After measuring the SBS threshold of the HNLFs, the FOPA based on these fibres can be set up to use pump powers that are either bound by the signal EDFAs or just below the SBS threshold power (by 1 dB). Using these power-maximised settings, the idler OSNRs and CEs are measured by observing the spectrum at the output of the HNLF. Moreover, the performance with OPC in the B2B configuration is also measured, as it is one of the ultimate figures of merit when choosing a HNLF for the OPC module.

For fair comparison, the signal band configuration is identical for each set of measurements. These measurements use two 3-channel signal bands that are each modulated on a 50 GHz grid with 16 QAM at 10 GBd, with a total power per band of 17 dBm. The OPC module used is the third version as in Figure 6.6.

Under these conditions, Table 6.3 shows the different CEs and B2B performance for the strained HNLFs previously characterised. From the table, it can be seen that Ge-doped HNLFs have higher CEs than the Al-doped ones, and the CE increases with the length of the fibre. As expected, this trend demonstrates that the CE increases with the fibre nonlinear coefficient and fibre length. In terms of B2B performance, due to its lower nonlinear coefficient at 6 /W/km and the upper limit of the pump powers used, the Al-doped 100 m HNLF is only able to provide B2B performance with OPC at 9.1 dB in terms of Q factor for DP signals. Ge-doped HNLFs, on the other hand, offer B2B performance beyond 9.8 dB with the exception of the 300 m one, which is not able to maintain a stable operation for DP signals. It is believed that large PMD is the reason of this instability, and this is going to be discussed in the next section. So far, Ge-doped 100 m and 160 m HNLFs provide similar performance. However, it must be emphasised that the 300 m Ge-doped HNLF has shown the best performance when single-polarization signals are to be used.

HNLF	CE	B2B performance in terms of Q factor
Ge-doped 100 m	-8 dB	DP: 9.8 dB
Ge-doped 160 m	-6 dB	DP: 9.8 dB
Ge-doped 300 m	-3 dB	DP: N/A
Al-doped 100 m	-11 dB	DP: 9.1 dB

TABLE 6.3: CEs and B2B performance in terms of Q factors for different strained HNLFs

6.1.3.3 Polarisation mode dispersion

As previously mentioned, the PMD parameter is the other important factor to be taken into account when choosing a suitable HNLF. PMD introduces signal and idler gain fluctuations as well as affecting the shape of the gain profile of the FOPA [Lin and Agrawal (2004a)]. The time variation in the signal gain is also well-known and is associated with environmental factors such as the acoustic vibration, temperature, etc.

The following experiments attempt to quantify the time variation of the B2B OPC performance for different HNLFs. Based on the scales of the time variation, proper HNLFs suitable for different applications can be determined.

Table 6.4 summarises the time scales of the variation of performance for the three Ge-doped strained HNLFs. The recorded time is the time during which the maximum Q factors in every minute vary by 0.1 dB for 6-channel DP-16 QAM signals in the 800 km DUC link. The actual time scales for stable operation depend on a variety of factors that randomly vary from time to time, so the time recorded corresponds to the most typical circumstances and is indicative only. Generally, the time scale increases as the length of the HNLF decreases, which is in agreement with the (sub-) linear dependence of PMD time delay on the length of the fibre, as given in Equation 2.10. Specifically, Ge-doped 100 m fibre offers the most stable operation, while the Ge-doped 300 m is not able to maintain the performance for DP signals over ten seconds. The former is the best candidate in the experiments involving transmission of DP signals in Chapter 4.

HNLF	Time of stable operation
Ge-doped 100 m	$\approx$60 min
Ge-doped 160 m	5 min
Ge-doped 300 m	$\ll$5 min

TABLE 6.4: Time of stable operation for different Ge-doped HNLFs

The longer and less stable Ge-doped 300 m HNLF offers a better idler OSNR than the shorter yet more stable Ge-doped 100 m fibre, in special scenarios, a trade-off has to be made, and the choice in the end depends on whether the signals are SP or DP. DP signals are more susceptible to the time variation of HNLF birefringence. Therefore,

the Ge-doped 100 m HNLF is used in experiments with DP signals, while the Ge-doped 300 m HNLF is used in experiments with SP signals.

To further enhance the duration for stable operation, a polarisation tracking scheme will be used and will be discussed in subsequent sections.

6.1.4 Pump placement

Given certain dispersion properties, the pump wavelength and separation have a crucial impact on the OPC performance in terms of uniform broadband operations. The pump placement requires the considerations of 1) phase matching, 2) signal band bandwidth, and 3) the gain bandwidth of the two FOPAs.

$$\Delta\beta = 2[\beta_{\text{even}}(\Delta\omega_s) - \beta_{\text{even}}(\Delta\omega_p)] \tag{6.2}$$

Chapter 3 discussed the phase-matching conditions for a dual-pump FOPA. As given in Equation 3.14, the pump wavelength separation term acts as a variable term which can counter-balance the finite linear phase-mismatch that combines the contributions from both the signal wavelength separation term and the even-order dispersion parameters at the central wavelength of the FOPA. Therefore, the pump spacing affects directly the CE, hence the OSNR and the performance of the idler outputs. The pump powers also contribute to the overall phase mismatch combining the contributions from nonlinear phase shift on the pumps. By experimenting with pump placement, the idler OSNR can be maximised, and the bandwidth within which the OSNR is maintained optimal can be determined.

As will be discussed in Section 6.2.1, in our experiments, the pump spacing is required to be and was set to 1.1 THz and 1.5 THz for the 3-channel WDM and the 7-channel Nyquist WDM cases, respectively, according to the signal placement principle which dictates optimal pump spacing for a given signal bandwidth. Idler CE can be analytically calculated based on the FOPA theories provided in Section 3.2. The variation of idler CE within the pumps separated by 1.1 THz or 1.5 THz determines the idler CE flatness. Figure 6.10(a) and Figure 6.10(b) displays the idler CE as a function of signal detuning from the centre frequency between the pumps. A sweeping of the centre frequency is carried out and illustrated as the third dimension in the two colour-graded plots.

The optimal phase-matching is achieved in the part of the plots where the surface formed by idler CE resembles a plateau, which means no significant idler CE dip in wavelengths close to the centre frequency. The centre frequency 192.65 THz used in the experiments falls exactly into this range. The analytically calculated idler CE profiles are plotted as in Figure 6.11

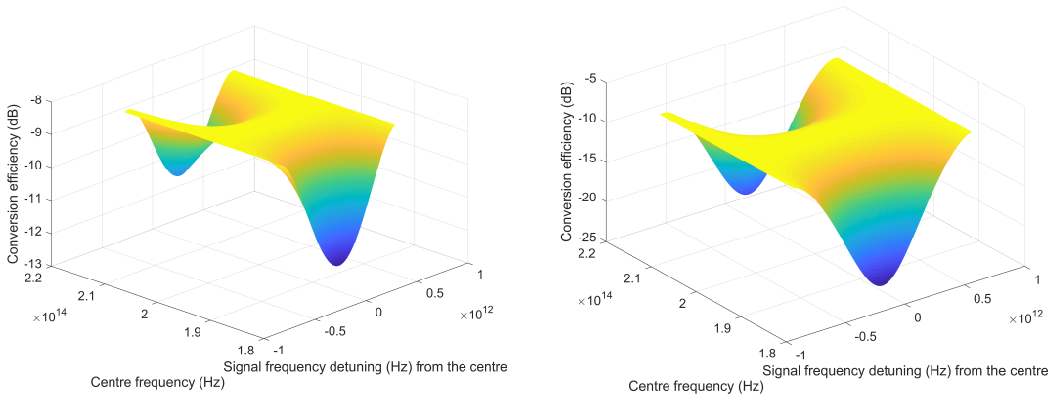

(a) For 1.1 THz pump separation (b) For 1.5 THz pump separation

FIGURE 6.10: Idler CE as functions of the 2p-FOPA centre frequency and signal detuning from the centre frequency

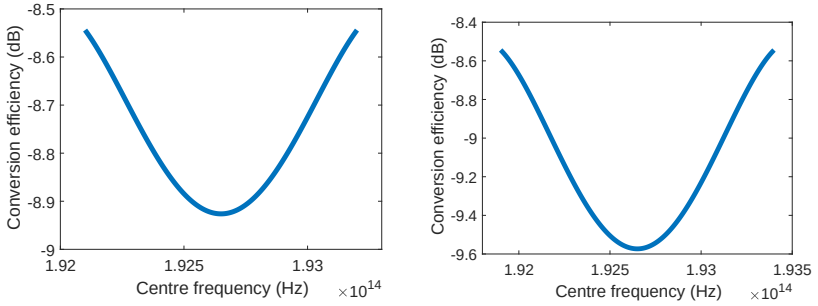

(a) For 1.1 THz pump separation (b) For 1.5 THz pump separation

FIGURE 6.11: Idler CE as a function of signal detuning from the centre frequency

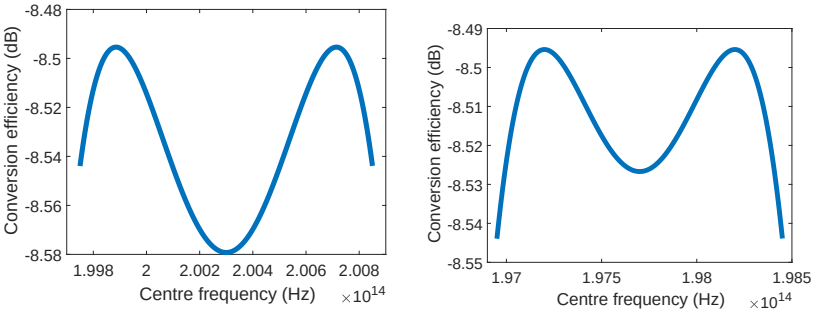

(a) For 1.1 THz pump separation (b) For 1.5 THz pump separation

FIGURE 6.12: Idler CE profiles at the 2p-FOPA centre frequency that provides maximum CE flatness

The maximum CE variations across the entire pump spacings shown in the figures are 0.5 dB and 1.0 dB. As a result, the B2B performance variations are measured to be in the range of ±0.1 dB in terms of Q factors, indistinguishable from experimental errors. Therefore, the idler CE profiles of this FOPA for both 3-channel and 7-channel cases are considered to be flat. For comparison, the idler CE profiles at centre frequencies providing the least variations are also shown in Figure 6.12, where the maximum CE

variations are about 0.05 dB. However, these two optimal centre wavelengths are 1497 nm and 1516 nm for 1.1 THz and 1.5 THz pump separation, respectively, completely outside C band. Most experimental devices in the lab operate only in C band, and a slight deviation from the optimum phase-matching condition is tolerable considering the B2B Q factor variations can be kept to about 0.1 dB when the centre frequency is set to 192.65 THz or 1556.2 nm.

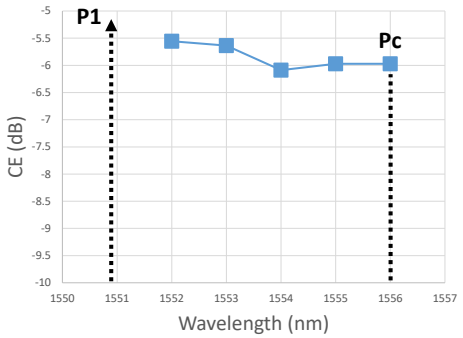

FIGURE 6.13: One-sided gain profile of the FOPA in the OPC module; P_1 is the shorter wavelength pump, and P_c is the centre between the two pumps

The 3 dB gain bandwidth of each FOPA in the OPC module is experimentally confirmed to be beyond the 1.5 THz for the OPC module. The specific value of the maximum 3 dB gain bandwidth is not determined, as it is larger than the maximum pump spacing that is allowed by the operating wavelength ranges of the pump filters. The link performance when the OPC is inserted for 14-channel DP-256 QAM NWDM signals varies on the order of only ±0.1 dB in terms of SNR when the pumps, each at a power of 22 dBm, are separated in the range between 0.9 THz and 1.5 THz (all centred at 192.65 THz). The variation of CE has been within 1 dB. For example, Figure 6.13 shows an experimentally measured one-sided gain profile, between the shorter wavelength pump and the centre between the two pumps, for a pump spacing of 1.25 THz. Note that the two pumps are co-polarised in this case to obtain maximum CEs. The CE for orthogonally-polarised pumps is about 2 dB lower than displayed. The CE is rather flat, having a maximum variation of 0.5 dB, across the measured spectral range, and possibly between the entire pump spacing since the CE profile is mostly symmetric about the centre.

6.2 Optimisation

6.2.1 Signal band placement and limitation

In principle, the two signal bands can occupy the entire bandwidth between the two pumps, if leaving enough guard bands around the pumps and the centre. In practice, even though such signal band placement provides the most efficient bandwidth utilisation, however, this comes at the expense of sub-optimal performance. The reason behind

this lies mainly in the interference of undesired FWM terms. These FWM terms can overlap with either the signal or idler bands, thereby degrading the performance of the idler output.

In Ref. [Marhic (2007)] numerical simulation using SSFM based on the NLSE of a typical dual-pump FOPA was carried out to determine the major FWM interference terms. The dominant interference terms are originated from the pump-signal FWM processes. These terms are idlers generated by either the pump-degenerated FWM process among the pump and the signal (PS) or the non-degenerated FWM process among the pump, the signal, and the idler (PSI), as illustrated in Figure 6.14. Since the PS and PSI terms are indistinguishable in terms of the bandwidth they occupy, they are not separately treated.

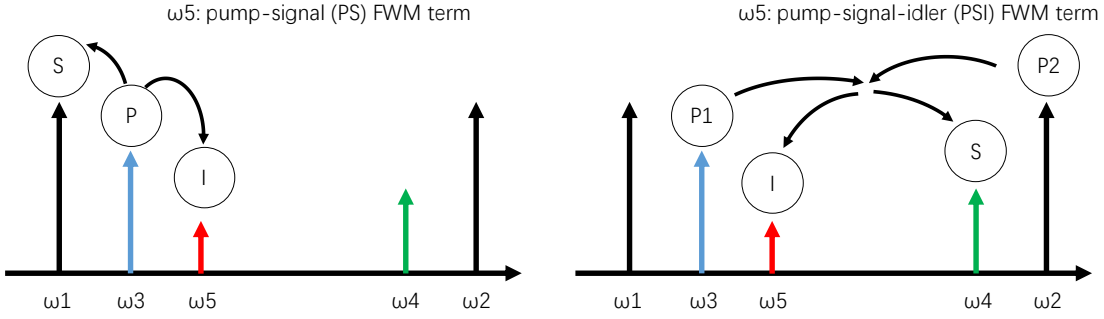

FIGURE 6.14: The origin of the dominant FWM interference terms; P, S, and I are used to denote the interacting waves in a FWM process; the unwanted FWM interference terms are named as PS (left) and PSI (right) terms, respectively.

To avoid the PSI (PS) interference terms when placing the signal band, they first need to be located. If the signal band occupies $[\omega_{s1}, \omega_{s2}]$, where ω_{s1} and ω_{s2} are used to denote the shortest and longest wavelengths by which the signal band is bounded, the PSI (PS) terms are expected to occupy $[\omega_1 + 2(\omega_{s1} - \omega_1), \omega_1 + 2(\omega_{s2} - \omega_1)]$, in which ω_1 and ω_2 are the frequencies of the two pumps. Note that the square brackets are used to show the endpoints are included. Based on this bandwidth relation, Figure 6.15 enumerates the most common signal band placement schemes, grouped by the signal band bandwidth as a fraction of the pump spacing, from half to one sixth of the pump spacing. The signal band, the idler band, and the PSI term are denoted by blue, green, and red blocks. Their different heights indicate their relative power to each other. The principle of choosing a signal band placement scheme is to find the widest signal band that avoids the overlapping of the PSI (PS) interference term with both the signal and the idler band.

Based on this criterion, both scheme 1 and 2 in Figure 6.15 provide a maximum signal band bandwidth of one sixth of the pump spacing. However, in a dual-band OPC configuration such as in this thesis, scheme 2 requires a guard band between the two neighbouring channels at the inner edges of the two signal bands in order for the WSS to split them. If the channels are densely packed, as for example in the NWDM case with

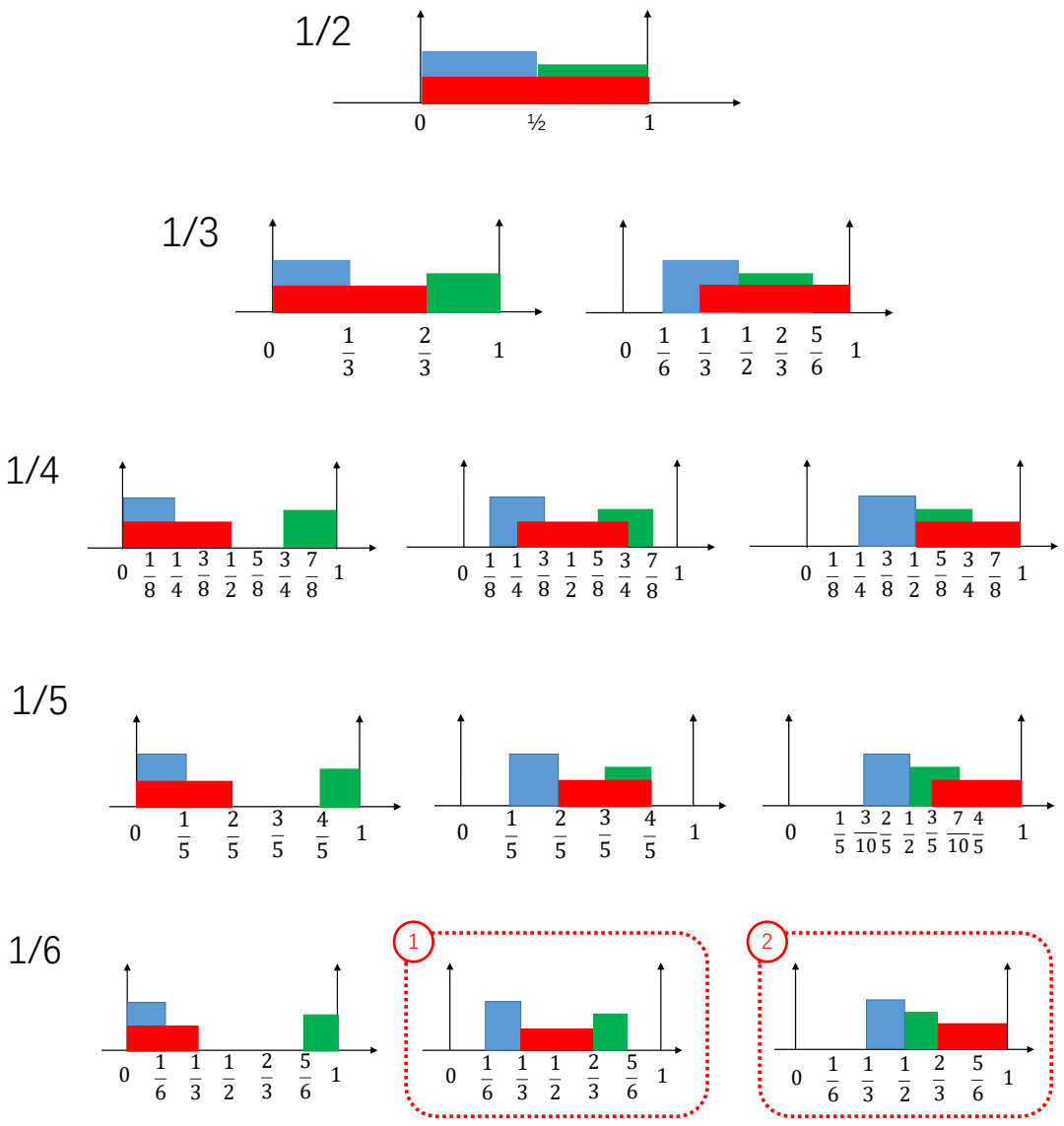

FIGURE 6.15: Enumeration of signal band placement schemes, grouped by the signal band bandwidth as a fraction of the pump spacing; blue: the signal band, green: the idler band, red: the PSI (PS) FWM interference terms; scheme 1 and 2 are labelled with red dotted squares.

no guard band at all between consecutive channels, scheme 2 is not practical. Scheme 1, in which the signal and idler bands occupy the frequency ranges $[\omega_1 + (\omega_2 - \omega_1)/6, \omega_1 + (\omega_2 - \omega_1)/3]$ and $[\omega_c + (\omega_2 - \omega_1)/6, \omega_1 + (\omega_2 - \omega_1)/3]$, respectively $(\omega_c = (\omega_1 + \omega_2)/2)$, is used in all OPC experiments in this thesis. Note that the parentheses are used to show the endpoints are excluded. The signal and idler bands swap their bandwidths for the other FOPA in the OPC module.

The spectrum in Figure 6.16 show an actual example of scheme 1. The transmitted signals are 7-channel NWDM signals, respectively. Note that the FWM interference terms fall between the signal and idler bands as designed.

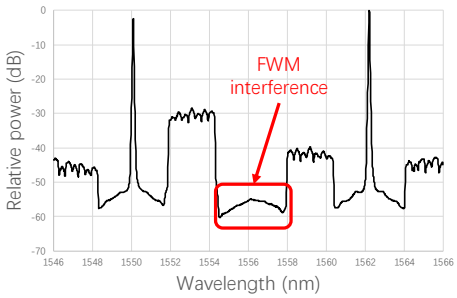

FIGURE 6.16: The PSI(PS) FWM interference for 7-channel NWDM signals

6.2.2 Signal powers into OPC module

The signal power into the OPC is an important factor on which the OPC performance depends. For a given FOPA operating in the small-signal regime, the idler power is proportional to the signal power as in Equation 3.10. As the signal power increases, the OSNR of both the signals and the idlers are increased, leading to improved performance, until reaching a point where the performance, degraded by the excessive signal-signal FWM interference that grows exponentially with the signal power if phase-matched, overweighs the improvements brought about by the additional signal OSNR. Therefore, there exists a peak performance at an optimal signal input power, at which point the OPC module should be operated.

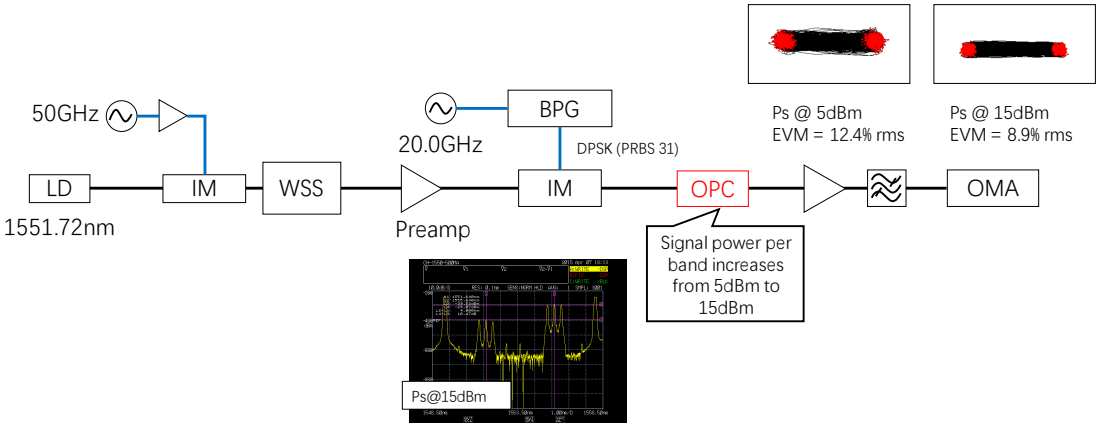

FIGURE 6.17: The performance (top right insets: constellations of the middle channel) improves as the signal input power per band increases in the OPC module

A 3-channel DPSK transmitter is set up for B2B OPC performance measurement using the EVM as the performance metric. For the second version of the OPC module, the EDFA output power before the WSS is set to 5 dBm and 15 dBm for comparison. Therefore, the signal band power at the input of the HNLF is less than stated in this section. Note that a 10 dB attenuation exists between the WSS outputs and the HNLF inputs due to the 7 dB coupler and the insertion loss of the circulator, the PC, etc. The EVM decreases from 12.4%rms to 8.9%rms after the signal input power is increased,

showing that up until the maximum allowable power of 15 dBm for the second version OPC module, the performance improves with increased signal input power.

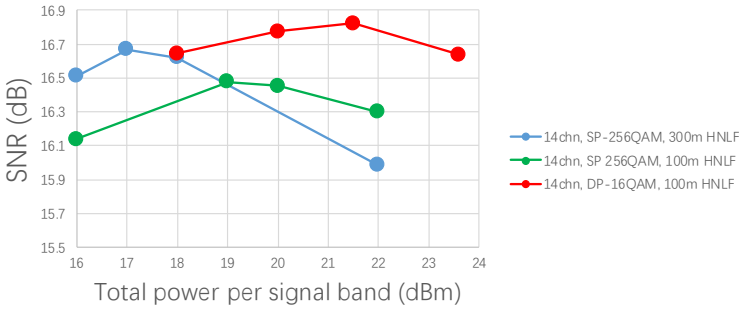

FIGURE 6.18: Performance as a function of signal input power per band

For the third version OPC module as in Figure 6.6, the signal input power per band can be further increased to more than 20 dBm per band. Note that there is also a 10 dB attenuation between the EDFA output and the input of the HNLF. Figure 6.18 shows the performance in terms of SNR of the 440 km DUC link with mid-link OPC as a function of the total signal input power per band. In this case, seven Nyquist WDM (NWDM) 256 QAM signals at 40 GBd per band are used. Table 6.5 summarises the optimal total signal input power per band for the two HNLFs that have been chosen. The signals with the 300 m Ge-doped HNLF offers better peak performance, and the optimal total signal input power per band is approximately 17 dBm, whereas 100 m Ge-doped HNLF offers a slightly lower peak performance at a 2 dB higher optimal total signal input power per band of 19 dBm, due to its shorter length. A third set of data deals with DP signals when using the Ge-doped 100 m HNLF and shows that the optimal total signal input power is 22 dBm, which is also 19 dBm per polarisation, i.e. identical to the SP case. This implies that the optimal total signal power per channel per polarisation for this type of transmitted NWDM signals should be about 10.6 dBm (i.e. 0.6 dBm at the HNLF input), regardless of the modulation format and the use of PolMux. Relevant OPC experiments will make use of these findings.

Table 6.5 also includes a measurement on dual-band 6-channel DP-16QAM signals, which confirms the conclusions above. These signals will be used in the experiments described in Chapter 7.

HNLF	Signal configuration	Optimal signal input power per band in dBm	Peak SNR in dB
Ge-doped 300 m	SP-256 QAM 7chn NWDM	17	16.6
Ge-doped 100 m	SP-256QAM 7chn NWDM	19	16.4
Ge-doped 100 m	DP-16QAM 7chn NWDM	22	16.8 for XPol
Ge-doped 100 m	DP-16QAM 6chn WDM	17	Q factor: 9.8dB

TABLE 6.5: Optimal signal input powers per band for different HNLFs and modulation formats

6.2.3 Signal polarisation insensitivity

6.2.3.1 Assessment of pump orthogonality

Insensitivity to the polarisation of the input signals is an indispensable feature of OPC since the SOP of the transmitted signals is prone to random changes with time. To assess the polarisation sensitivity of the OPC module, the system with a PC in place, before the OPC signal input, is tested in transmission. The manual PC is able to sweep the SOP of the input signals randomly across the Poincare sphere. The sweeping of the SOP of signals is expected to emulate the variation of the signals' SOP over time, due to a combination of factors such as the temperature and sound vibration along the link.

The transmitted signals comprise two 7-channel NWDM bands modulated with DP-256 QAM at 40 GBd. The OPC follows 220 km transmission. After the OPC module is set up and tuned maximising the orthogonality of the two pumps, the PC at the signal input is manually adjusted to ten different positions, and the corresponding performance is recorded at the receiver. The performance in terms of SNR remains almost unchanged, with SNR variations in the range of +/- 0.1 dB, which is within experimental error. This result demonstrates that the orthogonality of the pumps, hence the signal polarisation insensitivity, allows a polarisation-independent performance of the OPC module in a link.

However, the ten random positions of the input PC do not cover every region on the entire Poincare sphere, and the polarisation-independent performance may have been obtained only by chance. One way to test all regions of the Poincare sphere is to have a polarisation scrambled signals at the place of the input PC. This method is used in the following section to test the effectiveness of the pump polarisation tuning technique.

6.2.3.2 Verification of the pump polarisation tuning technique

It is the orthogonally polarised dual-pump FOPA configuration that enables the signal polarisation insensitivity. The control of the SOP of the two pumps is critical for setting up the OPC module.

As shown in the setup of the OPC module in Figure 6.6, the SOP of the two pumps are directly controlled by the PCs that follow each of them. Another pair of PCs are on each optical path connecting the pump and signal waves to the HNLF. They are inserted in order to adjust the SOPs of the two pumps so that they are aligned with the principal axes of the HNLF. In the dual-pump FOPA spectrum as in Figure 6.19, the PP term is defined to be the idler generated in the FWM process that involves the FOPA pumps as the pump and the signal.

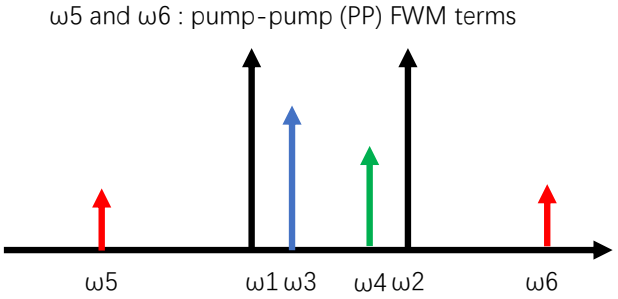

FIGURE 6.19: The pump-pump (PP) FWM terms are generated in the FWM process between the two pumps; ω_1 to ω_1 are the pump1, pump2, signal, and the idler of the FOPA.

Monitoring and reducing the two PP terms allows the two pumps to stay orthogonally polarised. They should be reduced to zero under ideal conditions. In practice, due to the finite co-polarised pump components, the PPs should have finite values. Minimising this finite value ensures the maximised orthogonality between the two pumps. Figure 6.20 shows a typical spectrum where both PPs are close to being minimised.

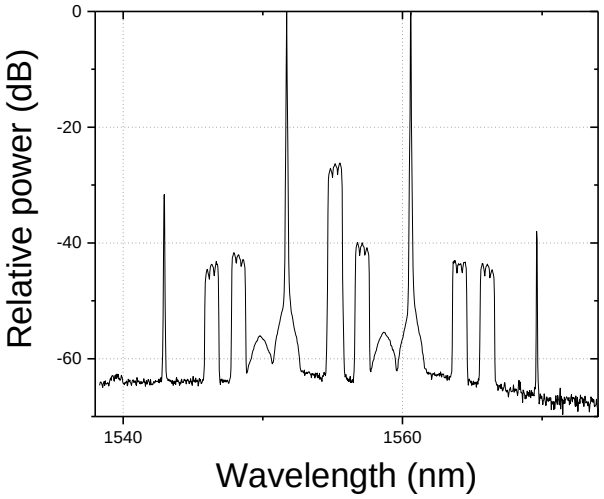

FIGURE 6.20: A spectrum showing the relative powers of the PP

Automated polarisation control is a desirable feature of the OPC module, as an automated scheme can track the time variation of the HNLF's birefringence as well as reducing the manual labour of the PC tuning. For manual tuning, an OSA can be used to monitor the power of the two PPs, whilst the four PCs are used to minimise them. In an automated scheme as in Figure 6.21, a polarisation tracker is inserted between the pump laser and the pump EDFA to change the pump polarisation directly upon the reception of a control signal, which is issued from a photon detector (PD) that monitors the PP power at one of the outputs of the HNLF. The function of the polarisation tracker is hence to minimise the PP it monitors. This automated scheme was implemented by Kyle R. H. Bottrill. The frequency of the polarisation tracker is 2 kHz so the time for

the tracker to settle and remain stable is almost instantaneous. The polarisations of the other PPs are controlled manually.

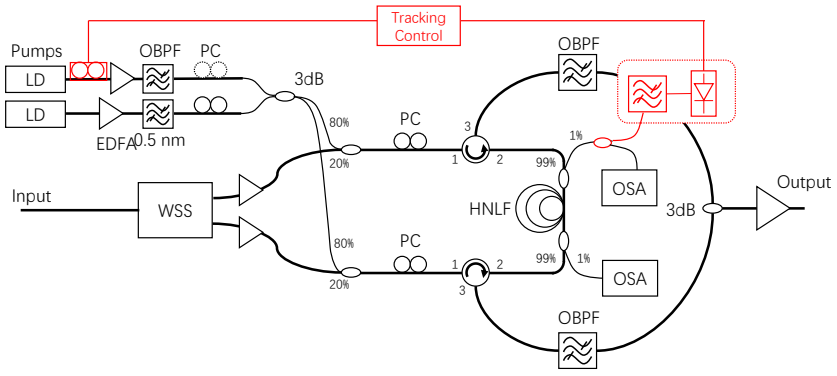

FIGURE 6.21: OPC module setup with the addition of a polarisation tracker

A set of experiments have been set up to assess the correct operation of the automated scheme and, more importantly, to investigate the relation between the power of PP and the OPC performance. Ideally, it should be confirmed from this experiment that the performance of the OPC module, either standalone or in a link, improves as the powers of both the PPs decrease.

The signal SOP is scrambled at high frequency to emulate the birefringence variation over time. The effect of the distortion in a perfectly signal polarisation insensitive OPC module would be negligible. Any residual co-polarised pump polarisation components would cause performance variations. The variations are calculated from the eye diagram on a DCA. Assuming the noise is Gaussian, SNRs that are directly measurable from the colour-graded eye diagram can be used as the performance metric to quantify the performance variation due to the residual signal polarisation dependence.

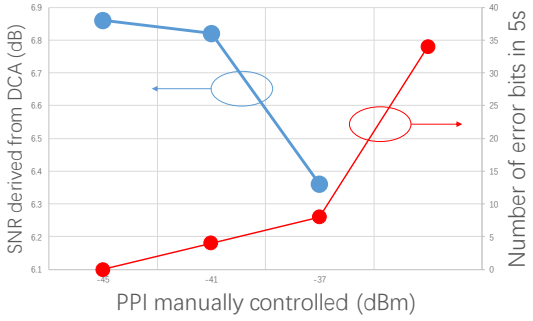

FIGURE 6.22: The B2B performance with OPC in terms of SNRs or numbers of error bits as a function of the PP powers

The experiment for this B2B configuration with OPC is set up. A polarisation scrambler, having a polarisation scrambling frequency of 2 MHz, is installed at the signal input of the OPC module and before the WSS. The transmitter provides a single-channel 40 GBd OOK signal. The SNR is measured in a colour-graded eye diagram with a DCA as the receiver.

A reduction in the PP powers should improve the SNR of a polarisation-scrambled signal derived from the eye diagram by the receiver DCA.

Figure 6.22 shows the experimental results. As the PP power increases from -45 dBm to -37 dBm, the SNR of the OOK signal decreases from 6.86 dB to 6.36 dB. The relation is monotonic. The receiver is swapped to a bit error counter to obtain the BERs, and the BERs are also shown to increase with increasing PP powers. These experimental results confirm that such a monotonic relationship exists, which validates the effectiveness of this pump polarisation tuning technique that is based on monitoring and minimising PP powers.

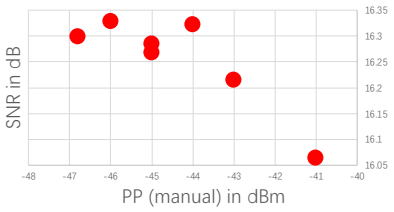

FIGURE 6.23: The link performance with OPC as a function of the PP powers

To account for the combined effect with the time variation of the signal input polarisation, the same validation process is also carried out in the transmission link instead of for B2B configuration alone. The experiment is set up in the 440 km link for fourteen DP-256 QAM NWDM signals with the OPC module in the mid-point. SNRs are measured as the performance metrics. In general, the SNR decreases with the PP power as in Figure 6.23, showing the effectiveness of the PP technique in a link environment. This tuning technique is hence used in all experiments of both SP and DP signals.

It is worth discussing that, unlike in laboratory settings, none of the HNLFs, especially the Ge-doped 300 m fibre, can sustain a stable operation for practical applications if only one PP term is monitored. Complete polarisation tracking requires monitoring both PP terms for both parametric processes. Under this scenario, simultaneous tracking and minimising all of the four unwanted PP idler terms is expected to offer stable operation for sufficiently long to sustain practical applications as well as close to perfect pump orthogonality hence signal polarisation insensitivity. Issues such as the demand on balancing the intensity of the four terms during this process are easy to envisage, considering that the intensity of the four terms is inter-related and that minimising that of one may increase those of the others.

Due to the limited availability of polarisation trackers and time constraint, this full automation scheme has not been implemented. As no previous investigation has been found in literature, the potential obstacles to its proper function remain to be discovered as a future work.

6.3 Characterisation

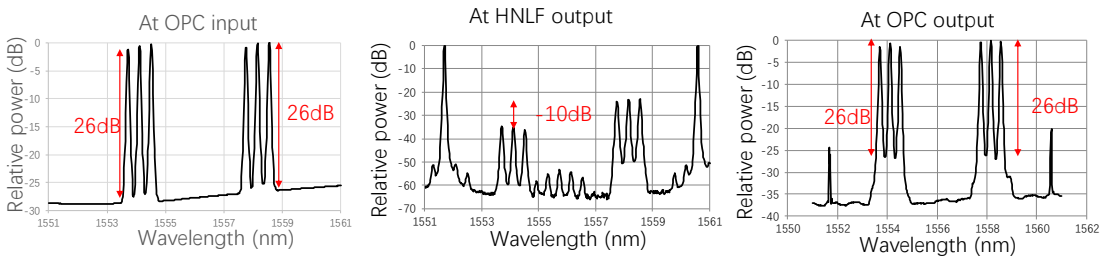

FIGURE 6.24: The spectra at the OPC input (left), the HNLF output (middle), and the OPC output (right) when the OPC module is placed in a link

OSNR is a direct indication of the signal quality, and the OSNR degradation may be readily available by rough estimation from the spectra. Figure 6.24 show the spectra taken at the input, within, and the output of the OPC module. The signals are dual-band 6-channel DP-16 QAM at 10 GBd and are transmitted in the 800 km DM link with the OPC placed at the mid-point. The definitions of different OSNRs are given in Figure 6.25.

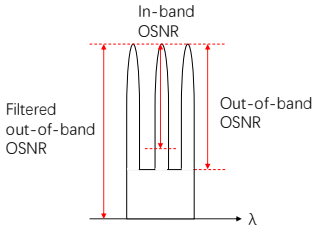

FIGURE 6.25: Three different OSNRs defined

By observing Figure 6.24, the out-of-band OSNR is not degraded inside the OPC module, which does not reflect the fact that noises have been added at the pre- and post-OPC EDFAs and in the FOPAs themselves. Therefore, the in-band OSNR cannot be directly deduced from the out-of-band OSNR by means such as interpolation. The quantification of the performance of the OPC module has to resort to the direct measurement of the OPC module performance in the B2B configuration.

The actual performance of the OPC module is quantified by comparing the B2B performance for various types of signals of interest for the cases when OPC is and is not used. This section provides the experimental results for B2B performance for various types of signals that are going to be used in experiments involving transmission. These various types of signals include SP-16 QAM and DP-16 QAM.

In general, the performance is degraded after applying the OPC, due to a combination of factors such as the transfer of pump noise onto the idler and the additional ASE noise from the built-in EDFAs. The baud rate is also related to the B2B performance whether the OPC is in place or not. If the transmitter is operating close to its performance limit,

the signal waveforms with a lower baud rate are more accurately defined, which improves the signal quality.

All results can be used as a reference for comparison with the link performance. The B2B performance of these different transmitted signals set an upper limit for the link performance without or with the OPC in place.

No.	Signals	The HNLF	B2B Q factor w/o OPC for the middle channel	B2B Q factor with OPC for the middle channel
1	SP-16 QAM at 10 GBd	Ge-doped 300 m	10.4 dB	10.3 dB
2	SP-16 QAM at 5 GBd	Ge-doped 300 m	11.2 dB	11.0 dB
3	SP-16 QAM at 2.5 GBd	Ge-doped 300 m	11.5 dB	10.9 dB
4	DP-16 QAM at 10 GBd	Ge-doped 100 m	10.4 dB	9.8 dB

TABLE 6.6: B2B performance without and with OPC for different HNLF and signals

6.4 Summary

This chapter begins by listing the design requirements of an OPC design and discusses the approaches of its implementation to achieve features such as the efficient bandwidth utilisation and the signal polarisation insensitivity. The implementation cost is also taken into account.

The OPC module setup design evolution is described and discussed. The main motivation is to increase the pump and signal powers delivered to the HNLF input while retaining the essential features of the OPC design.

The choice of the nonlinear medium is discussed. Different HNLFs are evaluated regarding the idler CE and the typical time of stable operation. Trade-offs have to be made in balancing the need of high nonlinearity, high SBS threshold power, small PMD, and various other parameters.

The impact on OPC performance of different pump spacing is also tested and discussed.

The chapter continues with the optimisation of the OPC module. Signal band placement is found to be critical in optimising the OPC performance. An optimum signal band placement scheme is devised by identifying and avoiding the major FWM interference terms that fall between the two pumps in the spectrum.

The optimal signal band power into the HNLF is found for various signals. These power settings strike a balance between the signal-signal FWM interference and the signal OSNR.

The techniques to monitor and to tune the pump polarisation orthogonality is devised and implemented. The effectiveness of these automated techniques is tested and verified.

This chapter is concluded with a B2B performance characterisation without and with the OPC module in place for the most typical signals in transmission. These performance evaluations suggest that the OPC module is ready to be integrated into the transmission system for nonlinearity mitigation as it will be described in the following chapter.

Chapter 7

Nonlinearity mitigation by OPC

7.1 Introduction

This chapter evaluates the performance of the OPC module placed at about the mid-point of different transmission links using a variety of modulated signals and numbers of WDM channels. The primary aim of this series of experiments is to prove the effectiveness of our OPC scheme, and, most importantly, this technique in general for the mitigation of nonlinearity-induced impairments under different scenarios. Furthermore, these experiments endeavour to relate the performance improvements by OPC to key transmission system parameters such as the modulation format, the PolMux, the WDM channel count, the transmission distance, and the use of optical inline dispersion management. Ideally, performance improvements brought about by mid-link OPC is expected to be agnostic to the types of the transmitted signals such as the modulation format, a certain extent to the WDM channel count, and the use of PolMux, but influenced by the link characteristics such as the transmission distance, power symmetry about the mid-link, the use of DM, etc. The effects of these different system parameters are experimentally tested. In this chapter, based on these evaluations and comparisons, mid-link OPC is shown to be capable of compensating for nonlinear impairments in conventional EDFA lump-amplified field-installed SMF-based transmission systems. A 3 dB improvement in terms of Q factor has been observed in DM links, and up to 0.5 dB in DUC links, as will be discussed in this chapter.

7.2 6-channel and 13-channel SP-16 QAM signals in a 400 km DM link

The first set of experiments investigates the effectiveness of the nonlinearity mitigation capability of the OPC module that has been introduced and characterised in the previous

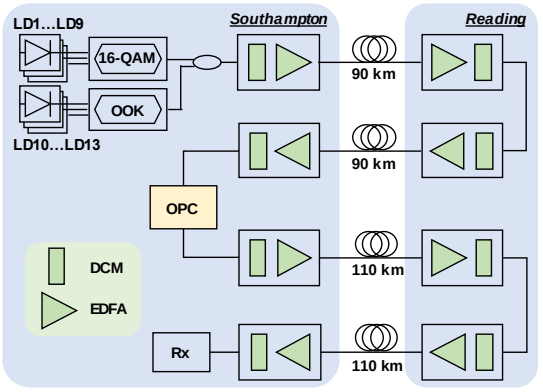

FIGURE 7.1: The link setup for the 400 km DM link with 13-channel signals modulated with 16 QAM or OOK at 10 GBd

chapter. In this section, the OPC module used is the second version (refer to Figure 6.5) in which the total signal input power per band is limited to 17 dBm, which corresponds to 12 dBm per channel for three channels per band. In this version of the OPC module, after passing through the WSS, the ASE noise outside the signal bands is effectively filtered out, and the signal band power is further reduced typically by about 4 dB. The OPC module is placed in the 400 km DM link connecting Southampton to Reading, with the addition of 34 km SMF spools in the Southampton lab to help match the total dispersion and dispersion slope of the entire link. The link setup schematic is given in Figure 7.1. The transmitter generates 6-channel 16 QAM signals at 10 GBd, grouped into two signal bands, each on a 50 GHz grid and centred at 1558.17 nm (192.4 THz) and 1554.13 nm (192.9 THz) respectively.

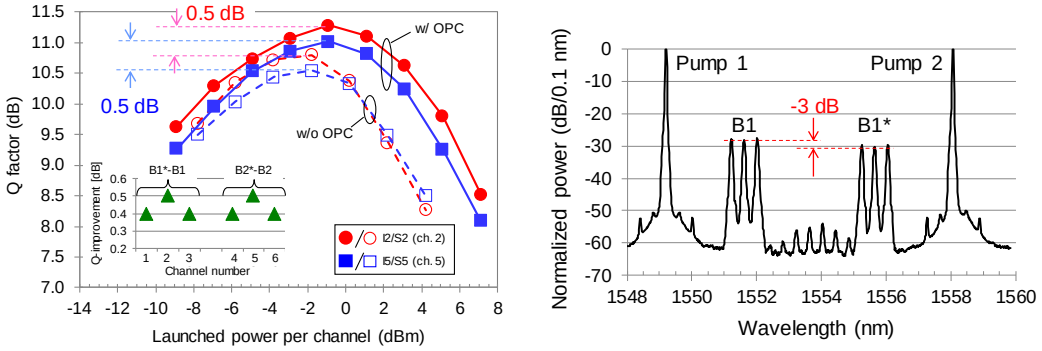

FIGURE 7.2: The performance in terms of Q factor against the launch power per channel for 6-channel signals (left) and the spectrum at the output of the HNLF (right) in this case

The link conditions for mid-link OPC are not ideal. Firstly, the OPC is not placed at the exact physical centre of the link. Secondly, the power profile is asymmetric with respect to the ideal mid-link OPC configurations, owing to the use of conventional lumped amplification by EDFAs.

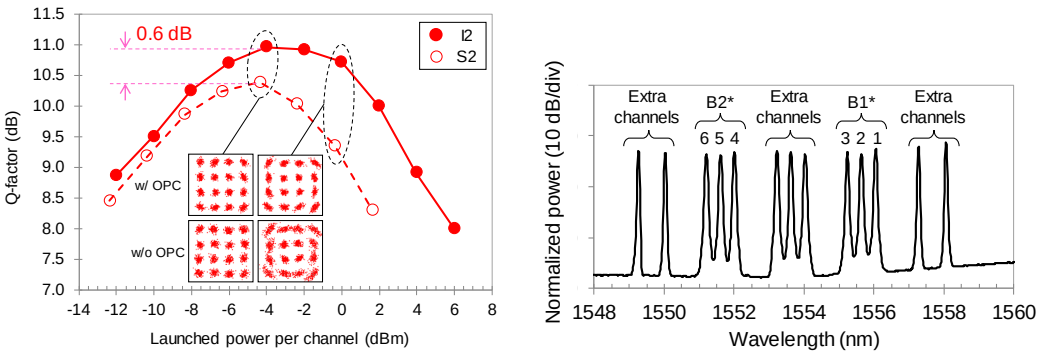

FIGURE 7.3: The performance in terms of Q factor against the launch power per channel for 13-channel signals (left) and the spectrum at the input of the receiver (right) in this case

The idler CE is in the vicinity of -3 dB as shown in the spectrum on the right in Figure 7.2, which is taken at one of the outputs of the HNLF. Under these conditions, Figure 7.2 (left) shows the measured performance in terms of Q factor as a function of launch power per channel for the cases without and with OPC for the two middle channels. As shown in the plots, the optimal launch power is increased by 1 dB and the peak performance in terms of Q factor after applying OPC is improved by 0.5 dB for both of the middle channels in the two signal bands, reaching a value in excess of 11.0 dB, almost comparable to the B2B performance as summarised in Table 7.1. The rest of the six channels show similar improvements as shown in the inset of Figure 7.2. Compared to that for the case of the 800 km link introduced later in this chapter, this improvement is relatively small, which may be attributed to the non-ideal link conditions and the noisy OPC module. The small Q factor improvement can be translated into a mere marginal transmission reach enhancement as the Q factor is linearly related to the OSNR.

There is a possibility that the performance improvement increases with the number of WDM channels since the signal-signal and signal-noise FWM interference also increases with the number of the WDM channels. To investigate whether the increase of the WDM channel count further enhances the OPC performance improvement, the channel count is increased to thirteen. The additional channels are inserted between and outside the existing two signal bands to set up an evenly spaced WDM configuration expanded from the 6-channel case. Figure 7.3 (right) is the received spectrum at the input of the receiver, showing the arrangement of channel wavelengths. Note that those channels that are outside the original signal bands are modulated with OOK signals at 10 GBd. Only the two original signal bands are phase conjugated in the OPC module.

The overall peak performance with OPC is slightly reduced compared to the 6-channel case, while the performance improvement is about 0.6 dB for one of the middle channels, close to that of the 6-channel case. As the nonlinear impairments are more severe, the optimal launch power per channel is reduced from -1 dBm to -4 dBm. The Insets in Figure 7.3 show the constellation without and with OPC. The outer constellation points

show significant spread of phase noise, which is reduced when the OPC is in place, indicating the effective nonlinear phase noise reduction.

In this section, the OPC module proposed is shown to have mitigated part of the nonlinearity in the SMF-based EDFA-amplified field-installed transmission system for WDM signals with advanced modulation formats. Similar performance improvements are observed when the number of WDM channels are increased from six to thirteen.

7.3 6-channel SP-64 QAM signals in a 400 km DM link

The previous section has studied the nonlinearity mitigation by OPC of 16 QAM signals in a field-installed link. Since it is known that the performance is increasingly susceptible to nonlinear impairments as the order of modulation formats increase [Agrawal (2012)], such a higher order modulation format namely 64 QAM is tested for the same link transmitter and link setup. The 6-channel 64 QAM signals at 10 GBd are sent over the same 400 km DM link as in Figure 7.1. The received signal spectrum is given in Figure 7.4. The coherent receiver detects the signals and produces BER measurement results by offline processing. These results are also converted into Q factors in order to be comparable with the results from other sets of experiments. The BER performance as a function of launch power per channel is summarised in Figure 7.5 for the two middle channels of the two signal bands. The performance imbalance between the two signal bands is the result of the non-uniform gain profile of the EDFAs across the spectrum as described in Chapter 5. The Q factor improvements, after converting from BER to Q factor using the equation $Q = 20\log_{10}(\sqrt{2}\mathrm{erfc}^{-1}(2\mathrm{BER}))$, amount to 1.8 dB and 2.5 dB for the two middle channels respectively. These figures are much larger than those for the 16 QAM case, and should be attributed to the use of the higher order modulation formats. More specifically, 64 QAM signals are more prone to the nonlinear impairments due to the much smaller Euclidian distances among neighbouring constellation points. Another reason of the much larger increase in performance improvement lies in the limited transmitter performance, especially the limited bandwidth (9.6 GHz) and the effective number of bits (ENOB) of the AWG that is used to generate the electrical input of the IQ modulator. In Figure 7.5, the B2B BER is about 0.03 for both channels, which can be converted to a Q factor of 5.5 dB, worse than the signal quality for the 16 QAM case. This indicates that the transmitter exhibits considerable noise due to its performance limitation. The transmitter noise interacts with the signals along the first half of the link generating signal-transmitter noise nonlinear interference, and this interference is reversed and compensated for in the second half, as suggested in [Galdino et al. (2017a)]. Ideally, the performance degradation due to transmitter signal-noise interaction can be effectively alleviated by OPC. As a result, assuming the transmitter

noise and signal FWM interference is one of the major factors of performance degradation, the corresponding performance improvement by OPC may increase in cases the transmitter noise is high.

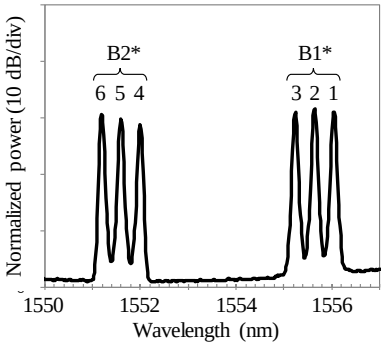

FIGURE 7.4: The typical spectrum at the input of the receiver with labelled channels

The plots for all six channels without and with OPC are shown in Figure 7.6. It can be observed that the six channels exhibit similar optimal launch powers without and with OPC at about -4 dBm and 2 dBm, respectively. The Q factor improvements for the six channels are between 1.2 dB and 2.5 dB, as summarised in Figure 7.7. The middle channels experience the greatest performance improvement as they suffer more from signal-signal FWM interference [Goebel and Hanik (2008)], hence allowing themselves to benefit the most from the reduction of nonlinearity.

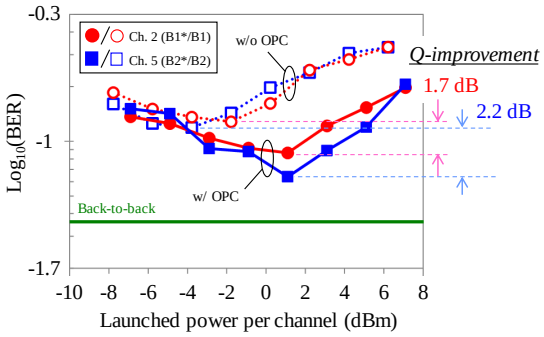

FIGURE 7.5: Performance in terms of BER as a function of launch power per channel for the two middle channels in the two signal bands

The spectra at key locations along the transmission link are given in Figure 7.8. As can be seen, the channel powers are equalised at the mid-link. The shorter wavelength signal band initially is set to be 3 dB higher than the longer (Figure 7.8 (top left)) so that at the mid-link (Figure 7.8 (top right)) the power of the two signal bands are equalised. The imbalance in gain continues, and the power difference is reversed. When reaching the receiver, the power of the shorter signal band is 3 dB lower (Figure 7.8 (bottom left and right)) regardless of the use of OPC.

In this section, the order of the modulation format is further pushed to 64 QAM, higher performance improvements by OPC are observed.

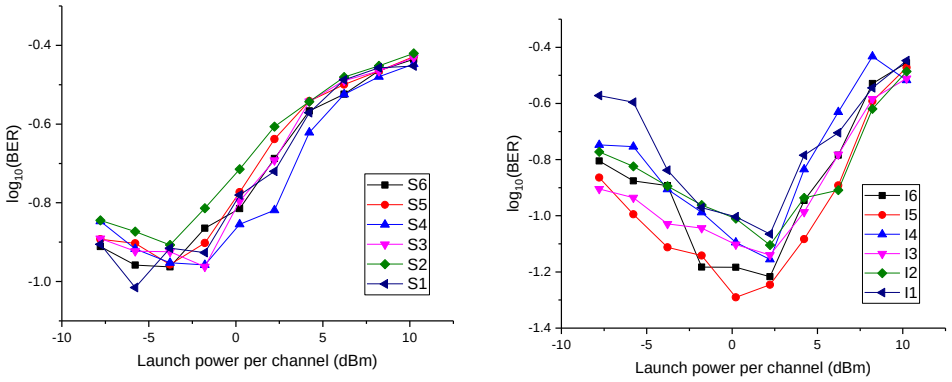

FIGURE 7.6: Performance in terms of BER as a function of launch power per channel for transmission of all six channels without (left) and with (right) OPC

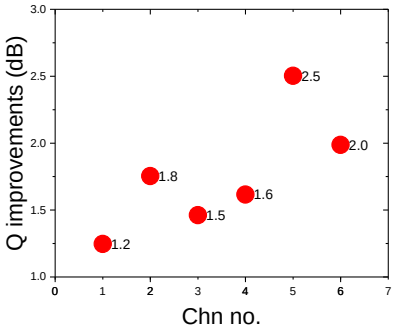

FIGURE 7.7: Q factor improvements for the six channels

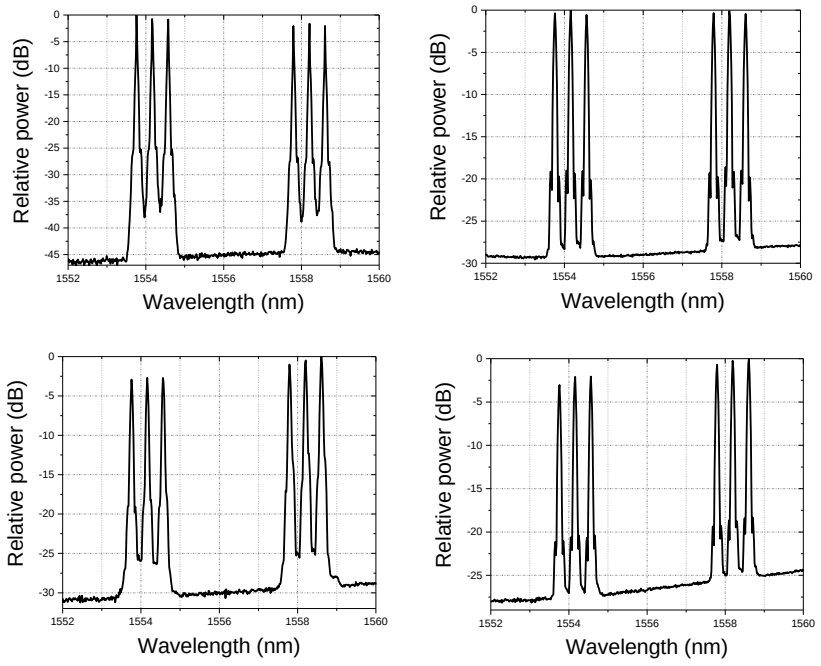

FIGURE 7.8: The spectra at the output of the transmitter (top left), the mid-link (top-right), the input of the receiver without (bottom left) and with (bottom right) OPC

7.4 6-channel DP-16 QAM signals in an 834 km DM link

Our OPC scheme is designed to be insensitive to the polarisation of the input signals as discussed in Chapter 6. The signals in the previous experiments are modulated on a single polarisation, and there is no adjustment of the signal polarisation at the input of the OPC module. To exploit further its polarisation-insensitive operation and to verify its compatibility with PolMux signals, the transmitter is set up to provide the same 6-channel signals but a PolMux emulator is added to the setup to generate DP-16 QAM as in Chapter 5. The equivalent bitrate is thus doubled to 0.48 Tbps when a total of six channels at 10 GBd are used.

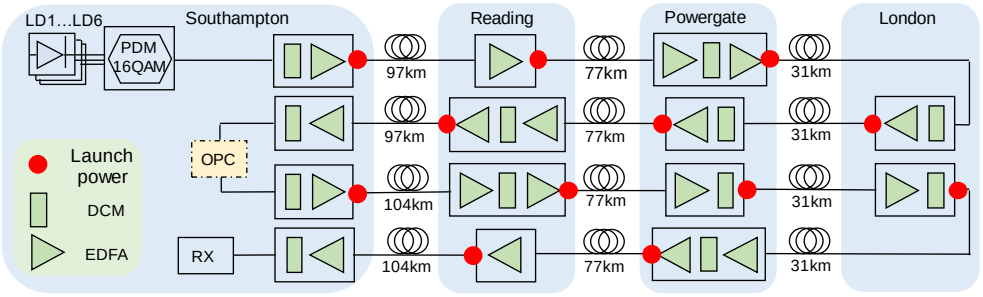

FIGURE 7.9: Transmission link setup for the 834 km DM link between Southampton and Telehouse, London

The transmission distance is another factor that affects the total nonlinear impairments incurred, as it is evident that the nonlinearity is proportional to the total effective length of the fibre. Signals with increased nonlinear impairments may benefit more from mid-link OPC, which remains to be tested. The field-installed transmission link is extended to Telehouse, London, doubling the distance from 400 km to 834 km, to test this OPC module and its compensation capability in a longer link where the span lengths now vary (with different span lengths of 97 km (104 km), 77 km, and 31 km, as shown in Figure 7.9) and the power profile symmetry further deteriorates. The link setup is given in Figure 7.9. The performance improvement may decrease, due to these non-ideal link conditions for OPC, or increase due to the greater nonlinear impairments the signals in the longer link suffer. The net result hence needs to be experimentally investigated in this section.

Before extending the link, the performance improvement is measured for the DP-16 QAM signals in the original 400 km link. Figure 7.10 shows the performance of the two middle channels versus their launch power. The performance improvement in terms of Q factors is approximately 0.3 dB, which is comparable to that for the SP-16 QAM case. Similar performance improvement is seen for the remaining channels, indicating that the OPC module can handle PolMux signals without deterioration in its performance.

After extending the link to 834 km, the same set of measurements has been taken again, the result of which are summarised in Figure 7.11 11 (left). The figure represents BER

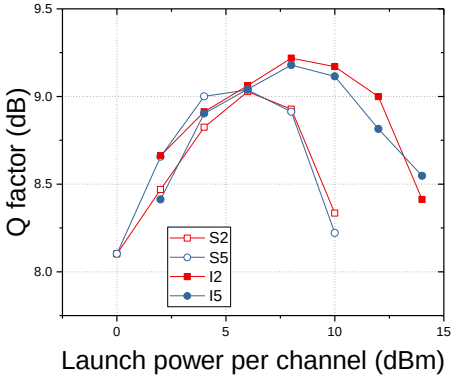

FIGURE 7.10: Performance in terms of Q factor as a function of launch power per channel for the two middle channels in a 400 link

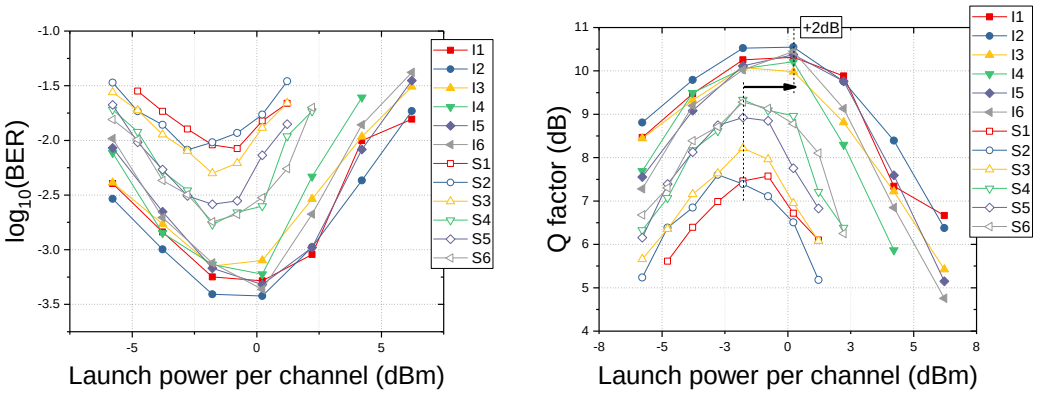

FIGURE 7.11: Performance in terms of BER (left) and Q factor (right) as a function of launch power per channel

of the DP-16 QAM signals as calculated by offline-processing using data received by the coherent receiver and the real-time oscilloscope. For comparison, Q factors are extracted from the BER values, and are presented in Figure 7.11 (right). The idler CEs are about -10 dB, as the HNLF used is now the Ge-doped 100m fibre which exhibits a lower CE than the 300m fibre used in the SP-16 QAM and SP-64 QAM experiments. Their differences have been discussed in Chapter 6.

The distinctive Q factor improvements range between about 1 dB to 3 dB as shown in Figure 7.12. Compared to 0.5 dB for the SP-16 QAM case and 0.3 dB for the DP-16 QAM obtained previously, the much larger improvements are apparently due to the doubled transmission distance, which is the only variable that has been altered.

These results imply that in this particular link setup, the doubled transmission distance inflicts stronger nonlinear impairments, which are then mitigated to a larger extent by OPC, hence the resulting significant increase in performance improvements. This shows that mid-link OPC may benefit more transmission systems with longer distances.

The optimal launch power per channel increases by 2 dB from -2 dBm to 0 dBm when OPC is in place, confirming the reduction of nonlinearity by OPC. The constellation

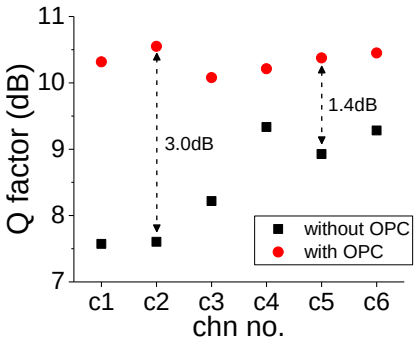

FIGURE 7.12: Q factors and improvements for the six channels

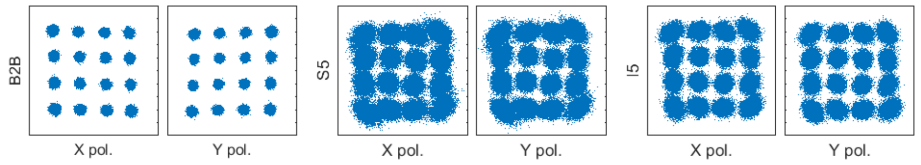

FIGURE 7.13: Constellation diagram for one of the middle channels when in B2B configuration, transmission without OPC, and with OPC, respectively

diagrams for channel 5, one of the middle channels, are shown in Figure 7.13. The reduction of nonlinearity induced noise is clearly visible through the reduced spread of both amplitude and phase noise.

In this section, DP signals are used in the OPC experiments, and it has been demonstrated that the use of PolMux does not have a large impact on the performance improvement. Moreover, the link distance has been doubled to 834 km, and the performance improvement is greatly increased regardless of the increase of link power asymmetry.

7.5 6-channel DP-16 QAM signals in a DUC link

Compared to DM links, the signals in DUC links are less afflicted by nonlinearity thanks to the removal of optical inline DCMs and the corresponding EDFAs. At the same time, the link maintains the complete compensation of dispersion and dispersion slope of the signals by EDC, for example, at the receiver end. Not only does the simplicity of the DUC link setup has appealed to the current generation of deployed SMF transmission systems, the higher local dispersion also results in broadening of the signal pulses, which in turn reduces the peak power of these pulses, thereby reducing the overall induced nonlinear effects, hence increasing the overall transmission reach.

Therefore, for the same link setup transformed from DM to DUC by removing all inline DCMs and corresponding EDFAs, the performance without OPC is expected to be

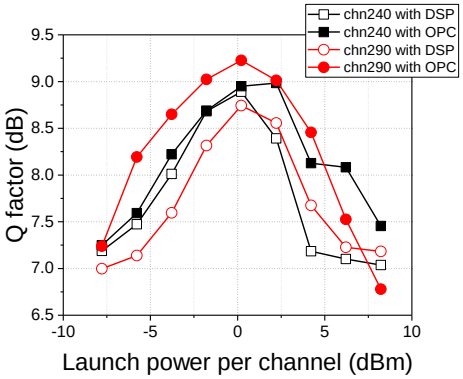

FIGURE 7.14: Performance in terms of Q factors as a function of launch power per channel for the two middle channels

better, due to the reduction in linear noise and nonlinear impairments from the above-mentioned sources. The potential performance improvements that the mid-link OPC brings about is hence expected to be lower than in DM links.

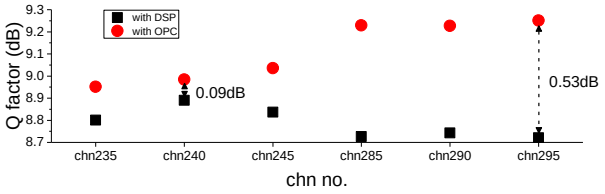

FIGURE 7.15: Q improvements and peak performance without and with OPC for six channels

A set of experiments for DP-16 QAM signals in the 800 km DUC link have been performed to investigate the impact of this change. The 800 km DUC link setup is identical to that of the previous DM link but without the inline DCMs and the corresponding EDFAs. The link is prepared as in Chapter 5, and is schematically shown in Figure 5.21. The transmitter is identical to the one used in the six-channel DP-16 QAM experiment. The channel powers are equalised at the mid-link before the OPC input, and the spectra at various positions in the link are shown in Figure 7.16. The shorter signal band initially is given a higher power (Figure 7.16 (left)) such that the accumulated EDFA gain tilt eliminates the initial power imbalance at the mid-link (Figure 7.16 (middle)). The power difference at the transmitter is 5 dB, higher than the 2 dB for the 434 km link, due to the doubled transmission distance. The performance comparison between using the OPC module alone to compensate simultaneously the dispersion and nonlinearity and using the EDC DSP alone at the receiver to compensate for the dispersion is shown in Figure 7.14. The optimal launch power of one of the middle channels is increased by 2 dB, while the peak performance of the other middle channel is increased by 0.5 dB. These results indicate the effective nonlinearity mitigation for both signal bands. The Q factor improvement obtained for the various channels without and with OPC is summarised in Figure 7.15. The wavelength-dependence of the improvement is due to the

non-uniform gain profile of the EDFAs. Compared to Figure 7.11, the optimal launch power with OPC is 2 dB higher in the DUC link than in the DM link. This is a direct result of the reduction of the accumulated nonlinear impairments after removing all the DCMs and corresponding EDFAs.

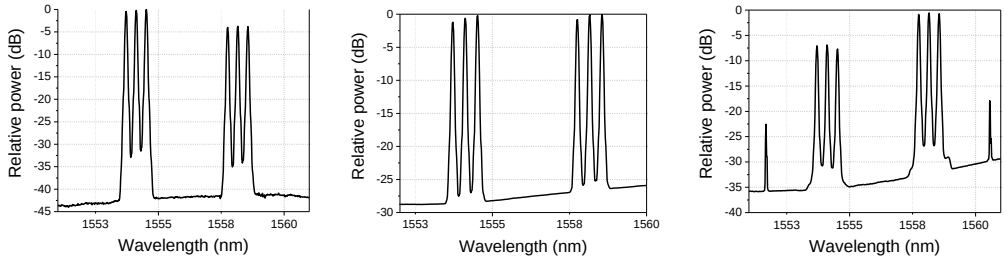

FIGURE 7.16: The spectra taken at the transmitter output (left), the mid-link (middle), and the receiver input (right)

In this section, the DM links in the previous experiments have been transformed to DUC links. The performance improvement is reduced due to the removal of inline DCMs and corresponding EDFAs. The performance improvement for the six channels ranges from 0.1 dB to 0.5 dB.

7.6 14-channel Nyquist-WDM DP-256 QAM at 40 GBd in a 440 km DUC link

Our OPC scheme, hence mid-link OPC in general, has proven its compensation capability for nonlinear impairments for SP-16 QAM, SP-64 QAM and DP-16 QAM signals in DM links. In order to exploit the spectral efficiency further, we collaborated with the Optical Networks Group of University College London (UCL) to gain access to their specialised high-capacity high-spectral efficiency transmitters. In particular, at maximum, 14-channel Nyquist-spaced WDM DP-256 QAM signals have been generated at UCL in London for these experiments. The transmitter is placed alongside the receiver, 220 km away from Southampton where the mid-link OPC is located, connected by the same NDFIS field-installed transmission network via Reading. For this transmitter configuration, the equivalent throughput is 5.7 Tbps, a record high for OPC experiments at the time. It is also the first demonstration of 256 QAM WDM signals in this field. The link configuration and its characterisation is given Chapter 5. The total transmission distance amounts to 440 km. Similar to the previous case with DP-16 QAM in the DUC link, the receiver offline DSP compensates for the dispersion when the OPC is not in place, and, for fair comparison, a WSS replaces the OPC to filter out the out-of-band ASE noise accumulated up to the mid-link with an EDFA to compensate for its loss.

The spectrum at one of the HNLF output is shown as in Figure 7.17, showing the signal band placement relative to the two pumps. The idler CE is about -10 dB. The

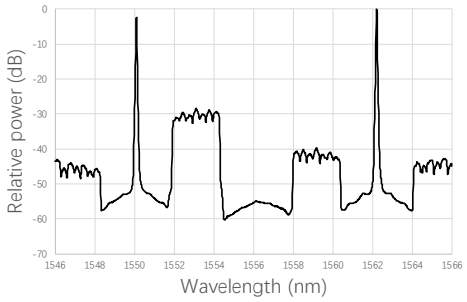

FIGURE 7.17: The spectrum taken at the output of the HNLF in the OPC module

performance in terms of SNR as a function of launch power per channel is plotted for the 3-channel case (left) and the 14-channel case (right) in Figure 7.18. The OPC does not improve the peak performance and the performance in the linear regime due to the additional noise introduced in the OPC module, but the improved performance in the nonlinear regime is clearly shown in both two cases. This is an indication of the reduction of nonlinear impairments. The operating window of launch power is also increased overall as a result.

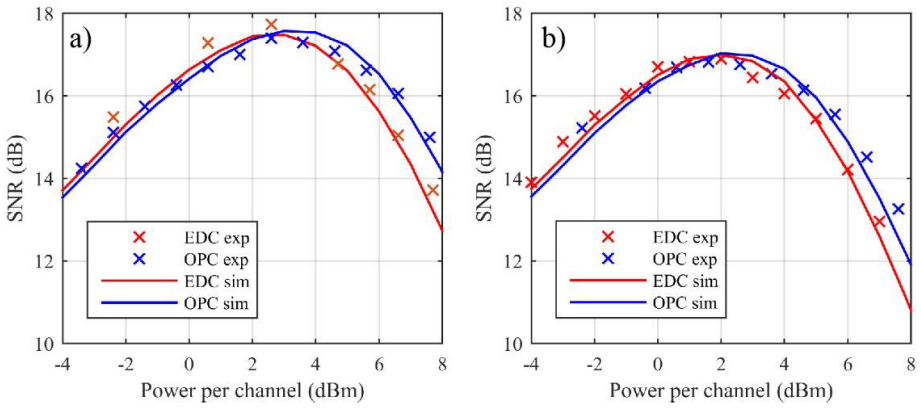

FIGURE 7.18: The performance in terms of SNR as a function of launch power per channel for single-band 3-channel (left) and dual-band 14-channel (right) signals

The peak SNR drops as the number of channels increases. This is the result of the increase of signal-signal and signal-noise FWM interference with the number of channels during transmission. Numerical simulations using the SSFM on Manakov equations for fibre propagation performed by Gabriel Saavedra from the UCL are in agreement with these experimental results as given by the curves in Figure 7.18. The same two sets of experiments are carried out for 16 QAM signals for both 3-channel and 14-channel cases. Similar patterns can be found in the linear and nonlinear regimes.

Channel performance measurements in terms of MI are shown in Figure 7.19 across all fourteen channels, confirming the OPC module's consistent performance when the total signal bandwidth is increased. More importantly, the MI, which determines the achievable bitrate, is above 10 bit/symbol for each channel, larger than the required

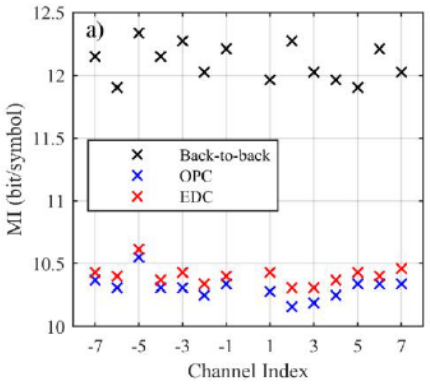

FIGURE 7.19: Channel performance in terms of MI for 14-channel signals

MI of 8bit/symbol for DP-256 QAM, indicating the possibility of post-FEC error free transmission for the 5.7 Tbps throughput.

In this section, the signal bandwidth, the order of modulation formats, and the baud rate are further pushed to higher levels to investigate the effectiveness of OPC. The limited improvements are identified to be the result of the non-ideal link conditions. The performance improvement is not affected by the signal bandwidth increase from 120 GHz for 3-channel signals to 560 GHz for 14-channel signals, resulting in a record high WDM capacity of 5.7 Tbps for OPC experiments.

7.7 Summary

The mid-link OPC technique is well-known for its nonlinearity compensating capability. Under ideal link conditions, mid-link OPC can effectively mitigate nonlinear impairments, agnostic to the signal modulation format, baud rate, bandwidth, and the use of PolMux. Mid-link OPC is therefore a competitive rival of the digital and other optical nonlinearity compensation techniques. OPC under ideal link conditions has been shown able to improve the performance both theoretically and experimentally. The effectiveness of the mid-link OPC technique remains to be demonstrated under realistic link conditions where the field-installed transmission link is based on standard SMFs and amplified by conventional EDFAs. The experiments in this chapter have addressed this issue.

Various types of signals and different sizes of signal bandwidth have been tested on a variety of realistic link setups. Table 7.1 summarises the experiments in this chapter. The signals generated at the transmitter output, the link parameters, the peak performance improvement, the optimal launch power, etc. are given in the table. The overall discovery from these experiments is in agreement with the expectation from OPC, and is summarised into two points.

No.	Format	Channel count	DM	Distance	Peak Q *	Improve in Q **	Optimal P_L ***
1	SP-16 QAM	6	DM	400	11.3 dB	0.5 dB	-1 dBm
2	SP-16 QAM	13	DM	400	10.9 dB	0.6 dB	-4 dBm
3	SP-64 QAM	6	DM	400	4.2 dB	2.5 dB	0 dBm / 2 dBm
4	DP-16 QAM	6	DM	400	9.2 dB	0.3 dB	0 dBm
5	DP-16 QAM	6	DM	834	10.5 dB	3.0 dB	0 dBm
6	DP-16 QAM	6	DUC	800	9.3 dB	0.5 dB	0 dBm / 2 dBm
7	DP-16 QAM	3 NWDM	DUC	440	17.2 dB SNR	0 dB SNR	2.5 dBm
8	DP-16 QAM	14 NWDM	DUC	440	16.9 dB SNR	0 dB SNR	2 dBm
9	DP-256 QAM	3 NWDM	DUC	440	17.5 dB SNR	0 dB SNR	3 dBm
10	DP-256 QAM	14 NWDM	DUC	440	17.0 dB SNR	0 dB SNR	2 dBm

TABLE 7.1: A summary of all experiments discussed in this chapter; *****: Peak performance in terms of Q factor if not indicated otherwise; ******: Performance improvement in terms of Q factor if not indicated otherwise; *******: Optimal launch power per channel

Firstly, the performance improvement increases with the use of DM and the transmitter noise. This may be understood by the fact that nonlinear interaction between propagating signals and the discreet addition of linear noises heavily distorts the signals, which translate to increased potential of performance gain by OPC. This is in line with the peer works discussed following Table 4.1.

To be more specific, the links in cases number 5 and 6 differ only by the use of DM. Note that although the link lengths have a discrepancy of 34 km, this amounts to only an insignificant fraction of the total length. After the use of DM, the performance improvement increases significantly from 0.5 dB to 3.0 dB. This more than two fold of increase of performance improvement has been attributed to the nonlinear impairments incurred by the inline DCMs and the related extra EDFAs. This result implies that DM links may be a more favourable link condition for the employment of OPC techniques.

Discreet source of linear noise also exists in transmitters. They usually stem from the non-ideal properties of transmitter electronics. Its nonlinear interaction with signals along the entire link may severely limit the achievable performance, therefore allowing an increased performance gain by OPC. As an example of this phenomenon, the transmitted signals in case number 1 and 3 differ only by the modulation formats. The transmitters in both cases comprise the same AWG that has a limited performance due to its bandwidth and ENOB. In this particular case, the transmitter noise increases with the order of modulation formats. OPC reduces the impact of signal-transmitter noise nonlinear interference during transmission [Galdino et al. (2017b)], thereby increasing the performance improvement.

Secondly, the performance improvement is not significantly affected by the use of PolMux signals (case number 1 and 4), the WDM channel count (case number 1 and 2, 9 and 10), and the order of modulation formats (case number 7 and 8). These comparisons demonstrate the advantages of using OPC that is an all-optical means for NLC. These inherent merits of OPC include the bitrate- and modulation format-transparency and the compatibility with WDM (including Nyquist-WDM) and PolMux signals. Although

not so revealing, these results are in agreement with the fundamental expectations from OPC.

Chapter 8

Discussions and future works

One of the targets of our project is to design a BW efficient OPC module that exploit the full BW offered by the transmitted signal band. Additionally a counter-propagation scheme is used to allow the two polarisation insensitive FWM processes take place in a single HNLF. The three design criteria are satisfied, and the proposed OPC module has been implemented, modified, refined, and finally put into use for transmission experiments. The OPC module has successfully demonstrated its proper functioning in practice, which help us achieve the second target of this project that is to verify the practicality of OPC in real-world transmission links. The experimental results are novel in the sense that they are the first to show the potential of employing OPC in contemporary and legacy links and they have pushed the limit of ever advanced spectrally efficient signal types in OPC-assisted systems.

A few points will be raised in this chapter in order to discuss some issues that have not been, yet should be, expanded from the main chapters. The issues are often related to potentially proposed future works that will help provide further insights on the some of the key aspects of OPC.

As mentioned in Chapter 6, the pump-signal FWM interference terms in the FOPA inevitably contaminate the signal and idler bands that occupy the same BW. This inherent problem of 2p-FOPA prevents the spectral range between pumps from its full utilisation. A potential solution that allows neglecting the pump-signal interference is to have significantly increased pump powers, thus increasing the pump-signal pump ratio, which, as has been discussed in Chapter 3, in turn reduces the relative power of the interference terms. Signal and idler bands can then be safely placed on top of the interference, causing possibly negligible performance degradation. This approach relies heavily on a high pump power, which may be limited by SBS. The other direction to avoid the impact of pump-signal FWM interference is to use a large pump spacing, since the flat gain BW of FOPAs can exceed hundreds of nm in record or at least tens of nm

in most practical cases. The signal bands in this case can be placed within the central one third spectral range between the pumps, as in [Al-Khateeb et al. (2017b)].

The performance improvements by OPC for our field-installed transmission systems were positive, ranging from 0.5 dB to 3.0 dB in terms of Q factors. A summary of these results can be found in Chapter 7. These results indicate effective NLC in practical links, albeit relatively moderate as a result of link asymmetry. The degree of link asymmetry, in terms of both dispersion and power profile, is mainly attributed to the lumped amplification by EDFAs and the non-uniform span lengths determined by geographical locations. The power asymmetry of the link is quantifiable as in [Hesketh and Petropoulos (2016), Rosa et al. (2015)]. However, the NLC efficiency is determined jointly by both the accumulated dispersion as well as the power profile. To my knowledge, such quantification of link asymmetry taking into account both profiles is still absent in literature and may be an interesting research topic.

Nonlinear interaction between transmitter noise and the signals added by inline EDFAs can be effectively mitigated by mid-link OPC, as discussed in Chapter 4. In our experiments, severe transmitter noise relates to enhanced performance improvements by OPC, which may imply that the mitigation of nonlinear interaction of signals and transmitter noise is the major source of performance improvements. This may be corroborated by the difference in transmitter B2B performance provided that a performance metric that directly compares different modulation formats is used [Galdino et al. (2017a)]. A systemic investigation of the impact of transmitter noise on NLC efficiency by OPC may still be helpful in gaining more insight into this particular aspect.

The experimental results as concluded in Chapter 7 are also in agreement with the characteristics of OPC in general. It was shown, for practical transmission systems with an emphasis on the field-installed lump-amplified SMF links, that OPC benefits the transmission performance in the presence of nonlinearity, at the same time agnostic to bitrate, modulation formats and the use of PolMux and is compatible with WDM and densely packed super-channel signals. However, an issue some of these results raise is related to the operating BW of OPC. It was shown that increasing the WDM channel count outside of the operating BW of the OPC module does not negatively impact NLC efficiency, yet the improvements were even slightly increased in one particular case. It is assumed that the nonlinear interference generated within the NLC BW can be effectively mitigated. If the nonlinear interference originated completely or partially from the outside of the operating BW, it may be treated as stochastic nonlinear interference noise [Dar and Winzer (2017)], which may fit the Gaussian noise (GN) model [Poggiolini et al. (2014)] and its variants. The investigation on its characteristics and mitigation by OPC is still absent from literature to the author's knowledge.

Multiple OPC

The cascadability of the OPC module is an important design consideration if multiple

OPC is to be employed. The feasibility of multiple inline OPC replacing or supplementing EDFAs for nonlinearity mitigation has been under discussion [Ellis et al. (2015), Solis-Trapala et al. (2016), Namiki et al. (2017), Hu et al. (2017)]. Noise and nonlinear distortions introduced by the OPC module or its OSNR degradation is the primary factor that determines its cascadability. The noise figure (NF) of our OPC scheme may be improved by providing optimised CE with less noise and nonlinear crosstalk among co-propagating channels. Multiple inline OPC has been experimentally verified [Hu et al. (2017)] to have provided SMF-based backward-pumped-Raman-amplified transmission systems both improved peak performance and increased optimal launch power, demonstrating its practicality for nonlinearity mitigation. However, only three FOPA-based OPC modules are used in this experiments. A larger number of multiple OPC has been analytically and numerically confirmed to bring about sublinear monotonic improvements, scaling with $\sqrt{1+N_{\mathrm{OPC}}}$ in performance with increasing number of OPC modules, N_{OPC} [Ellis et al. (2015)], provided that PMD and TOD may be neglected. Multiple OPC is expected theoretically to outperform its digital counterparts due to its capability to reverse periodically the accumulated nonlinear signal-noise interference and to interrupt and limit the impact of PMD within the largest inter-OPC fibre segment. However, the analytical prediction anticipating at least a 50% SNR improvement [Ellis et al. (2015)] over uncompensated links often failed to be delivered in practical experiments, mostly with a limited 1 dB to 2 dB SNR gain. Twelve OPC devices in a recirculating loop have demonstrated both improved optimal launch power and improved peak performance [Solis-Trapala et al. (2016)]. Although this set of experiments are based on DRA links with shorter than usual span lengths (12 km), not to mention the use of recirculating loops instead of actual continuous fibres, the results are still indicative of the practicality of multiple OPC.

Practical restrictions towards ideal implementations of OPC devices often find their resolutions within the OPC devices themselves. The largest potential source of signal nonlinear distortion comes from the additive pump-signal and signal-signal nonlinear interference terms. Careful manipulation of the signal band placement is able to help remove pump-signal interference, and its magnitude and severity can be alleviated by increasing the relative pump power with respect to the signal power per channel. On the other hand, signal-signal interference spectral components falling onto either the signal or the idler band is unavoidable simply through manipulation of the signal band wavelengths. It can, instead, be controlled by reducing the signal power per channel for a given channel count, since the individual power of each of these FWM interference terms scales cubically to signal channel power. Signal-signal interference, therefore, as an inherent source of signal quality degradation during the phase conjugation process [Morshed et al. (2013b)], poses an ultimate constraint on the cascadability of wideband spectrally efficient OPC devices.

From the perspective of HNLF design [Marhic (2007)], having a fibre with large β_3

increases D, hence reducing the FWM efficiency of both pump-signal and signal-signal interference terms. A larger β_3, at the same time, does not alter the gain spectra of FOPAs, as the linear phase mismatch depends only on even order dispersion terms of the fibre. This approach requires delicate fibre design and manufacturing.

Phase noise is another potential source of signal quality degradation. The pump phase noise transfers to the converted idlers with a magnifying factor of two. Dithering of the pump may also induce unintentional residual idler spectral broadening. On the other hand, multiplicative nonlinear phase noise (NLPN), originating inside OPC devices through the interplay between ASE noise and Kerr nonlinearity, is experimentsally shown to be negligible after the cascade of twelve OPC devices as in [Solis-Trapala et al. (2016)] inside a recirculating loop. This may be a result of the limited nonlinear interaction length permitted by HNLFs of the order of a hundred metres.

The overall noise performance of OPC devices can be summarised and quantified by NF measurements. For OPC devices that require pre- or post-OPC optical amplifications by EDFAs to compensate for the signal band power loss inside the devices, the NF of the EDFA sets an upper limit for the overall NF of the OPC. Therefore, in this regard, a power transparent OPC device that parametrically amplifies the signal band compensating for all loss incurred without resorting to EDFAs definitely provides enhanced noise performance. Cascadability similar to EDFAs can be achieved if the corresponding NF of OPC devices is comparable to that of EDFAs, which is often the case since the 3 dB quantum-limited NF of phase-insensitive optical amplifiers is more readily approached in practice by FOPAs. A 4.3 dB NF has been measured for a recent 20 dB-gain full C-band 1p-FOPA [Takasaka (2013)], lower than that of a typical EDFA. Other low NF FOPAs in literature, such as in [Wang et al. (2008)] where a Raman-assisted FOPA exhibit a NF of 3.6 dB and in [Tong et al. (2010)] where NF close to 4 dB has been achieved, all show their potential as cascadable OPC devices. Last but not least, it is worth mentioning that Raman effects induce additional minor NF penalty, especially at the gain edges [Tang et al. (2004)]. It is not, however, as severe a source of noise as those aforementioned. Resolving the issue with cascadability of OPC devices is a first step towards the practical implementation of multiple OPC schemes, with the hope to release the full potential of OPC as a versatile and comprehensive solution for amplification, dispersion compensation,and NLC.

The research presented in this thesis has formed the basis for a new research proposal prepared by our group on the theme of OPC. The new EPSRC project PHOS will further the scope of the work presented in the thesis, and is anticipated to offer answers to many of the topics discussed in the previous paragraph.

Appendix A

List of publications

1. Gabriel Saavedra, **Yujia Sun**, Kyle R. H. Bottrill, Lidia Galdino, Zhixin Liu, Francesca Parmigiani, David J. Richardson, Periklis Petropoulos, Robert Killey, Polina Bayvel, "Optical Phase Conjugation in Installed Optical Networks", in *OFC* (2018), W3E.2.

2. **Yujia Sun**, Kyle R. H. Bottrill, Francesca Parmigiani, David J. Richardson, Periklis Petropoulos, "Optical Phase Conjugation for Simultaneous Dispersion and Nonlinearity Compensation Performed over an 800-km long Field-installed Transmission Link", in *ECOC* (2017), Th.1.F.2.

3. **Yujia Sun**, Abel Lorences-Riesgo, Francesca Parmigiani, Kyle R.H. Bottrill, Satoshi Yoshima, Graham D. Hesketh, Magnus Karlsson, Peter A. Andrekson, David J. Richardson, and Periklis Petropoulos, "Optical Nonlinearity Mitigation of 6 x 10 GBd Polarization-division Multiplexing 16QAM Signals in a Field-installed Transmission Link", in *OFC* (2017), Th3J.2.

4. Satoshi Yoshima, **Yujia Sun**, Zhixin Liu, Kyle R. H. Bottrill, Francesca Parmigiani, David J. Richardson, and Periklis Petropoulos, "Mitigation of Nonlinear Effects on WDM QAM Signals Enabled by Optical Phase Conjugation with Efficient Bandwidth Utilization", *Journal of Lightwave Technology*, 35, 971-978 (2017).

5. Periklis Petropoulos, Francesca Parmigiani, Kyle R.H. Bottrill, Satoshi Yoshima, **Yujia Sun**, and David J. Richardson, "Multi-channel All-optical Signal Processing Based on Parametric Effects", in *OFC* (2016), W4D.3.

6. Satoshi Yoshima, Zhixin Liu, **Yujia Sun**, Kyle R. H. Bottrill, Francesca Parmigiani, Periklis Petropoulos, and David J. Richardson, "Nonlinearity Mitigation for Multi-channel 64-QAM Signals in a Deployed Fiber Link through Optical Phase Conjugation", in *OFC* (2016), Th4F.4.

7. Satoshi Yoshima, **Yujia Sun**, Kyle R. H. Bottrill, Francesca Parmigiani, Periklis Petropoulos, and David J. Richardson, "Nonlinearity Mitigation through Optical Phase Conjugation in a Deployed Fibre Link with Full Bandwidth Utilization," in *ECOC* (2015), We.2.6.3.

Bibliography

Govind P. Agrawal. *Nonlinear Fiber Optics*. Elsevier Science Publishing Co Inc, fifth edition, October 2012. ISBN 0123970237.

Mohammad A. Z. Al-Khateeb, Mary E. McCarthy, and Andrew D. Ellis. Experimental verification of four wave mixing in lumped optical transmission systems that employ mid-link optical phase conjugation. In *Conference on Lasers and Electro-Optics*. OSA, 2017a. ISBN 978-1-943580-27-9.

Mohammad A. Z. Al-Khateeb, Mary E. McCarthy, and Andrew D. Ellis. Performance enhancement prediction for optical phase conjugation in systems with 100km amplifier spacing. In *2017 European Conference on Optical Communication (ECOC)*, Th.1.F. IEEE, Sep 2017b. ISBN 9781538656242.

Mohammad A. Z. Al-Khateeb, Mary E. McCarthy, Christian Sánchez, and Andrew D. Ellis. Nonlinearity compensation using optical phase conjugation deployed in discretely amplified transmission systems. *Optics Express*, 26(18):23945, Aug 2018. ISSN 1094-4087.

Abdallah A. I. Ali, Christian S. Costa, Mohammad A. Z. Al-Khateeb, Filipe M. Ferreira, and Andrew D. Ellis Aston. Four-wave mixing in optical phase conjugation system with pre-dispersion. In *2017 Opto-Electronics and Communications Conference (OECC) and Photonics Global Conference (PGC)*. IEEE, Jul 2017.

Abhishek Anchal, K Pradeep Kumar, Sean O'Duill, Prince M. Anandarajah, and Pascal Landais. Experimental demonstration of optical phase conjugation using counter-propagating dual pumped four-wave mixing in semiconductor optical amplifier. *Optics Communications*, 369:106–110, Jun 2016. ISSN 0030-4018.

Brian Anderson, Angel Flores, Roger Holten, and Iyad Dajani. Comparison of phase modulation schemes for coherently combined fiber amplifiers. *Optics Express*, 23(21): 27046, Oct 2015. ISSN 1094-4087.

F.A. Callegari, J.M.C. Boggio, and H.L. Fragnito. Spurious four-wave mixing in two-pump fiber-optic parametric amplifiers. *IEEE Photonics Technology Letters*, 16(2): 434–436, Feb 2004.

John C. Cartledge, Fernando P. Guiomar, Frank R. Kschischang, Gabriele Liga, and Metodi P. Yankov. Digital signal processing for fiber nonlinearities [invited]. *Optics Express*, 25(3):1916, jan 2017.

Ronen Dar and Peter Winzer. Nonlinear interference mitigation: Methods and potential gain. *Journal of Lightwave Technology*, 2017. ISSN 0733-8724.

Henrik Eliasson, Pontus Johannisson, Magnus Karlsson, and Peter A. Andrekson. Mitigation of nonlinearities using conjugate data repetition. *Optics Express*, 23(3):2392, Jan 2015. ISSN 1094-4087.

Henrik Eliasson, Samuel L.I. Olsson, Magnus Karlsson, and Peter A. Andrekson. Comparison between coherent superposition in DSP and PSA for mitigation of nonlinearities in a single-span link. In *2014 The European Conference on Optical Communication (ECOC)*. IEEE, Sep 2014. ISBN 9782954944401.

A. D. Ellis, M. E. McCarthy, M. A. Z. Al-Khateeb, and S. Sygletos. Capacity limits of systems employing multiple optical phase conjugators. *Optics Express*, 23(16):20381, Jul 2015. ISSN 1094-4087.

A. D. Ellis, M. E. McCarthy, M. A. Z. Al Khateeb, M. Sorokina, and N. J. Doran. Performance limits in optical communications due to fiber nonlinearity. *Advances in Optics and Photonics*, 9(3):429, July 2017. ISSN 1943-8206.

A.D. Ellis, M.A.Z. Al Khateeb, and M.E. McCarthy. Impact of optical phase conjugation on the nonlinear shannon limit. In *Optical Fiber Communication Conference*, TH4F.2. OSA, 2016. ISBN 978-1-943580-07-1.

Robert Elschner, Thomas Richter, and Colja Schubert. Characterization of FWM-induced crosstalk for WDM operation of a fiber-optical parametric amplifier. In *37th European Conference and Exposition on Optical Communications*. OSA, 2011. ISBN 978-1-55752-932-9.

Robert A. Fisher, B. R. Suydam, and D. Yevick. Optical phase conjugation for time-domain undoing of dispersive self-phase-modulation effects. *Optics Letters*, 8(12):611, Dec 1983.

A. Gajda, F. Da Ros, E. P. da Silva, A. Peczek, E. Liebig, A. Mai, M. Galili, L. K. Oxenløwe, K. Petermann, and L. Zimmermann. Silicon waveguide with lateral p-i-n diode for nonlinearity compensation by on-chip optical phase conjugation. In *Optical Fiber Communication Conference*, W3E.4. OSA, 2018.

Lidia Galdino, Daniel Semrau, Domaniç Lavery, Gabriel Saavedra, Cristian B. Czegledi, Erik Agrell, Robert I. Killey, and Polina Bayvel. On the limits of digital back-propagation in the presence of transceiver noise. *Optics Express*, 25(4):4564, Feb 2017a. ISSN 1094-4087.

Lidia Galdino, Daniel Semrau, Domaniç Lavery, Gabriel Saavedra, Cristian B. Czegledi, Erik Agrell, Robert I. Killey, and Polina Bayvel. On the limits of digital back-propagation in the presence of transceiver noise. *Optics Express*, 25(4):4564, feb 2017b.

Guanjun Gao, Xi Chen, and William Shieh. Influence of PMD on fiber nonlinearity compensation using digital back propagation. *Optics Express*, 20(13):14406, jun 2012a.

Guanjun Gao, Xi Chen, and William Shieh. Limitation of fiber nonlinearity compensation using digital back propagation in the presence of PMD. In *Optical Fiber Communication Conference*, OM3A.5. OSA, 2012b. ISBN 978-1-55752-938-1.

Bernhard Goebel and Norbert Hanik. Analytical calculation of the number of four-wave-mixing products in optical multichannel communication systems. *Technical Report, Technische Universitat Munchen*, 2008.

L. Gruner-Nielsen, M. Wandel, P. Kristensen, C. Jorgensen, L. V. Jorgensen, B. Edvold, B. Palsdottir, and D. Jakobsen. Dispersion-compensating fibers. *Journal of Lightwave Technology*, 23(11):3566–3579, Nov 2005. ISSN 0733-8724.

Lars Gruner-Nielsen, Soren Herstrom, Sonali Dasgupta, David Richardson, Dan Jakobsen, Carl Lundstrom, Peter A. Andrekson, Martin E. V. Pedersen, and Bera Palsdottir. Silica-based highly nonlinear fibers with a high SBS threshold. In *IEEE Winter Topicals 2011*. IEEE, Jan 2011. ISBN 9781424484287.

J. Hansryd, F. Dross, M. Westlund, P.A. Andrekson, and S.N. Knudsen. Increase of the SBS threshold in a short highly nonlinear fiber by applying a temperature distribution. *Journal of Lightwave Technology*, 19(11):1691–1697, 2001. ISSN 0733-8724.

Graham D. Hesketh and Periklis Petropoulos. Minimizing inter-channel cross-phase modulation with optical phase conjugation in asymmetric fibre links. *Optics Express*, 24(18):20270, Aug 2016. ISSN 1094-4087.

Min-Chen Ho, M.E. Marhic, K.Y.K. Wong, and L.G. Kazovsky. Narrow-linewidth idler generation in fiber four-wave mixing and parametric amplification by dithering two pumps in opposition of phase. *Journal of Lightwave Technology*, 20(3):469–476, Mar 2002. ISSN 0733-8724.

H. Hu, R. M. Jopson, A. H. Gnauck, Dario Pilori, S. Randel, and S. Chandrasekhar. Fiber nonlinearity compensation by repeated phase conjugation in 2.048-tbit/s WDM transmission of PDM 16-QAM channels. In *Optical Fiber Communication Conference*, TH4F.3. OSA, 2016. ISBN 9781943580071.

Hao Hu, Robert M. Jopson, Alan H. Gnauck, Sebastian Randel, and S. Chandrasekhar. Fiber nonlinearity mitigation of WDM-PDM QPSK/16-QAM signals using fiber-optic parametric amplifiers based multiple optical phase conjugations. *Optics Express*, 25 (3):1618, jan 2017.

Hao Hu, Rahman Nouroozi, Reinhold Ludwig, Carsten Schmidt-Langhorst, Hubertus Suche, Wolfgang Sohler, and Colja Schubert. 110 km transmission of 160 gbit/s RZ-DQPSK signals by midspan polarization-insensitive optical phase conjugation in a ti:PPLN waveguide. *Optics Letters*, 35(17):2867, Aug 2010. ISSN 1539-4794.

Chaoran Huang, Yajun Wu, Xiaojie Guo, Ming Li, and Chester Shu. Improving the nonlinear tolerance of fiber-based optical phase conjugation. *IEEE Photonics Technology Letters*, 27(4):439–442, Feb 2015a. ISSN 1041-1135.

Chaoran Huang, Yajun Wu, Xiaojie Guo, Ming Li, and Chester Shu. Mitigation of nonlinear distortion in OPC module with backward raman pumping. In *Optical Fiber Communication Conference*, W1K.1. OSA, 2015b. ISBN 9781557529374.

K. Inoue, T. Kominato, and H. Toba. Tunable gain equalization using a mach-zehnder optical filter in multistage fiber amplifiers. *IEEE Photonics Technology Letters*, 3(8): 718–720, Aug 1991.

Ezra Ip. Nonlinear compensation using backpropagation for polarization-multiplexed transmission. *Journal of Lightwave Technology*, 28(6):939–951, mar 2010.

S.L. Jansen, D. van den Borne, B. Spinnler, S. Calabro, H. Suche, P.M. Krummrich, W. Sohler, G.-D. Khoe, and H. de Waardt. Optical phase conjugation for ultra long-haul phase-shift-keyed transmission. *Journal of Lightwave Technology*, 24(1):54–64, Jan 2006. ISSN 0733-8724.

R.M. Jopson, A.H. Gnauck, and R.M. Derosier. Compensation of fibre chromatic dispersion by spectral inversion. *Electronics Letters*, 29(7):576, 1993.

P. Kaewplung, T. Angkaew, and K. Kikuchi. Simultaneous suppression of third-order dispersion and sideband instability in single-channel optical fiber transmission by midway optical phase conjugation employing higher order dispersion management. *Journal of Lightwave Technology*, 21(6):1465–1473, Jun 2003. ISSN 0733-8724.

Pasu Kaewplung and Kazuro Kikuchi. Simultaneous cancellation of fiber loss, dispersion, and kerr effect in ultralong-haul optical fiber transmission by midway optical phase conjugation incorporated with distributed raman amplification. *Journal of Lightwave Technology*, 25(10):3035–3050, Oct 2007.

Inwoong Kim, Olga Vassilieva, Paparao Palacharla, and Motoyoshi Sekiya. The impact of spectral inversion placement for nonlinear phase noise mitigation in non-uniform transmission links. In *2014 IEEE Photonics Conference*. IEEE, Dec 2014. ISBN 9781457715044.

Inwoong Kim, Olga Vassilieva, Paparao Palacharla, Motoyoshi Sekiya, and Tadashi Ikeuchi. Analysis of nonlinearity mitigation using spectral inversion for superchannel transmission. *IEEE Photonics Journal*, 8(5):1–8, Oct 2016. ISSN 1943-0655.

Shiva Kumar and Ling Liu. Reduction of nonlinear phase noise using optical phase conjugation in quasi-linear optical transmission systems. *Optics Express*, 15(5):2166, 2007.

Son Thai Le, Mary E. McCarthy, Naoise Mac Suibhne, Mohammad A. Z. Al-Khateeb, Elias Giacoumidis, Nick Doran, Andrew D. Ellis, and Sergei K. Turitsyn. Demonstration of phase-conjugated subcarrier coding for fiber nonlinearity compensation in CO-OFDM transmission. *Journal of Lightwave Technology*, 33(11):2206–2212, Jun 2015a. ISSN 0733-8724.

Son Thai Le, Mary E. McCarthy, Naoise Mac Suibhne, Andrew D. Ellis, and Sergei K. Turitsyn. Phase-conjugated pilots for fibre nonlinearity compensation in CO-OFDM transmission. *Journal of Lightwave Technology*, 33(7):1308–1314, Apr 2015b. ISSN 0733-8724.

Gordon K. P. Lei and Michel E. Marhic. Amplification of DWDM channels at 128 tb/s in a bidirectional fiber optical parametric amplifier. *Optics Express*, 22(7):8726, Apr 2014. ISSN 1094-4087.

Gabriele Liga, Tianhua Xu, Alex Alvarado, Robert I. Killey, and Polina Bayvel. On the performance of multichannel digital backpropagation in high-capacity long-haul optical transmission. *Optics Express*, 22(24):30053, Nov 2014.

Qiang Lin and Govind P. Agrawal. Effects of polarization-mode dispersion on fiber-based parametric amplification and wavelength conversion. *Optics Letters*, 29(10): 1114, May 2004a. ISSN 0146-9592.

Qiang Lin and Govind P. Agrawal. Vector theory of four-wave mixing: polarization effects in fiber-optic parametric amplifiers. *Journal of the Optical Society of America B*, 21(6):1216, Jun 2004b. ISSN 0740-3224.

Xiang Liu, A. R. Chraplyvy, P. J. Winzer, R. W. Tkach, and S. Chandrasekhar. Phase-conjugated twin waves for communication beyond the kerr nonlinearity limit. *Nature Photonics*, 7(7):560–568, May 2013. ISSN 1749-4885.

Lars Lundberg, Mikael Mazur, Abel Lorences-Riesgo, Magnus Karlsson, and Peter A. Andrekson. Joint carrier recovery for DSP complexity reduction in frequency comb-based superchannel transceivers. In *2017 European Conference on Optical Communication (ECOC)*, Th.1.D. IEEE, Sep 2017.

M. E. Marhic, N. Kagi, T.-K. Chiang, and L. G. Kazovsky. Cancellation of third-order nonlinear effects in amplified fiber links by dispersion compensation, phase conjugation, and alternating dispersion. *Optics Letters*, 20(8):863, Apr 1995. ISSN 0146-9592.

Michel E. Marhic. *Fiber Optical Parametric Amplifiers, Oscillators and Related Devices*. CAMBRIDGE UNIV PR, December 2007. ISBN 0521861020.

Michel E. Marhic, Peter A. Andrekson, Periklis Petropoulos, Stojan Radic, Christophe Peucheret, and Mahmoud Jazayerifar. Fiber optical parametric amplifiers in optical communication systems. *Laser & Photonics Reviews*, 9(1):50–74, Sep 2014. ISSN 1863-8880.

J. Marti and F. Ramos. Compensation for dispersion-induced nonlinear distortion in subcarrier systems using optical-phase conjugation. *Electronics Letters*, 33(9):792, 1997. ISSN 0013-5194.

Motoharu Matsuura and Naoto Kishi. Simultaneous multichannel transmission of intensity- and phase-modulated signals based on optical phase conjugation using a quantum-dot SOA. In *Optical Fiber Communication Conference/National Fiber Optic Engineers Conference 2013*, OTH1C.7. OSA, 2013.

M. E. McCarthy, M. A. Z. Al Kahteeb, F. M. Ferreira, and A. D. Ellis. PMD tolerant nonlinear compensation using in-line phase conjugation. *Optics Express*, 24(4):3385, Feb 2016. ISSN 1094-4087.

C. J. McKinstrie, S. Radic, and C. Xie. Reduction of soliton phase jitter by in-line phase conjugation. *Optics Letters*, 28(17):1519, sep 2003.

R.J. Mears, L. Reekie, I.M. Jauncey, and D.N. Payne. Low-noise erbium-doped fibre amplifier operating at 1.54µm. *Electronics Letters*, 23(19):1026, 1987.

D. Mechin, J. D. Harvey, and C. J. McKinstrie. Experimental demonstration of a 180nm wavelength conversion based on a potentially noise-free bragg scattering process. In *2006 European Conference on Optical Communications*. IEEE, Sep 2006. ISBN 9782912328397.

Marc D. Mermelstein. SBS threshold measurements and acoustic beam propagation modeling in guiding and anti-guiding single mode optical fibers. *Optics Express*, 17 (18):16225, Aug 2009.

P. Minzioni, I. Cristiani, V. Degiorgio, L. Marazzi, M. Martinelli, C. Langrock, and M.M. Fejer. Experimental demonstration of nonlinearity and dispersion compensation in an embedded link by optical phase conjugation. *IEEE Photonics Technology Letters*, 18 (9):995–997, May 2006. ISSN 1041-1135.

Paolo Minzioni. Nonlinearity compensation in a fiber-optic link by optical phase conjugation. *Fiber and Integrated Optics*, 28(3):179–209, may 2009.

Partha P. Mitra and Jason B. Stark. Nonlinear limits to the information capacity of optical fibre communications. *Nature*, 411(6841):1027–1030, Jun 2001.

M. Morshed, L. B. Du, B. Foo, M. D. Pelusi, and A. J. Lowery. Optical phase conjugation for nonlinearity compensation of 1.21-tb/s pol-mux coherent optical ofdm.

In *2013 18th OptoElectronics and Communications Conference held jointly with 2013 International Conference on Photonics in Switching (OECC/PS)*, 1–2, June 2013a.

Monir Morshed, Liang B. Du, Benjamin Foo, Mark D. Pelusi, Bill Corcoran, and Arthur J. Lowery. Experimental demonstrations of dual polarization CO-OFDM using mid-span spectral inversion for nonlinearity compensation. *Optics Express*, 22(9): 10455, Apr 2014. ISSN 1094-4087.

Monir Morshed, Liang B. Du, and Arthur J. Lowery. Performance limitation of coherent optical OFDM systems with non-ideal optical phase conjugation. In *IEEE Photonics Conference 2012*, 394–395. IEEE, sep 2012. ISBN 9781457707339.

Monir Morshed, Liang Bangyuan Du, and Arthur James Lowery. Mid-span spectral inversion for coherent optical OFDM systems: Fundamental limits to performance. *Journal of Lightwave Technology*, 31(1):58–66, Jan 2013b. ISSN 0733-8724.

Monir Morshed, Arthur J. Lowery, and Liang B. Du. Improving performance of optical phase conjugation by splitting the nonlinear element. *Optics Express*, 21(4):4567, Feb 2013c. ISSN 1094-4087.

Shu Namiki, Karen Solis-Trapala, Hung Nguyen Tan, Mark Pelusi, and Takashi Inoue. Multi-channel cascadable parametric signal processing for wavelength conversion and nonlinearity compensation. *Journal of Lightwave Technology*, 35(4):815–823, Feb 2017. ISSN 0733-8724.

Samuel L. Olsson, Bill Corcoran, Carl Lundstrom, Martin Sjodin, Magnus Karlsson, and Peter A. Andrekson. Phase-sensitive amplified optical link operating in the nonlinear transmission regime. In *European Conference and Exhibition on Optical Communication*. OSA, 2012. ISBN 978-1-55752-950-3.

Samuel L. I. Olsson, Bill Corcoran, Carl Lundstrom, Tobias A. Eriksson, Magnus Karlsson, and Peter A. Andrekson. Phase-sensitive amplified transmission links for improved sensitivity and nonlinearity tolerance. *Journal of Lightwave Technology*, 33 (3):710–721, Feb 2015. ISSN 0733-8724.

Mark D. Pelusi. Fiber looped phase conjugation of polarization multiplexed signals for pre-compensation of fiber nonlinearity effect. *Optics Express*, 21(18):21423, Sep 2013. ISSN 1094-4087.

Mark D. Pelusi and Benjamin J. Eggleton. Optically tunable compensation of nonlinear signal distortion in optical fiber by end-span optical phase conjugation. *Optics Express*, 20(7):8015, Mar 2012. ISSN 1094-4087.

David M. Pepper and Amnon Yariv. Compensation for phase distortions in nonlinear media by phase conjugation. *Optics Letters*, 5(2):59, Feb 1980.

V.E. Perlin and H.G. Winful. On distributed raman amplification for ultrabroad-band long-haul WDM systems. *Journal of Lightwave Technology*, 20(3):409–416, Mar 2002. ISSN 0733-8724.

I.D. Phillips, M. Tan, M.F.C. Stephens, M. E. McCarthy, E. Giacoumidis, S. Sygletos, P. Rosa, S. Fabbri, S. T. Le, T. Kanesan, S. K. Turitsyn, N. J. Doran, P. Harper, and A. D. Ellis. Exceeding the nonlinear-shannon limit using raman laser based amplification and optical phase conjugation. In *Optical Fiber Communication Conference*, M3C.1. OSA, 2014. ISBN 9781557529930.

W. Pieper, C. Kurtzke, K. Petermann, R. Schnabel, H.G. Weber, R. Ludwig, and D. Breuer. Nonlinearity-insensitive standard-fibre transmission based on optical-phase conjugation in a semiconductor-laser amplifier. *Electronics Letters*, 30(9):724–726, Apr 1994.

P. Poggiolini, G. Bosco, A. Carena, V. Curri, Y. Jiang, and F. Forghieri. The GN-model of fiber non-linear propagation and its applications. *Journal of Lightwave Technology*, 32(4):694–721, Feb 2014. ISSN 0733-8724.

Pierluigi Poggiolini. The GN model of non-linear propagation in uncompensated coherent optical systems. *Journal of Lightwave Technology*, 30(24):3857–3879, Dec 2012. ISSN 0733-8724.

S. Radic, C.J. McKinstrie, R.M. Jopson, J.C. Centanni, and A.R. Chraplyvy. All-optical regeneration in one- and two-pump parametric amplifiers using highly nonlinear optical fiber. *IEEE Photonics Technology Letters*, 15(7):957–959, Jul 2003. ISSN 1041-1135.

Danish Rafique and Andrew D. Ellis. Impact of signal-ASE four-wave mixing on the effectiveness of digital back-propagation in 112 gb/s PM-QPSK systems. *Optics Express*, 19(4):3449, Feb 2011a. ISSN 1094-4087.

Danish Rafique and Andrew D. Ellis. Various nonlinearity mitigation techniques employing optical and electronic approaches. *IEEE Photonics Technology Letters*, 23 (23):1838–1840, dec 2011b.

Victor J. Rancaño, Francesca Parmigiani, Periklis Petropoulos, and David J. Richardson. 100ghz grid-aligned reconfigurable polarization insensitive black-box wavelength converter. In *Optical Fiber Communication Conference/National Fiber Optic Engineers Conference 2013*, JTH2A.19. OSA, 2013. ISBN 978-1-55752-962-6.

A. Redyuk, M.F.C. Stephens, and N.J. Doran. Suppression of WDM four-wave mixing crosstalk in fibre optic parametric amplifier using raman-assisted pumping. *Optics Express*, 23(21):27240, Oct 2015. ISSN 1094-4087.

M. Reimer, A. Borowiec, X. Tang, C. Laperle, and M. O'Sullivan. Direct measurement of nonlinear WDM crosstalk using coherent optical detection. In *IEEE Photonics Conference 2012*. IEEE, Sep 2012. ISBN 9781457707315.

Haisheng Rong, Simon Ayotte, Walid Mathlouthi, and Mario Paniccia. Mid-span dispersion compensation via optical phase conjugation in silicon waveguides. In *OFC/NFOEC 2008 - 2008 Conference on Optical Fiber Communication/National Fiber Optic Engineers Conference*. IEEE, Feb 2008.

F. Da Ros, M. Lillieholm, M. P. Yankov, P. Guan, H. Hu, S. Forchhammer, M. Galili, and L. K. Oxenlowe. Impact of signal-conjugate wavelength shift on optical phase conjugation-based transmission of QAM signals. In *2017 European Conference on Optical Communication (ECOC)*. IEEE, sep 2017.

F. Da Ros, I. Sackey, R. Elschner, T. Richter, C. Meuer, M. Nolle, M. Jazayerifar, K. Petermann, C. Peucheret, and C. Schubert. Kerr nonlinearity compensation in a 5 x 28-GBd PDM 16-QAM WDM system using fiber-based optical phase conjugation. In *2014 The European Conference on Optical Communication (ECOC)*. IEEE, sep 2014.

F. Da Ros, M. P. Yankov, E. P. da Silva, M. Lillieholm, S. Forchhammer, M. Galili, and L. K. Oxenløwe. Link-placement characterization of optical phase conjugation for nonlinearity compensation. In *Optical Fiber Communication Conference*, W3E.3. OSA, 2018. ISBN 978-1-943580-38-5.

Paweł Rosa, Son Thai Le, Giuseppe Rizzelli, Mingming Tan, and Juan Diego Ania-Castañón. Signal power asymmetry optimisation for optical phase conjugation using raman amplification. *Optics Express*, 23(25):31772, Dec 2015. ISSN 1094-4087.

Paweł Rosa, Giuseppe Rizzelli, and Juan Diego Ania-Castañón. Link optimization for DWDM transmission with an optical phase conjugation. *Optics Express*, 24(15):16450, Jul 2016. ISSN 1094-4087.

A. Royset, S.Y. Set, I.A. Goncharenko, and R.I. Laming. Linear and nonlinear dispersion compensation of short pulses using midspan spectral inversion. *IEEE Photonics Technology Letters*, 8(3):449–451, Mar 1996. ISSN 1041-1135.

I. Sackey, F. Da Ros, T. Richter, R. Elschner, M. Jazayerifar, C. Meuer, C. Peucheret, K. Petermann, and C. Schubert. Design and performance evaluation of an OPC device using a dual-pump polarization-independent FOPA. In *2014 The European Conference on Optical Communication (ECOC)*. IEEE, Sep 2014. ISBN 9782954944401.

Isaac Sackey, Francesco Da Ros, Johannes Karl Fischer, Thomas Richter, Mahmoud Jazayerifar, Christophe Peucheret, Klaus Petermann, and Colja Schubert. Kerr nonlinearity mitigation: Mid-link spectral inversion versus digital backpropagation in

5×28-GBd PDM 16-QAM signal transmission. *Journal of Lightwave Technology*, 33 (9):1821–1827, may 2015.

Isaac Sackey, Carsten Schmidt-Langhorst, Robert Elschner, Tomoyuki Kato, Takahito Tanimura, Shigeki Watanabe, Takeshi Hoshida, and Colja Schubert. Waveband-shift-free optical phase conjugator for spectrally efficient fiber nonlinearity mitigation. *Journal of Lightwave Technology*, 36(6):1309–1317, mar 2018.

Carsten Schmidt-Langhorst, Isaac Sackey, Robert Elschner, Tomoyuki Kato, Takahito Tanimura, Shigeki Watanabe, Takeshi Hoshida, and Colja Schubert. Fiber nonlinearity mitigation in 800-km transmission of a 1.6-tb/s superchannel using waveband-shift-free optical phase conjugation. In *2017 European Conference on Optical Communication (ECOC)*, Th.1.F. IEEE, Sep 2017. ISBN 9781538656242.

Morteza H. Shoreh. Compensation of nonlinearity impairments in coherent optical OFDM systems using multiple optical phase conjugate modules. *Journal of Optical Communications and Networking*, 6(6):549, May 2014. ISSN 1943-0620.

Karen Solis-Trapala, Takashi Inoue, and Shu Namiki. Nearly-ideal optical phase conjugation based nonlinear compensation system. In *Optical Fiber Communication Conference*, W3F.8. OSA, 2014a. ISBN 9781557529930.

Karen Solis-Trapala, Takashi Inoue, and Shu Namiki. Signal power asymmetry tolerance of an optical phase conjugation-based nonlinear compensation system. In *2014 The European Conference on Optical Communication (ECOC)*. IEEE, Sep 2014b.

Karen Solis-Trapala, Mark Pelusi, Hung Nguyen Tan, Takashi Inoue, and Shu Namiki. Optimized WDM transmission impairment mitigation by multiple phase conjugations. *Journal of Lightwave Technology*, 34(2):431–440, Jan 2016. ISSN 0733-8724.

Karen Solis-Trapala, Mark Pelusi, Hung Nguyen Tan, Takashi Inoue, Satoshi Suda, and Shu Namiki. Doubled transmission reach for DP-64qam signal over field-deployed legacy fiber systems enabled by MSSI. In *2015 European Conference on Optical Communication (ECOC)*. IEEE, sep 2015.

M. F. C. Stephens, M. Tan, I. D. Phillips, S. Sygletos, P. Harper, and N.J. Doran. 1thz-bandwidth polarization-diverse optical phase conjugation of 10×114gb/s DP-QPSK WDM signals. In *Optical Fiber Communication Conference*, W3F.6. OSA, 2014. ISBN 9781557529930.

Shigehiro Takasaka. Flat amplification over c-band by quasi phase-matched fiber optical parametric amplifier using pump-phase shifers. In Werner Weiershausen, Benjamin B. Dingel, Achyut K. Dutta, and Atul K. Srivastava, editors, *Optical Metro Networks and Short-Haul Systems VI*. SPIE, dec 2013.

Hung Nguyen Tan, Takashi Inoue, and Shu Namiki. Highly cascadable all-optical wavelength conversions of DP-QPSK, DP-16qam, and DP-64qam signals. In *2015 European Conference on Optical Communication (ECOC)*. IEEE, Sep 2015. ISBN 9788460817413.

Hung Nguyen Tan, Takashi Inoue, Ken Tanizawa, Stephane Petit, Yoichi Oikawa, Shigehiro Takasaka, Takeshi Yagi, and Shu Namiki. Counter-dithering pump scheme for cascaded degenerate FWM based wavelength converter. In *Optical Fiber Communication Conference*, W3F.4. OSA, 2014. ISBN 9781557529930.

Renyong Tang, Paul L. Voss, Jacob Lasri, Preetpaul Devgan, and Prem Kumar. Noise-figure limit of fiber-optical parametric amplifiers and wavelength converters: experimental investigation. *Optics Letters*, 29(20):2372, oct 2004.

Zhi Tong, Adonis Bogris, Magnus Karlsson, and Peter A. Andrekson. Full characterization of the signal and idler noise figure spectra in single-pumped fiber optical parametric amplifiers. *Optics Express*, 18(3):2884, jan 2010.

K. Torii and S. Yamashita. Efficiency improvement of optical fiber wavelength converter without spectral spread using synchronous phase/frequency modulations. *Journal of Lightwave Technology*, 21(4):1039–1045, Apr 2003. ISSN 0733-8724.

T. Torounidis, P.A. Andrekson, and B.-E. Olsson. Fiber-optical parametric amplifier with 70-dB gain. *IEEE Photonics Technology Letters*, 18(10):1194–1196, May 2006. ISSN 1041-1135.

Victor Torres-Company and Andrew M. Weiner. Optical frequency comb technology for ultra-broadband radio-frequency photonics. *Laser & Photonics Reviews*, 8(3):368–393, Dec 2013.

T. Umeki, T. Kazama, H. Ono, Y. Miyamoto, and H. Takenouchi. Spectrally efficient optical phase conjugation based on complementary spectral inversion for nonlinearity mitigation. In *2015 European Conference on Optical Communication (ECOC)*. IEEE, Sep 2015. ISBN 9788460817413.

Takeshi Umeki, Takushi Kazama, Akihide Sano, Kohki Shibahara, Kenya Suzuki, Masashi Abe, Hirokazu Takenouchi, and Yutaka Miyamoto. Simultaneous nonlinearity mitigation in 92 $\times$ 180-gbit/s PDM-16qam transmission over 3840 km using PPLN-based guard-band-less optical phase conjugation. *Optics Express*, 24(15):16945, Jul 2016. ISSN 1094-4087.

Dragana Vukovic, Jochen Schroder, Francesco Da Ros, Liang Bangyuan Du, Chang Joon Chae, Duk-Yong Choi, Mark D. Pelusi, and Christophe Peucheret. Multichannel nonlinear distortion compensation using optical phase conjugation in a silicon nanowire. *Optics Express*, 23(3):3640, Feb 2015. ISSN 1094-4087.

S. H. Wang, Lixin Xu, and P. K. A. Wai. Optimal noise figure for raman-assisted fiber optical parametric amplifiers. In *OECC/ACOFT 2008 - Joint Conference of the Opto-Electronics and Communications Conference and the Australian Conference on Optical Fibre Technology*. IEEE, jul 2008.

S. Watanabe, T. Chikama, G. Ishikawa, T. Terahara, and H. Kuwahara. Compensation of pulse shape distortion due to chromatic dispersion and kerr effect by optical phase conjugation. *IEEE Photonics Technology Letters*, 5(10):1241–1243, Oct 1993. ISSN 1041-1135.

S. Watanabe and M. Shirasaki. Exact compensation for both chromatic dispersion and kerr effect in a transmission fiber using optical phase conjugation. *Journal of Lightwave Technology*, 14(3):243–248, Mar 1996. ISSN 0733-8724.

Haiqing Wei and David V. Plant. Simultaneous nonlinearity suppression and wide-band dispersion compensation using optical phase conjugation. *Optics Express*, 12(9):1938, 2004.

Tianhua Xu, Gunnar Jacobsen, Sergei Popov, Jie Li, Evgeny Vanin, Ke Wang, Ari T. Friberg, and Yimo Zhang. Chromatic dispersion compensation in coherent transmission system using digital filters. *Optics Express*, 18(15):16243, Jul 2010.

Amnon Yariv, Dan Fekete, and David M. Pepper. Compensation for channel dispersion by nonlinear optical phase conjugation. *Optics Letters*, 4(2):52, Feb 1979. ISSN 0146-9592.

Xingwen Yi, Xuemei Chen, Dinesh Sharma, Chao Li, Ming Luo, Qi Yang, Zhaohui Li, and Kun Qiu. Digital coherent superposition of optical OFDM subcarrier pairs with hermitian symmetry for phase noise mitigation. *Optics Express*, 22(11):13454, May 2014. ISSN 1094-4087.

M. Yu, G.P. Agrawal, and C.J. McKinstrie. Effect of residual dispersion in the phase-conjugation fiber on dispersion compensation in optical communication systems. *IEEE Photonics Technology Letters*, 7(8):932–934, Aug 1995.

Xiang Zhou, Jianjun Yu, Ming-Fang Huang, Yin Shao, Ting Wang, Peter Magill, Milorad Cvijetic, Lynn Nelson, Martin Birk, Guodong Zhang, Sergey Y Ten, H. B. Matthew, and S. K. Mishra. 32Tb/s (320x114Gb/s) PDM-RZ-8QAM transmission over 580km of SMF-28 ultra-low-loss fiber. In *Optical Fiber Communication Conference and National Fiber Optic Engineers Conference*. OSA, 2009.